

Louisiana State University

LSU Scholarly Repository

LSU Historical Dissertations and Theses

Graduate School

1997

Cellulose-Reinforced Composites and SRIM and RTM Modeling.

Mohammad Fahrurrozi

Louisiana State University and Agricultural & Mechanical College

Follow this and additional works at: https://repository.lsu.edu/gradschool_disstheses

Recommended Citation

Fahrurrozi, Mohammad, "Cellulose-Reinforced Composites and SRIM and RTM Modeling." (1997). *LSU Historical Dissertations and Theses*. 6481.

https://repository.lsu.edu/gradschool_disstheses/6481

This Dissertation is brought to you for free and open access by the Graduate School at LSU Scholarly Repository. It has been accepted for inclusion in LSU Historical Dissertations and Theses by an authorized administrator of LSU Scholarly Repository. For more information, please contact gradetd@lsu.edu.

INFORMATION TO USERS

This manuscript has been reproduced from the microfilm master. UMI films the text directly from the original or copy submitted. Thus, some thesis and dissertation copies are in typewriter face, while others may be from any type of computer printer.

The quality of this reproduction is dependent upon the quality of the copy submitted. Broken or indistinct print, colored or poor quality illustrations and photographs, print bleedthrough, substandard margins, and improper alignment can adversely affect reproduction.

In the unlikely event that the author did not send UMI a complete manuscript and there are missing pages, these will be noted. Also, if unauthorized copyright material had to be removed, a note will indicate the deletion.

Oversize materials (e.g., maps, drawings, charts) are reproduced by sectioning the original, beginning at the upper left-hand corner and continuing from left to right in equal sections with small overlaps. Each original is also photographed in one exposure and is included in reduced form at the back of the book.

Photographs included in the original manuscript have been reproduced xerographically in this copy. Higher quality 6" x 9" black and white photographic prints are available for any photographs or illustrations appearing in this copy for an additional charge. Contact UMI directly to order.



A Bell & Howell Information Company
300 North Zeeb Road, Ann Arbor MI 48106-1346 USA
313/761-4700 800/521-0600

**CELLULOSE REINFORCED COMPOSITES
AND SRIM AND RTM MODELING**

A Dissertation

**Submitted to Graduate Faculty of the
Louisiana State University and
Agricultural and Mechanical College
in partial fulfillment of the
requirements for the degree of
Doctor of Philosophy**

in

The Department of Chemical Engineering

by

**Mohammad Fahrurrozi
B.S., Gadjah Mada University, Yogyakarta, Indonesia, 1989
M.S., Louisiana State University, 1993
August, 1997**

UMI Number: 9808738

**UMI Microform 9808738
Copyright 1997, by UMI Company. All rights reserved.**

**This microform edition is protected against unauthorized
copying under Title 17, United States Code.**

UMI
300 North Zeeb Road
Ann Arbor, MI 48103

ACKNOWLEDGMENTS

The author would like to express his most sincere appreciation to his major advisor, Dr. John R. Collier, for all his help, guidance, and encouragement through out these years. Special thanks also to Dr. Billie J. Collier and Dr. Joan I. Negulescu for all their help. The author also would like to thank Dr. Armando B. Corripio, Dr. Frank R. Groves, Jr., and Dr. Randall C. Gayda for serving in his advisory committee.

The financial support from the Louisiana Board of Regents for Louisiana Education Quality Support Fund grant and from National Institute of Standards and Technology (NIST) through the grant to Specialty Plastic Inc. are gratefully acknowledged. The author wishes to thank the Higher Education Development Project (P-PS2PT) and Jurusan Teknik Kimia, Gadjah Mada University, Indonesia, for giving the author the chance to pursue PhD program at Louisiana State University. The author deeply appreciates the financial support from the government of Indonesia through P-PS2PT through out his first 4.5 years at Louisiana State University.

The author also thanks Dr. Wei Ying Tao of SRRC, New Orleans, for her help in preparing needle punched mats. Thanks also for all members of Polymer Processing and Textile Groups for their significant contributions to this dissertation. Special thanks are for Maryoud Elsunni for his help and expert advice

in sugar cane mat preparation, Erick Commeoux for his help with DSC and TGA. Mircea Despa for his help with SEM and ESEM, and Bijan Seyfzadeh for his help with surface tension measurement. Thanks are extended to V. Paul Rodriguez, Robert J. Perkins, and all the student workers in the Chemical Engineering Shop.

Most of all the author wants to thank his parents, his wife Khonsaa and his daughters Fatimah and Maryam. The author would not have been able to finish this endeavor without their support, sacrifice and love.

TABLE OF CONTENTS

ACKNOWLEDGMENTS	ii
LIST OF TABLES	vii
LIST OF FIGURES	viii
ABBREVIATIONS	xii
ABSTRACT	xii
CHAPTER	
1 INTRODUCTION	1
PART I: SRIM CELLULOSE/PU COMPOSITES	9
2 LITERATURE REVIEW	10
2.1 Continuous Fiber Reinforced Composites	10
2.2 SRIM Process	12
2.2.1 Impingement Mixing	13
2.2.2 Mold Filling	14
2.3 Chemistry of PU SRIM	16
2.4 Chemical Reaction and Phase Separation	18
2.4.1 Chemical Reaction	18
2.4.2 Phase Separation	20
2.4.3 Chemical Formulation for SRIM	21
2.5 Preformed Mat From Sugar Cane Rind Fiber	22
2.5.1 Sugar Cane Rind Fiber	22
2.5.2 Mat Formation and Placement in the Mold	24
2.6 Material and Product Characterization	26
2.6.1 Fiber-matrix Adhesion	26
2.6.2 Mechanical Properties	27
3 EXPERIMENTAL	29
3.1 RIM Machine	29
3.2 The Mold	29

3.3	Material	30
3.3.1	Chemical Formulation	30
3.3.2	Preformed Mats	33
3.4	Experimental Procedures	34
3.4.1	Molding Experiment	34
3.4.2	Mechanical Testing	35
3.4.3	Kinetic Study	36
3.4.4	Other Experimental Procedures	37
4	RIM EXPERIMENTAL RESULTS AND DISCUSSIONS ...	39
4.1	Effect of Fiber Loading	39
4.2	Effect of Chemical Ratio	45
4.3	Resin-fiber Adhesion	47
4.4	Kinetic Study	52
5	CELLULOSIC COMPOSITES CONCLUSIONS	58
6	CELLULOSIC COMPOSITES RECOMMENDATIONS	61
PART II. SRIM AND RTM MODELING		62
7	LITERATURE SURVEY ON SRIM AND RTM MODELING	63
7.1	SRIM and RTM Modeling	65
7.2	Finite Difference Based Models	66
7.3	Finite Element Based SRIM Model	68
7.4	PC Based Modeling for Fully 3-D SRIM Mold Filling Problems	70
8	MATHEMATICAL REPRESENTATION FOR MOVING FRONT PROBLEMS IN RTM AND SRIM	72
8.1	Governing Equations	73
8.2	Permeability	75
8.3	Energy and Reaction Equations	79
8.4	Rheokinetic Model	81
8.5	Boundary Conditions.....	82
8.6	Front Tracking Methods	83
9	DEVELOPMENT OF THE NUMERICAL METHODS	85
9.1	Control Volume Finite Difference Formulation	86

9.2	Implementing Boundary Conditions	91
9.3	Convergence Consideration	94
9.4	Front Tracking	95
9.4.1	Approximate Method for Front Tracking	96
9.4.2	Volume of Fluid Method	97
9.5	Iterative Scheme	100
9.6	Programming Implementation	101
10	MODEL VERIFICATION AND DEMONSTRATION	104
10.1	Comparison with Experimental Data from Literature: Non Reactive System	105
10.2	Comparison with Results Obtained Using NIST's FE Program	107
10.3	Mold Filling and Curing Simulation	111
10.3.1	Adiabatic Solution	113
10.3.2	The Mold Thermal Effect	115
10.4	Comparison with molding Experimental Data with Cellulosic Preform	117
10.5	Simulation of Stub Flange Filling	119
11	MODELING CONCLUSIONS	125
12	MODELING RECOMMENDATIONS	127
REFERENCES		129
APPENDIXES		139
A	COMPUTER PROGRAM STRUCTURE	139
B	CHEMICAL STRUCTURES	141
C	A REVIEW ON MAPPING OF GOVERNING EQUATIONS	142
VITA		148

LIST OF TABLES

2.1	Viscosity and Gel Time for Typical PU Formulation for RIM/SRIM	21
2.2	Typical Commercial Polyurethane (PU) and Polyurea- urethane (PUU) Formulations	22
3.1	Some Important Properties of The Resins	32
4.1	TGA Analysis Result	47
4.2	Surface Tension Properties of The Resins and Mold Release Agents	48
4.3	Estimated Surface Energy	48
9.1	Expression for U, V, W and Γ	87
10.1	Thermal, Kinetic, and Rheological Parameters	113

LIST OF FIGURES

2.1	Theoretical Efficiency Factors for Various Fiber Configuration	11
2.2	SRIM Unit Operation (Macosko, 1989)	13
2.3	Isocyanate Reactions	17
2.4	Segmented Block PUU Copolymer	19
2.5	Molecular Structures of Cellulose, Lignin and Hemicellulose	24
3.1	The RIM Molds	31
3.2	Tensile Test Specimen Dimension	36
4.1	Effects of Fiber Loading on Tensile Properties of Spectrim® 50/Cheesecloth Composites for Various Chemical Ratio	40
4.2	Effect of Fiber Properties on The Mechanical Properties	41
4.3	Effect of Fiber Loading on Tensile Properties of Spectrim® MM 310/cotton Composites for Chemical Ratio = 1	42
4.4	Effect of Fiber Loading on Bending Properties of Spectrim® MM 310/Cellulosic Composites for Chemical Ratio = 1	43
4.5	Effect of Chemical Ratio on Tensile Properties of Spectrim® 50/Cheesecloth Composites	46
4.6	SEM Micrographs of Broken Parts of The Samples	49
4.7	Gate Pressure Profiles for 27.94 cm x 28.575 cm x 0.65 cm Center Gated Rectangular Mold	53
4.8	Experimental Temperature and The Kinetic Model Prediction	55

4.9	Conversion Versus Time	57
9.1	Control Volume for Two-dimensional Space	89
9.2	One-dimensional Diffusion Problem	93
9.3	An Illustration for The Approximate Boundary Conditions ...	94
9.4	Approximate Method for Front Movement	97
9.5	Iterative Algorithm	101
10.1	Simulation Results: Non Reactive System	106
10.2	Filling Patterns: Effect of Grid Refinement	107
10.3	Filling Patterns: Comparison of 2-D and 3-D Model Predictions	107
10.4	Comparison with NIST FE Solution: Filling Patterns	109
10.5	Comparison with NIST FE Solution: Gate Pressure Profiles...	110
10.6	Run Time versus The Number of Grid Points for The 2-D Model	110
10.7	Adiabatic Mold Filling and Curing	114
10.8	Young's Mold	116
10.9	Non-isothermal Reactive Systems: A Comparison with FE Solution	117
10.10	Non-isothermal Reactive Systems: Effect of Inlet Temperature	118
10.11	Molding Experimental Data with Sugar Cane Fiber	119
10.12	Matlab Screen Capture: Discretized Geometry and Multi-Blocking of Stub Flange	122

10.13 Simulation Result: Filling Patterns 124

LIST OF ABBREVIATION

ABBREVIATION	TERM
BDO	Butanediol
CFD	Computational fluid dynamic
CV	Control volume
DABCO	1,4-diazabicyclo (2,2,2)-octane
DBTDL	Dibutyltin dilaurate
DETDA	Diethyl toluene diamine
DSC	Differential scanning calorimetric
EO	Ethylene oxide
FD	Finite difference
FE	Finite element
FTIR	Fourier transform infrared spectroscopy
MDI	Methyl diphenyl diisocyanate
PI	Phenyl Isocyanate
PPO	Polypropylene oxide
PU	Polyurethane
PUU	Polyurethane-urea
RIM	Reaction injection molding
RTM	Resin transfer molding
SEM	Scanning electron microscopy
SRIM	Structural reaction injection molding
SRRC	USDA Southern Regional Research center
TGA	Thermal gravimetric analysis
UHMWPE	Ultra high molecular weight polyethylene

ABSTRACT

Structural reaction injection molding (SRIM) cellulosic/polyurethane composites were prepared from various forms of cellulosic mats, and elastomeric polyurea-urethane (PUU) and rigid polyurethane (PU) formulations. Mats (woven and non-woven) prepared from different sources of fibers with lignin content ranging from zero (cotton) to at least 10 % (sugar cane and kenaf fibers) performed comparably in PUU/cellulosic composites. Young's modulus and tensile strength of PUU/cellulosic composites were doubled with 5 % and 7 % fiber loading respectively. Young's modulus and tensile strength of PU/cellulosic composites were improved by 300 % and 30 % , respectively, with 7 % fiber loading, whereas their bending moduli and strengths were improved up to 100 % and 50 % , respectively, with 18 % fiber loading. However, the mechanical properties of PU composites were more sensitive to the fiber properties and fiber macroscopic arrangements. The study with chemical ratio variations indicates that as the fiber loading increases, the cellulose hydroxyl presence starts shifting the chemical balance and thus should be accounted for.

Mats prepared from sugar cane fibers extracted from rind with low alkali concentration (0.2 N) followed by steam explosion require lower injection pressures compared to the ones prepared from fiber obtained from higher alkali

treatment (above 0.5 N) without steam explosion. Hence, the steam exploded mats are more suitable for SRIM purposes.

The PU kinetics was studied using an adiabatic temperature rise method. An Arrhenius type empirical equation was used to fit the data. The fitted equation was second order to the partial conversion, and the gelling time at adiabatic condition is less than 5 seconds (much quicker than the 10 to 12 seconds in mold gel time quoted by the manufacturer).

FORTRAN programs were written to solve the SRIM model based on Darcy's equation. The model incorporated heat transfer and chemical reaction. The modeling was intended to aid in interpreting in-mold pressure data obtained from mat permeability characterization. The model also has other wider applications such as mold design and SRIM and resin transfer molding (RTM) simulation. The model predicts some experimental data from this work and the literature satisfactorily.

CHAPTER 1

INTRODUCTION

Reaction injection molding (RIM) is a process to manufacture plastic parts directly from low viscosity monomers or oligomers. In a RIM process, two reactive liquids are combined by impingement mixing just before entering a mold. Polymerization, that is quickly induced by this impingement mixing, proceeds rapidly, and when the gel point is exceeded, subsequent polymerization and solidification occur simultaneously. The solid structure results from cross-linking or phase separation or a combination of both, and the product can be demolded in times on the order of a minute. The combination of low viscosity materials and fast demolding allows high speed production of complex parts such as those used in the automobile industry (Macosko, 1989; Gum et al., 1992, Lindsay, 1993).

The development of RIM technology has mainly been driven by the need for flexible polyurethane (PU) facia in the US automobile industry (Macosko, 1989). This industry is still the major market for RIM products (Gum et al., 1992; Grulke, 1994; Lindsay, 1993), and PU and polyurea-urethane (PUU) constitute the two highest percentage components of the total RIM process production(Macosko, 1989; Ryan et al., 1991; Pannone and Macosko, 1987). Recent trends show that PUU is dominating in the automobile industry due to its superior mechanical and

processing properties compared to those of PU (Ryan et al., 1991; Pannone and Macosko, 1987).

The low viscosity mold filling RIM system has advantages over the injection molding of thermoplastics (Macosko, 1989). The low viscosity allows the use of a low injection pressure and production of reinforced parts (Lo, 1994; Lo, et al., 1994). Over half of RIM products are fiber filled or fiber reinforced (Macosko, 1989). The main motivations for using filler or reinforcement are to improve the dimensional stability and enhance the mechanical properties of the final products. For example, polymers typically have coefficients of thermal expansion (CTE) nearly ten times those of metals (Macosko, 1989). This can cause problems in many applications where polymers are layered over metal surfaces. The addition of fibers can greatly reduce the coefficient of thermal expansion. Using continuous fiber reinforcement with a high loading allows the production of polymer composites with flexural modulus and tensile strengths approaching those of laminate composites and metals, thereby enabling the use of the composite polymers in structural applications (Macosko, 1989). Another important reason for adding fillers to the polymer is to reduce the material cost of the final products.

Several fibers have been used as fillers in RIM materials, for example: hammer milled and chopped glass fibers, wollastonite, mica flakes and carbon fibers (Macosko, 1989). There were also efforts to use organic fibers such as nylon and ultra high molecular weight polyethylene (UHMWPE) (Macosko, 1989; Stanford,

1988; Williams et al., 1991). The degree of improvement in the physical properties of the composites follows the general principle of reinforcement which requires the optimization of the fiber content, the aspect ratio of the fiber (L/D), and the surface adhesion between the reinforcing and the matrix phases (Stanford, 1988; Richardson, 1977; Eagles et al., 1991; Williams et al., 1991).

The presence of fibers, for example as fillers, greatly increases the viscosity of the slurry (Macosko, 1989; Stanford, 1988); the viscosity increases with the fiber content and aspect ratio. This sets limits to the achievement of physical property improvement by using fiber fillers in composites. It has been reported that the maximum fiber loading in filled RIM material is 30 % when the reinforcement is injected as part of one reactant stream, i.e. in reinforced reaction injection molding (RRIM) (Macosko, 1989).

Using continuous fibers in a form of a pre-placed mat can extend the above mentioned limitations. In this approach a preformed mat is put in the mold before the reactants are injected into the mold. The process is often called structural reaction injection molding (SRIM). In this regard, SRIM is very similar to resin transfer molding (RTM), except that in RTM a single stream mixture of resin or resins and the catalyst is pumped into the mold and the reaction is initiated by catalyst and/or heating. It has been reported that glass fiber contents up to 60 % are realizable in the SRIM process (Macosko, 1989).

Beside the aspect ratio, the fiber-matrix adhesion also has a critical influence on the efficiency of the load transfer between the matrix and the fiber (Richardson, 1977; Eagles et al., 1991). Improvement of the adhesion between the reinforcing material and the matrix can be accomplished in two ways: surface treatment of the fiber (Williams et al., 1991) or adding coupling agents (Collier and Collier, 1993, Richardson, 1977). Both methods, however, add extra processing steps to the RIM operation, and usually extra cost.

J.R. Collier and B.J. Collier (1993) proposed the use of cellulose fibers as preformed mats for SRIM recently. Cellulose fibers have two advantages over most other fibers; firstly, they are produced naturally, so they are renewable; secondly, the primary hydroxyl groups react with isocyanates to form urethane bonds (Collier and Collier, 1993; Young and Rowell, 1986). Therefore good adhesion develops between the cellulosic fibers and the PU matrix. Therefore this research involves the effect of the presence of chemically active fibers, such as cellulosic fibers, on the chemical and mechanical properties of SRIM products.

Mechanical properties of both the fibers and the matrix as well as the adhesion between the two are the most critical factors determining mechanical properties of the composites (Richardson, 1977). The other factors influencing the level of the reinforcement are fiber aspect ratio, fiber arrangement in the mat, and fiber content in the composites (Richardson, 1977). Cellulosic fibers with different properties can be obtained from different sources, such as wood fiber, cotton fiber,

and sugar cane fiber, or from one source with different processing conditions such as different degrees of delignification (Collier et. al., 1992; Agarwal, 1992; Elsunni and Collier, 1996; Romanoschi et al., 1997(a) and 1997(b)). Two different arrangements of fibers can be obtained using two types of mats, woven and non-woven mats. The mat porosity can be varied by using different fiber loading in the mold. These factors give a wide property range of cellulose/PU composites suitable for different applications.

In SRIM composite production, matrix and composite are formed simultaneously. Consequently, the presence of the active fiber in the mold could influence the kinetics of the matrix formation. To have good fiber-matrix adhesion it is important for the resin to completely wet the fiber in a very short time during the mold filling (Macosko, 1989; Richardson, 1977; Eagles et al., 1991). Resin surface tension and fiber surface energy, control the wetting phenomena. In the PU RIM process, the molal ratio of the reactants is very critical and fully controlled. In order to achieve the design properties of the products, the amount of polyol must be adjusted to compensate for the influence of the mats since cellulosic hydroxyl groups in the mats compete with RIM chemical hydroxyl groups.

Mold filling is the most crucial step in the SRIM operation because in a very short time (on the order of seconds) the resin should be able to fill the mold, completely displace the air, and wet the reinforcing fibers. To achieve this, mold and

mold filling should be designed properly. Modeling tools that can aid in this are of practical importance.

The objectives of this research are:

1. To study the effects of variations of cellulosic fiber properties and arrangements on the mechanical properties of PU/cellulose composites.
2. To study the effects of fiber preparation conditions on moldability and the mechanical properties of the composites.
3. To study the fiber-matrix interaction in polyurethane/cellulose composites.
4. To develop a personal computer (PC) based SRIM/RTM model.

The first objective of this research is important from the PU/cellulosic composites application point of view. Quantitative information on the composite mechanical properties as well as on the factors influencing them will help in choosing proper application for the composites. This research is expected to give useful information in this matter.

The second objective is related to the cellulosic fiber preparation aspect. The need to obtain fibers that have a good performance mechanically should be balanced against the practicality of both fiber and the composite productions. This study is intended only to find some feasible operating conditions for fiber preparation. This work is part of a larger effort to study possible applications to add economic value to cellulosic agricultural by-products.

Since cellulosic fibers are technically also polyols, they can be expected to influence SRIM chemical balance. The study is limited to the identification of possible effects of the presence of the cellulosic fiber on the chemical balance in the SRIM system.

Although modeling tools can reduce the experimental cost to some degree, they are not always cheap and widely available for different types of users. Making the modeling tools available on PC's should enhance the use of this technology. The work done in this research is expected to contribute to developing a PC based SRIM model. The models developed in this work is applicable as well to RTM. Since mold filling occurs after mixing the two fluid streams, in SRIM, the filling aspects of SRIM and RTM are similar.

This dissertation is organized into two parts. The first part deals with the experimental aspects of PU/cellulosic composite preparation with SRIM, and the second part with the SRIM modeling. A literature review on various aspect of SRIM is presented in Chapter 2. Chapter 3 reports the experimental procedures, the equipment and the material used in this work. Chapter 4 presents the experimental results and the discussion. Finally the first part of this dissertation ends with conclusions (Chapter 5) and recommendations (Chapter 6). A literature survey on SRIM modeling is presented in chapter 7. Mathematical representation of the SRIM model is given in Chapter 8 followed by the numerical method development in Chapter 9. Chapter 10 presents model verification and

demonstration. Finally conclusions of the modeling work will be presented in Chapter 11 followed by recommendations (Chapter 12).

PART I

SRIM CELLULOSE/PU COMPOSITES

CHAPTER 2

LITERATURE REVIEW

As an introduction and a basis for the later discussions, a review of composites with continuous fiber reinforcement will be presented first. The next four sections will be devoted to various aspects of SRIM, followed by a literature review on preformed mats from sugar cane rind fiber. The last sections will focus on the material and composite characterization.

2.1 Continuous Fiber Reinforced Composites

In terms of fiber dimensions, there are two extreme cases in fiber reinforced composites, i.e. particulate composites and continuous fiber composites. While the aspect ratios are close to one in particulate composites, the corresponding ratios for continuous fiber reinforcement are technically considered to be infinity (Richardson, 1977). In actual situations, however, a composite containing fibers of a few tens cm in length and aspect ratios of 50-100 are considered a continuous fiber reinforcement composite (Richardson, 1977; Eagles, et al., 1976).

For continuous fiber composites, where the fibers run end to end in a long sample, the tensile strength of the composites can be modeled as (Macosko, 1989; Richardson, 1977):

$$\sigma = \sigma_m \phi + \varepsilon \sigma_f (1 - \phi) \quad (2.1)$$

Where ϕ is the porosity, ε an efficiency factor (depends on reinforcement efficiency). σ , σ_f , and σ_m are the tensile strength of the composites, fibers and the matrix respectively. The theoretical values of ε for different fiber orientations in the mats are given in the Figure 2.1 (Richardson, 1977). For random mats, ε takes a value of 3/8 (Macosko, 1989; Richardson, 1977).

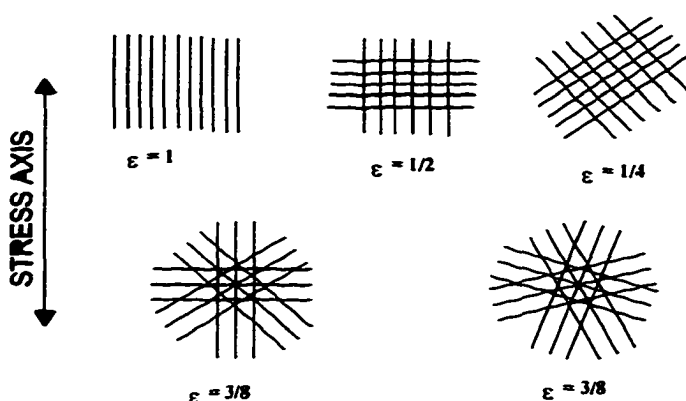


Figure 2.1 Theoretical Efficiency Factors for Various Fiber Configuration

Producing preforms with essentially infinite lengths of fibers is uneconomical in most practical situations; most fibers fall into the category of short fibers. In order for the performance of these fibers to be close to those of continuous fibers, their aspect ratio must be greater than a critical value (L_c/d) (Richardson, 1977; Eagles, et al., 1976), defined in terms of a critical length, L_c , divided by the fiber diameter.

Using a force balance between the tensile stress on the fibers and the shear stress on the fiber-matrix interface, the critical aspect ratio can be calculated as given by (Richardson, 1977; Eagles, et al., 1976):

$$\frac{L_c}{d} = \frac{\sigma_f}{2\tau_i} \quad (2.2)$$

where σ_f is the fiber tensile strength, and τ_i is the shear strength of the interface or the matrix, whichever is weaker. The fibers have to be much longer than L_c in order to have performance close to the continuous fibers (Macosko, 1989).

From equation (2.1) and (2.2), it can be concluded that the composite mechanical properties are influenced by the mechanical properties of the fibers and the matrix, the adhesion force between fibers and matrix, the fiber dimension and the fiber arrangement in the mat. The following discussions will elaborate on each of these considerations.

2.2 SRIM Process

The steps in production of SRIM materials can be described by the unit operations in Figure 2.2. Reviews on sugar cane rind cellulosic fibers and the mat formation from these fibers will be presented in separate sections. In this section, the discussion is focused on impingement mixing and mold filling, the two most crucial steps in SRIM processes; a detailed discussion on the SRIM unit operations can be found elsewhere (Macosko, 1989).

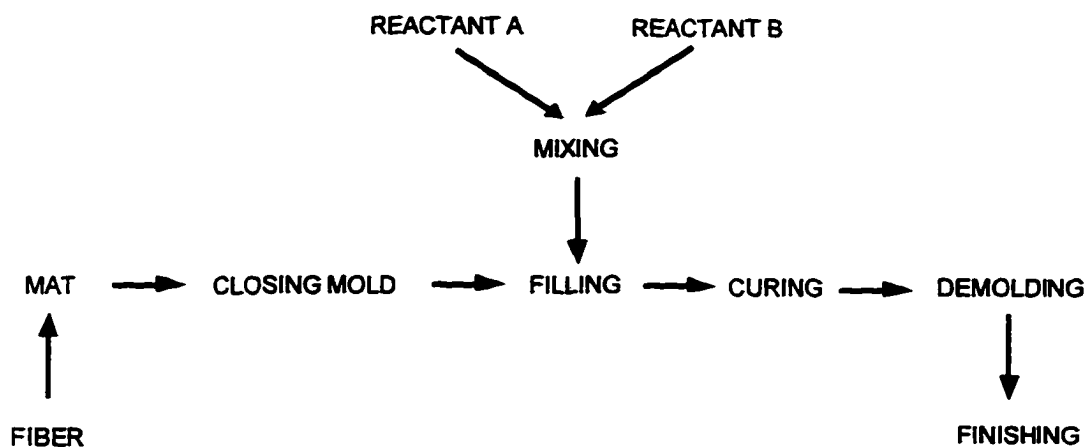


Figure 2.2 SRIM Unit Operation (Macosko, 1989)

2.2.1 Impingement Mixing

Impingement mixing is the heart of RIM as well as SRIM processes, since it is the impingement mixing that "initiates" the polymerization in these processes (Macosko, 1989). Impingement mixing is carried out in the mixing head that brings the two reactant streams into a uniform reaction. The mixing quality is usually described by the value of the Reynold's number and is given by:

$$Re_i = \frac{4\rho_i Q_i}{D_i \mu_i} \quad (2.3)$$

where ρ_i , μ_i , and Q_i are the density, viscosity and volumetric flowrate of stream i respectively; D_i is the diameter of the orifice.

A sufficiently high Reynold's number is necessary for good mixing. The value of the critical Reynold's number, however, depends on the design of the

mixing head and the chemical formulation for the SRIM process (Baser et al., 1993; Boukolbal et al., 1989). For PU systems the critical Reynold's number is about 300 (Macosko, 1989).

The flow around the fibers in the SRIM processes will improve the mixing and thus lower the critical Reynold's number (Macosko, 1989). However, the presence of the fiber mat in the mold will also increase the pressure drop needed in the mold, thereby reducing the pressure drop available for impingement mixing. These two effects can be balanced by proper mold design and careful selection of the chemical system and the operating conditions for the SRIM processes so that the viscosity of the resin remains suitably low until the mold filling is completed. This issue will be discussed in the next subsection.

2.2.2 Mold Filling

Mold filling is a very critical step in the SRIM process. In a very short time (on the order of one second), the resin must completely fill the mold and wet all the individual fibers while the reactions have not proceeded significantly (Macosko, 1989). Despite this fast process, the trapping of voids inside the composite must be avoided because they will greatly affect the mechanical properties of the composites (Macosko, 1989; Eagles, et al., 1976; McGeehan and Gillespie, J.R., 1993). Lack of complete wetting of the fibers will significantly reduce the effectiveness of the reinforcement (Macosko, 1989; Eagles, et al.,

1976). For these reasons, the analysis of fluid distribution in SRIM mold filling is of practical importance. From the mold filling analysis, a good mold design, a correct chemical formulation, fiber arrangement and operating condition can be obtained. This will be discussed further in the modeling section.

Fluid penetration into fiber bundles is driven by pressure and surface tension (Macosko, 1989). As a rough estimation of the surface tension effect, Macosko (Macosko, 1989) modeled the spaces between the parallel fibers as cylindrical channels. He used the capillary equation to calculate the penetration driving force as:

$$\Delta p_p = \frac{2\gamma \cos(\Theta)}{R} \quad (2.4)$$

where γ is the resin surface tension, θ is the resin-fiber contact angle, and R is an effective radius of the channel which was taken to be on the order of the fiber radius.

Equation (2.4) can be combined with Poiseuille's equation to estimate the penetration distance into a capillary tube as (Macosko, 1989):

$$L_p = \frac{R}{2} \left(\frac{\Delta p_p}{2\mu} \right)^{\frac{1}{2}} t^{\frac{1}{2}} \quad (2.5)$$

where L_p is the penetration distance, μ is the resin viscosity, and t is the penetration time. From the above equations, it is apparent that both a low viscosity

resin and a reasonably long filling time are necessary for complete penetration into the mat of fiber bundles.

To achieve a longer filling time, SRIM requires slower reactions compared to RIM reactions. This can be achieved by manipulating the amount of catalyst in the chemical formulation or by selecting a slower reaction system. This will be discussed in the following section.

2.3 Chemistry of PU SRIM

Basically, SRIM chemistry is analogous to RIM chemistry. Many good reviews on RIM chemistry are available in the literature (Macosko, 1989; Gum et al., 1992). In this section the discussion will be limited to pertinent issues related to PU/cellulosic composites only.

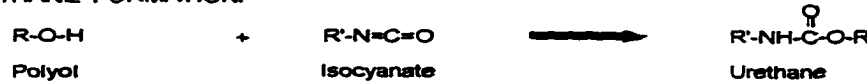
PU and PUU chemistry is characterized by the chemistry of isocyanates (Macosko, 1989). Isocyanates can react readily with compounds containing an active hydrogen (a hydrogen which is replaceable by a sodium atom) (Macosko, 1989). Isocyanate reactions with some important active hydrogen compounds in this work are given in the Figure 2.3. The reaction between amine and isocyanate will form polyurea and the reaction between isocyanate and an alcohol or polyol will produce urethane. Isocyanate can also react with urethane to form alphanate and with urea to form biuret (Macosko, 1989; Spathis et al., 1994; Kontou et al., 1990). These last two reactions greatly increase the solubility of the hard segment

in the soft segment and reduce phase separation in RIM and SRIM processes, by forming chemical crosslinking between the segments (Spathis et al., 1994; Kontou et al., 1990). In most RIM operations, equal stoichiometry between isocyanate and the polyol oligomer and chain extender is highly desirable (Macosko, 1989; Kontou et al., 1990).

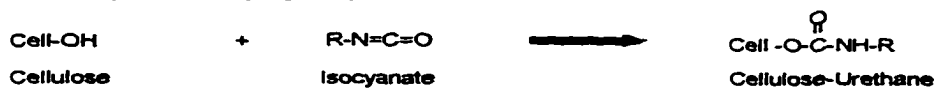
UREA FORMATION:



URETHANE FORMATION:



CELLULOSE-ISOCYANATE REACTION:



BIURET FORMATION



ALLOPHANATE FORMATION



Figure 2.3 Isocyanate Reactions

Many catalysts have been shown experimentally to have an influence on isocyanate reactions. Organometallic compounds such as dibutyltin dilaurate (DBTDL) greatly increase PU formation (Macosko, 1989; Luo et al., 1994; Pannone and Macosko, 1987), but do not show any effect on polyurea formation even at 2 mole % concentration. Tertiary amines such as 1,4-diazabicyclo (2,2,2)-

octane (DABCO) catalyze both reactions, but they show a stronger effect on urea formation than urethane (Pannone and Macosko, 1987). Isocyanate can also experience self condensation and addition (Macosko, 1989). Most of these reactions occur at relatively high temperatures or if suitable catalysts are present. No other reactions are important in SRIM or RIM processes except isocyanurate formation (self addition reaction of isocyanate) which is the basis of an emerging RIM/SRIM formulation (Macosko, 1989).

As mentioned before, most PU systems for RIM or SRIM are segmented block copolymers which form their structure from phase separation and/or crosslinking. This is illustrated in Figure 2.4. During the mold filling and curing, chemical reaction and phase separation occur simultaneously causing the modulus and viscosity of the polymer to rapidly increase. The relative speed of the two processes will determine the properties of the final products; this will be discussed in the following section.

2.4 Chemical Reaction and Phase Separation

2.4.1 Chemical Reaction

The two mechanisms, chemical reaction and phase separation, are connected to each other through two competing reactions. While isocyanate reacts with the oligomer to form the soft segments, its reaction with the chain extender

will form hard segments, thereby leading to the phase separation. The hard segment is generally thermodynamically incompatible with the soft segment.

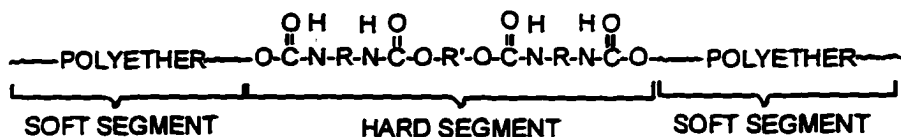


Figure 2.4 Segmented Block PUU Copolymer

A fast phase separation is desirable for polymer production, because it leads to fast demolding (Macosko, 1989). However, an extremely fast phase separation could lead to a brittle product, if the hard segment separates too quickly from the solution and traps the oligomer and the chain extender.

Usually, the chain extender is much more reactive than the oligomer polyol, especially in the PUU system where the chain extender is a low molecular weight diamine (Macosko, 1989; Pannone and Macosko, 1987). The aromatic diamine chain extender reaction with isocyanate is about 10 times faster than uncatalyzed polyether polyol reactions. However, to obtain good bonding (hydrogen-bonding) between the hard segment and the soft segment the relative activity of the chain extender and the oligomer should be close to each other (Ryan et al., 1991; Gao et al., 1994). This can be achieved by using catalysts such as DBTDL that speed up the PU formation (Macosko, 1989; Spathis et al., 1994; Pannone and Macosko,

1987). The reaction can also be increased by raising the temperature, but this method is not practical in RIM/SRIM processes where fast operations are required.

2.4.2 Phase Separation

The incompatibility can be increased by using higher molecular weight oligomer polyol and by lowering the temperature (Macosko, 1989; Spathis et al., 1994). Phase separation can also be increased by using more reactive chain extenders (Ryan et al., 1991; Gao et al., 1994).

The fraction of hard segment in the final product as well as its hydrogen bonding with the soft segment is very important for effective reinforcement (Ryan et al., 1991; Birch et al., 1989; Gao et al., 1994). If the reaction between the oligomer and isocyanate is too fast, the phases will be more compatible causing the interphase bonding to be stronger; however, the hard segment concentration will be lower. On the other hand, if the chain extender is too reactive such as 3-chloro, 3'-methylene, 4,4' diamino diphenyl methane (CMOMDA), the hard segment formation will be very fast and phase separation will be more developed; however, the bonding between phases will be weak, causing the product to be brittle (Gao et al., 1994).

For good mechanical properties of the products, hard segment content as well as the interphase bonding need to be controlled. This is done by choosing an appropriate chemical formulation.

2.4.3 Chemical Formulation for SRIM

From the previous discussions, it can be summarized that a good chemical formulation for SRIM should consider at least the three following factors:

1. a good fluid distribution in the mold
2. a complete wetting of all fibers
3. a good matrix phase formation (analogous to that of the RIM process).

Because of the first two considerations, typically SRIM chemical formulations have longer gel times and lower viscosities compared to those of RIM formulations (Macosko, 1989; Spathis et al., 1994) as shown in Table 2.1. Theoretically, commercial formulations for PU and PUU as shown in Table 2.2 can also be used for SRIM, except that SRIM requires a lower molecular weight oligomer (to lower the viscosity), and either a lower catalyst content or a less reactive chain extender (to increase gel time).

Table 2.1 Viscosity and Gel Time for Typical PU Formulation For RIM/SRIM

	RIM FORMULATION	SRIM FORMULATION
t_G, s	> 0.1	3 - 6
$\mu, \text{Pa.s}$	1	0.05 - 0.2

Table 2.2 Typical Commercial Polyurethane (PU) and Polyurea-urethane (PUU) Formulations

SPECTRIM 3101 Polyurethane(PU)	SPECTRIM 50¹ Poly Urea-Urethane (PUU)
Component A:	Component A:
Proprietary polyisocyanate: 100 %	MDI : 50-55 % MDI homopolymer : 2-5 % Proprietary MDI/ : 40-48 % polyether polyol pre-polymer
Component B:	Component B:
Proprietary polyether- : 29 % polyol Diethylene glycol : 19 % Proprietary polyol/glycol : 52 % blend	DETDA (chain extender) : 24 % Proprietary polyether : 76 % polyol, incorporating catalyst and additive
Catalyst:	
Tin Catalyst, : 0.05-0.25 % of Fomrez UL 382 B component	

2.5 Preformed Mat From Sugar Cane Rind Fiber

2.5.1 Sugar Cane Rind Fiber

Sugar cane is an important agriculture product in many southern states of the United States and is produced in large quantities (Collier et al., 1992; Agarwal, 1992; Elsunni and Collier, 1996; Chen, 1993). Sugar cane industries produce large

¹ Spectrim® is Dow Chemical's trade mark

² Fomrez® is Witco Chemical's trade name

volumes of cellulosic products that are essentially waste materials at present (Collier and Collier, 1993). Efforts have been made to develop higher economic value products containing the cellulosic fiber from sugar cane rind (Collier and Collier, 1993; Collier et al., 1992; Agarwal, 1992; Elsunni and Collier, 1996; Chen, 1993). Some practical uses of the fiber such as knitted textile fabrics and non woven mats for erosion control were studied experimentally (Collier and Collier, 1993).

In addition to cellulose fiber, sugar cane rind also contains approximately 18 % weight lignin and 30 % hemicellulose. As shown by their molecular structures in Figure 2.5, cellulose, lignin, and hemicellulose are basically polyols (Collier and Collier, 1993; Meister and Chang, 1992). As a polyol, the hydroxyl groups in cellulose should be as reactive with isocyanate as are the hydroxyls in the polyether or polyester polyol (Collier and Collier, 1993, Collier et. al., 1996).

All the natural polyols have potential application in the PU polymer (Meister and Chang, 1992; Feldman and Locasse, 1994). Studies have been done using lignin as filler for PU (Feldman and Locasse, 1994) and as a soft segment in PU segmented block copolymer (Meister and Chang, 1992). Since relatively high aspect ratio cellulosic fibers can be extracted from plants, it is of interest to study the application of cellulosic fibers as preformed mats in the SRIM process.

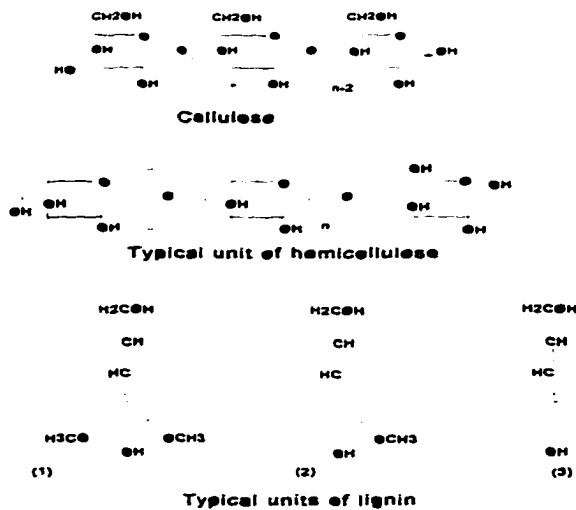


Figure 2.5 Molecular Structures of Cellulose, Lignin and Hemicellulose (Hon and Shiraishi, 1991)

The ultimate fiber length of the sugar cane rind fiber is approximately 2-3 mm (Collier et al., 1992). Using partial delignification followed by steam explosion, it is possible to produce fiber bundles of at least 5 cm length from sugar cane rind (Collier et al., 1992; Agarwal, 1992; Elsunni and Collier, 1996; Chen, 1993). The degree of delignification and the process conditions will influence the mechanical properties, the dimensions, and the chemical properties of the fibers. Elsunni and Collier (1996) found that sugar cane rind treated with 0.1 N alkali solution at 166° C for 1 hour, then followed by steam explosion, produced fibers that could be used for various textile applications. This type of fiber has dimensions and aspect ratios suitable for SRIM preformed mats.

2.5.2 Mat Formation and Placement in The Mold

The simplest way to produce a mat from sugar cane rind fiber is by directly discharging the fibers onto a screen or a web surface (Collier and Collier, 1993). If the fibers are sufficiently long and flexible they will entangle tending to form mats. Furthermore, the lignin residue in the fibers will help the formation of a self adhering cellulosic mat (Collier and Collier, 1993) and the paper matting character of the short fibers will also enhance adhesion.

A more uniform mat could be made from sugar cane fiber bundles using a textile needle punch process. In a needle punch process, a fibrous web is punched with a group of specially designed needles (Tortora and Collier, 1997). This process reorients the fibers and entangles them among each other giving some strength to the mat. But shorter fibers may result from additional mechanical treatment imposed prior to the needle punching. This method, nevertheless, enables mass production of the cellulosic mats from sugar cane rind fibers using standard textile industry machines, and is therefore relevant to commercial production of PU/Cellulosic fiber composites. However, it is important to determine the critical length and aspect ratio of the cellulosic fiber for PU composites, so the maximum acceptable degree of size reduction can be determined.

The simplest way to place the preformed mat in the mold is by putting several layers of the mat in the mold cavity (Macosko, 1989; Trevino et al., 1991). To prevent fluid channeling, mats must be cut to closely fit the edge of the cavity. The mat thickness prior to compression in the mold is usually several times that of the mold. Therefore, the friction force in the closed mold between the mold surface and the preform usually can hold the mat in place during mold filling with resin (Macosko, 1989; Trevino et al., 1991). A special placement device may be needed if the mat loading is low or if the mat has to be positioned at a specific place and does not fill the whole cavity.

2.6 Material and Product Characterization

Since the chemical formulation used in this research is a commercial PUU formulation, chemical properties of the resins were set by the supplier. Therefore, there is no significant chemical characterization needed. However, it is important to measure surface tension and contact angle properties of the resins for fiber wetting and mold filling studies. The most relevant characteristics of the composites to be identified in this work are: the bonding between the cellulosic fiber and the matrix and the mechanical properties of the composites.

2.6.1 Fiber-matrix Adhesion

Environmental scanning electron microscopy (ESEM) has been used to directly visualize the bonding between the core and the skin in fiber composites (Gao

et al., 1994). ESEM can be used to determine various phenomena in SRIM without requiring surface coating prior to examination (Collier and Collier, 1993). The adhesion between fiber and matrix can be studied qualitatively from the images of broken specimens using ESEM or scanning electron microscope (SEM).

In order to have good fiber-matrix adhesion, the resin should wet the fibers while it fills the mold cavity. Wettability of the fiber is related to the surface tension of the resin and surface energy of the fiber. Contact angles are determined by the surface tension of liquids and the surface energy of solids, which in turn controls the wetting of solids surface by liquids (Feldman and Locasse, 1994; Wu, 1982; Tadmor and Gogos, 1979). Since these physical properties are interrelated they can be measured using a single instrument, such as a dynamic tensiometer (Wu, 1982). Surface tension and contact angle measurement are based on force balances on a plate, fiber, or ring pulled out of the measured fluid, and are therefore very straightforward. The surface energy measurement requires measurement of contact angles and surface tension of different liquids on the measured solid (Feldman and Locasse, 1994). The solid surface energy is calculated using an equation of state that relates the contact angles to the surface tensions (Feldman and Locasse, 1994; Wu, 1982).

2.6.2 Mechanical Properties

The ultimate goal of the composite formation in this work is to improve the mechanical properties of the PU matrix, and these properties can be indirect

measures of adhesion (Collier and Collier, 1993). The tensile properties of the composites can be tested using standard instruments such as an Instron tester and according to ASTM D638 standard (Progelhof and Throne, 1993; Peebles, 1994; Peebles and Corripio, 1995). For load bearing composite applications, bending property characterization is also important; the three point bending test is widely used for this purpose and the most commonly referred bending test standard for plastic specimens is ASTM D790 (Progelhof and Throne, 1993). Methods for direct measurement of matrix-fiber adhesion are available. An example of those is what is called the single fiber fragmentation (SFF) test (Hedenberg and Gatenholm, 1995; Matthews and Rawlings, 1994). In this method, a tensile test is performed on a thin sheet (dog bone shaped) reinforced with a single oriented fiber until the reinforcing fiber fails. From the distribution of the length of the broken fiber, the adhesion force can be estimated (Hedenberg and Gatenholm, 1995). However for SRIM composites, the sample preparation for this test is very difficult. Therefore, this last method was not utilized in this work.

CHAPTER 3

EXPERIMENTAL

3.1 RIM Machine

The RIM machine used in this research is a Hi-Tech lab scale RIM machine series 114. The machine is capable of delivering two streams into the mixing head with a mass flowrate range of 0.9-6.8 kg/min for each stream and a maximum shot size of 300 gram for each stream. The machine is equipped with a control board that is connectable to a PC. Certain operating parameters such as the temperature set points for the chemical tanks and the timing parameters can be set through the control board or through the PC. This configuration also enables data collection from the RIM operation. For this purpose an extra input board and several input cards have been added to the system during the course of this work and the previous work by Peebles (1993). Using this set up, two linear pressure transducers and up to four thermocouples can be connected to the data collection system. This is useful for in mold pressure profile studies and adiabatic temperature rise studies for kinetic modeling. A more complete description of the control aspect of the machine can be found in Peebles' dissertation (1994).

3.2 The Mold

Two types of molds have been used in this study. The first type allows the preparation of two dog bone shaped specimens conforming to ASTM D638 for standard tensile testing of plastic materials. This mold was constructed from a mild

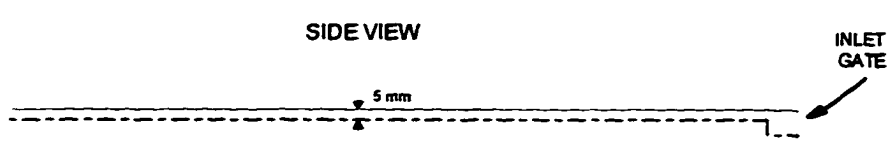
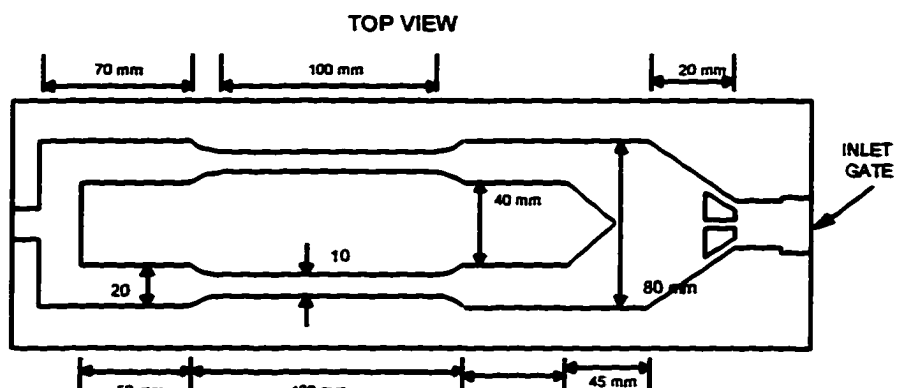
stainless steel. The second mold is an aluminum mold. It was designed for in-mold pressure and temperature measurement necessary for mat characterization or kinetic studies rather than for mechanical testing sample preparation. Several pressure transducer wells were drilled on the top plate of the second mold, whereas two inlet ports were drilled on the bottom part of the mold; one inlet is closed while the other is in use. This second mold will produce a plastic sheet from which samples for bending or tensile testing can be cut. The schematic diagrams and dimensions of the molds are depicted in Figure 3.1.

3.3 Material

3.3.1 Chemical Formulation

Two types of commercial chemical formulations were used in this study, namely: Spectrim® 50 and Spectrim® 310; both from Dow Chemical. The approximate chemical content of these formulations is shown in Table 2.2. Other pertinent properties are shown in Table 3.1. Spectrim® 50 is formulated to form an elastomeric PUU designed for reaction injection molding, therefore it has a relatively high viscosity and a low gel time. Spectrim® 310 was specially designed for the SRIM process used in manufacturing automobile facia. One-tenth percent by weight of organic tin catalyst (Fomrez® UL-38) was added to the B component of Spectrim® 310 prior to the RIM experiment. Fomrez® contains 100 % alkyltin

Bottom Part of Mold 1



Bottom Part of Mold 2

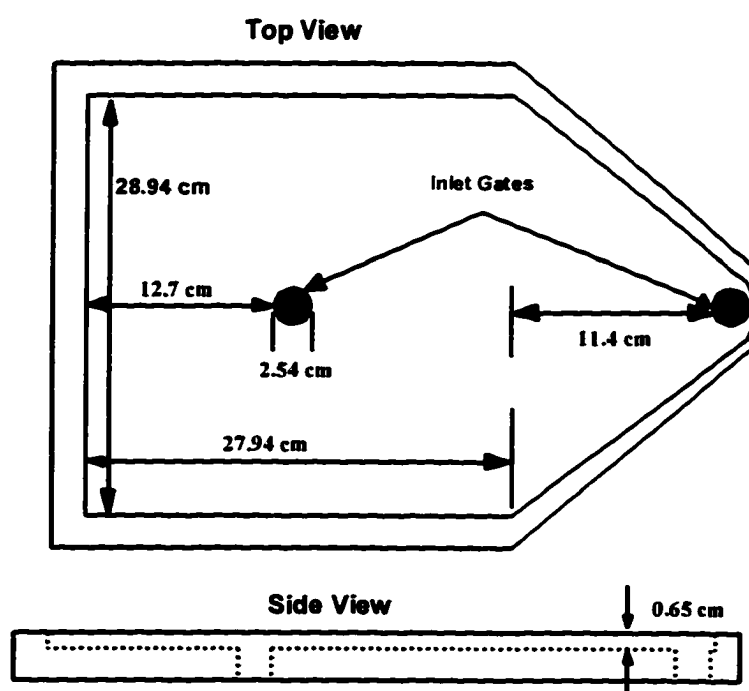


Figure 3.1 The RIM Molds

Table 3.1 Some Important Properties of The Resins

	Spectrim® 50	Spectrim® 310
<u>Component A:</u>		
-NCO Equivalent weight	234.6	134
Density at 25°C g/cm³	1.1516	1.2
Viscosity at 25°C (cp)	1323	180
<u>Component B:</u>		
Equivalent weight	233.9	113
Density at 25°C g/cm³	1.0311	1.053
Viscosity at 25°C (cp)	1371	430
Gel Time (sec)	order of second	10-12

carboxylate. Spectrim 50 has an internal mold release agent incorporated into component B. Mold Wiz F-57® a commercial external mold release agent, was also used to improve demolding. F-57® is a generic mold release agent for polyester, epoxies, phenolics and urethane elastomer molds. The “active” compound in this mold release is a buffered fluorocarbon dispersed in a volatile solvent. No internal mold release agent was added to Spectrim® 310, but a specialty external mold release agent (Chemtrend® RCT 101) was used. RCT 101 composition is 85-95 % hydrocarbon naphtha and 5-15 % wax blend.

3.3.2 Preformed Mats

Three different fiber sources were used: cotton fibers, sugar cane rind fibers, and kenaf fibers. The cotton fiber mats were used in the form of woven and non-woven mats. A commercial cheesecloth of 100 % cotton and a 100 % cotton needle punched mat were used. The cheesecloth is a woven textile fabric. In the composite field, the term mat includes fabrics. One batch of sugar cane rind fiber was prepared, according to the recommendation of Elsunni and Collier (1996), by partial delignification at 135 °C using 0.2 NaOH solution for one hour and then followed by a steam explosion. A second batch of the sugar cane rind fiber was prepared by delignification with higher normality NaOH (0.5 N) at 135 °C, and a third one was delignified with 1.0 N NaOH at atmospheric pressure. All batches were then sprayed with a water jet. Preform mats were prepared from these fibers by water laying on a screen. Kenaf fibers were used in the form of raw fibers (mechanically separated from the pith) and in the form of treated fibers prepared by Romanoschi et al. (1997), in a manner similar to the sugar cane fibers. The raw kenaf fibers were used in the form of water laid mats, while the treated kenaf fibers were used in the form of needle punched mats. All the needle punched mats were prepared by Dr. Wei Ying Tao of USDA SRCC in New Orleans.

For comparison purposes some composites were formed using fiber glass mats. The fiber glass was a commercial grade of E-glass formed into random mats. These mats are used commercially with Spectrim® 310.

3.4 Experimental Procedures

3.4.1 Molding Experiment

The mold cavity surfaces were cleaned first and sprayed with an appropriate external mold release agent. The mats were cut in the shape of the mold cavity using a fabric roller cutter and then laid into the mold cavity. Usually more than one layer was needed to obtain a desirable fiber content in the composites. The mold was then closed by tightening the bolts that clamped the bottom and the top parts of the mold together. For data collection, optional temperature and/or pressure transducers can be connected to the top part of the mold. A calculated amount of resin was then injected into the mold using the RIM machine. After a sufficient time was allowed for the thermosetting material to cure, the mold was opened and the composite was removed from the mold for fiber content determination and mechanical testing preparations.

The sample fiber content was determined by dividing the mat weight per unit area by the composite weight per unit area. To do so, several samples were cut from a molded sheet and their area and weight determined. The fiber content (weight fraction) is given by:

$$\omega_f = \frac{\frac{W_m}{A_m}}{\frac{W_c}{A_c}} \quad (3.1)$$

where ω_f is fiber weight fraction in the composite sample. W and A are weight and area, respectively. Subscript m refers to the preform mat and c to the composite sample.

3.4.2 Mechanical Testing

Tensile and three point bending tests were performed using an Instron 4301 tester. The tensile tests were done according to ASTM D638 and the bending tests were according to ASTM D790. Two specimens for tensile tests can be obtained from each shot using mold 1 (shown in Figure 3.1). Several samples for tensile and bending test could also be cut from a sheet molded using the second mold. The samples were then machined using Tensilekut® (manufactured by Sieburg Industries, Inc.) to conform with ASTM D638 or ASTM D790 standard. The sample thicknesses are equal to the mold cavity thicknesses (i.e. 0.5 cm for the first mold and 0.65 cm for the second mold). For bending tests, the samples are machined into 1.8 cm x 15 cm rectangular shapes. The shape and dimension of tensile test samples are given in Figure 3.2. These samples can be obtained directly from the first mold or by machining samples cut from a sheet prepared using the second mold.

The tensile test was emphasized on samples prepared from Spectrim® 50. The bending test is more relevant for Spectrim® MM 310 because this material was designed for load bearing applications. Therefore bending tests were done only for samples prepared from this later resin.

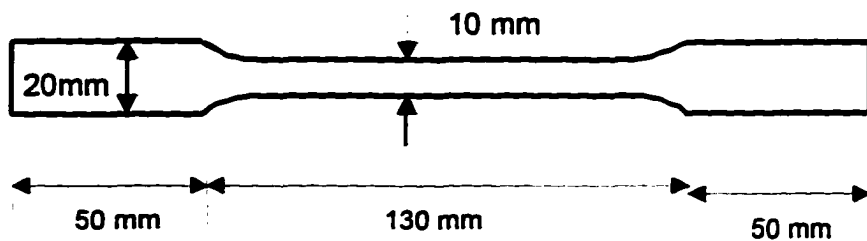


Figure 3.2 Tensile Test Specimen Dimension

3.4.3 Kinetic Study

Kinetic studies were performed only for Spectrim® 310. A kinetic study for Spectrim® 35 was done previously by Peebles and Corripio (1995). Since the Spectrim® 50 composition is very similar to Spectrim® 35, its kinetic properties should not be far different from that of Spectrim® 35. A thermal method was used to study the kinetics of the polyurethane reaction. Because the reaction is very fast, it is difficult to use the differential scanning calorimeter (DSC) to study the kinetics without losing significant information. Therefore the adiabatic temperature rise method was used in this study. Since the catalyst content was so low (manufacturer recommendation is between 0.05-0.25 %) the experiment with catalyst content variation was not performed since this would require a very tedious cleaning of the machine. All experiments with Spectrim 310 were performed with a catalyst content of 0.1 % by weight of the B component (polyol).

The equipment set-up for the kinetic measurements was similar to the one used by S.M. Peebles and A.B. Corripio (1996) except that the shot was made into an insulated container. The temperature profile was read using a thermocouple that was inserted into an insulated plastic container and then recorded using the data acquisition system of the Hi-Tech RIM machine. The size of the shot was set to about 150 grams with the chemical mol ratio equal to 1 . A well insulated cup with a thermocouple in it was placed directly in the front of the mixing head. For each shot, temperature versus time data were collected and saved into a PC file. The temperature data were recorded about three times in every second. The data were then fitted using an Arrhenius type empirical equation.

3.4.4 Other Experimental Procedures

Surface tensions of the resins and the mold release agents were determined with the plate method using a Kruss K14 Surface Tensiometer. The surface energies of the fibers were also determined from contact angle measurement using the Kruss K14. From contact angle measurements using two liquids, the surface energy of the fiber was determined using a harmonic average (Wu, 1982). To determine contact angles between the fibers and the liquid, the perimeters of the fibers need to be known. The perimeters of the fibers were determined by measuring the force needed to compensate for the force from the surface tension of fully wetting fluid (hexane was used for this purpose). This measurement was also done using the Kruss K14. The fiber perimeter can be calculated from:

$$P_f = \frac{F}{\sigma \cos(\theta)} \quad (3.2)$$

where σ is the wetting liquid surface tension and θ is the contact angle which is zero for a fully wetting liquid. F is the force to balance the surface tension force.

The moisture content of the fibers was determined using the thermal gravimetric analysis (TGA). The mats were usually kept in oven at 100 °C for at least two hours prior the RIM process, and the same preparation was used before TGA analysis. To study the moisture take up by the mat during the molding preparation, several samples were also kept at room temperature after the oven conditioning for at least 45 minutes and then analyzed with TGA.

To visualize fiber-matrix adhesion, several samples were cut from broken specimens after the mechanical testing. The sample were then analyzed with scanning electron microscopy (SEM).

CHAPTER 4

RIM EXPERIMENTAL RESULTS AND DISCUSSIONS

4.1 Effect of Fiber Loading

Figure 4.1 shows the effects of fiber loading on tensile properties of PUU cellulosic composites. The figure shows that the tensile strength and Young's modulus of the PUU-cheesecloth composites are doubled compared to those of neat PUU with only 7 and 5 % fiber loading respectively. Similar trends were observed for chemical ratios between 0.77 - 1.11. Cellulosic fiber tensile properties are so dominant that the plots of tensile strength, Young's Modulus and strain at break versus fiber loading are close to each other for chemical ratios between 0.77-1.11. This is due to the effective load transfer between the matrix and the reinforcing fiber. Similar trends could be observed from the plot of the reduced tensile strength (the composite tensile strength divided by the neat matrix tensile strength) and reduced Young's modulus versus fiber loading for PUU/cellulosic composites prepared with fibers from various sources and slightly different chemical formulation as shown in Figure 4.2 (Collier et. al., 1996). PUU/cellulosic composites were prepared from various sources of cellulosic fibers in the form of woven, needle punched, and water laid mats. The SRRC kenaf fiber was in the form of needle punched mat, while LSU kenaf, sugar cane, and wood fibers were in the form of water laid mats. The matrix was either Spectrim® 50 or Spectrim® 35.

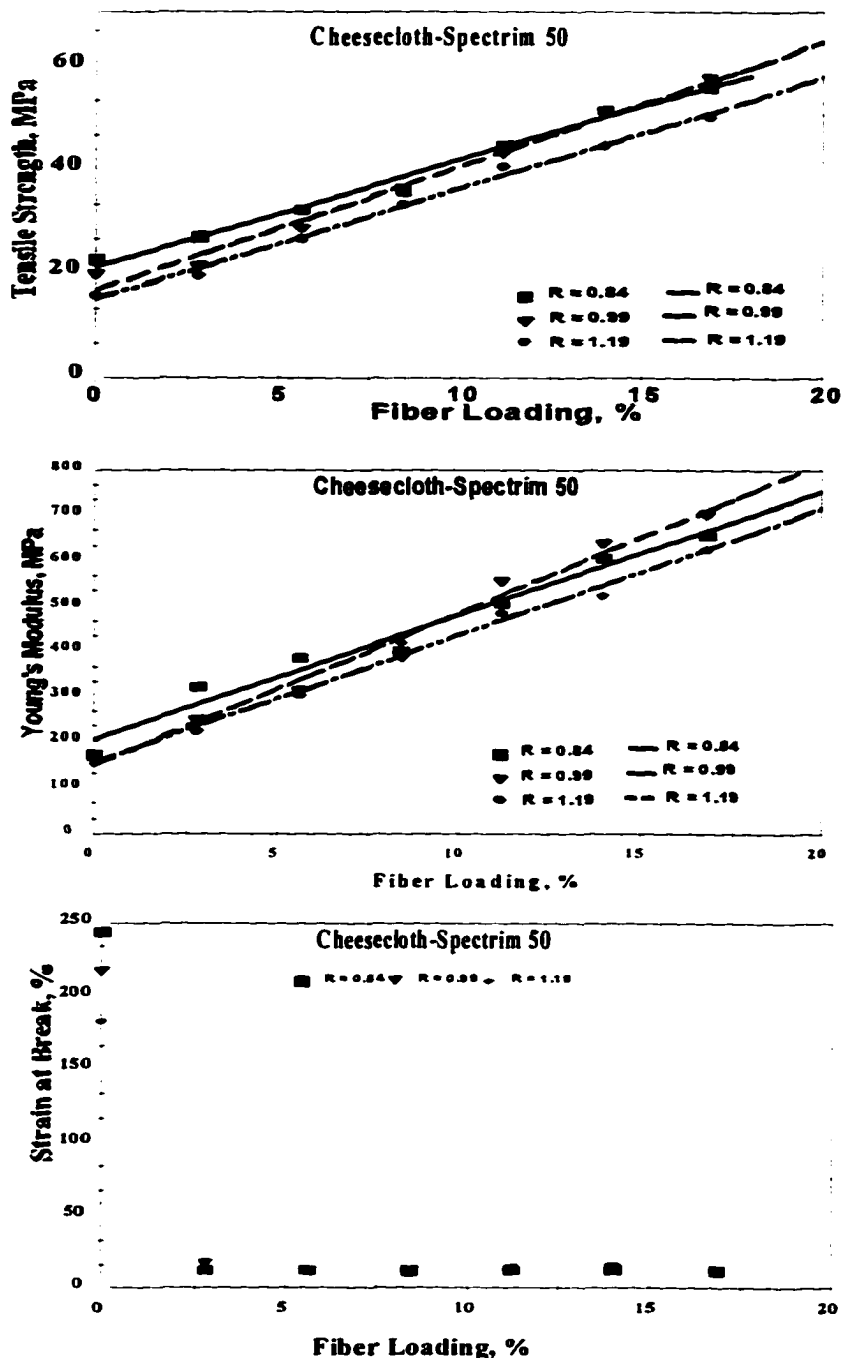


Figure 4.1 Effects of Fiber Loading on Tensile Properties of Spectrim® 50/Cheesecloth Composites for Various Chemical Ratio

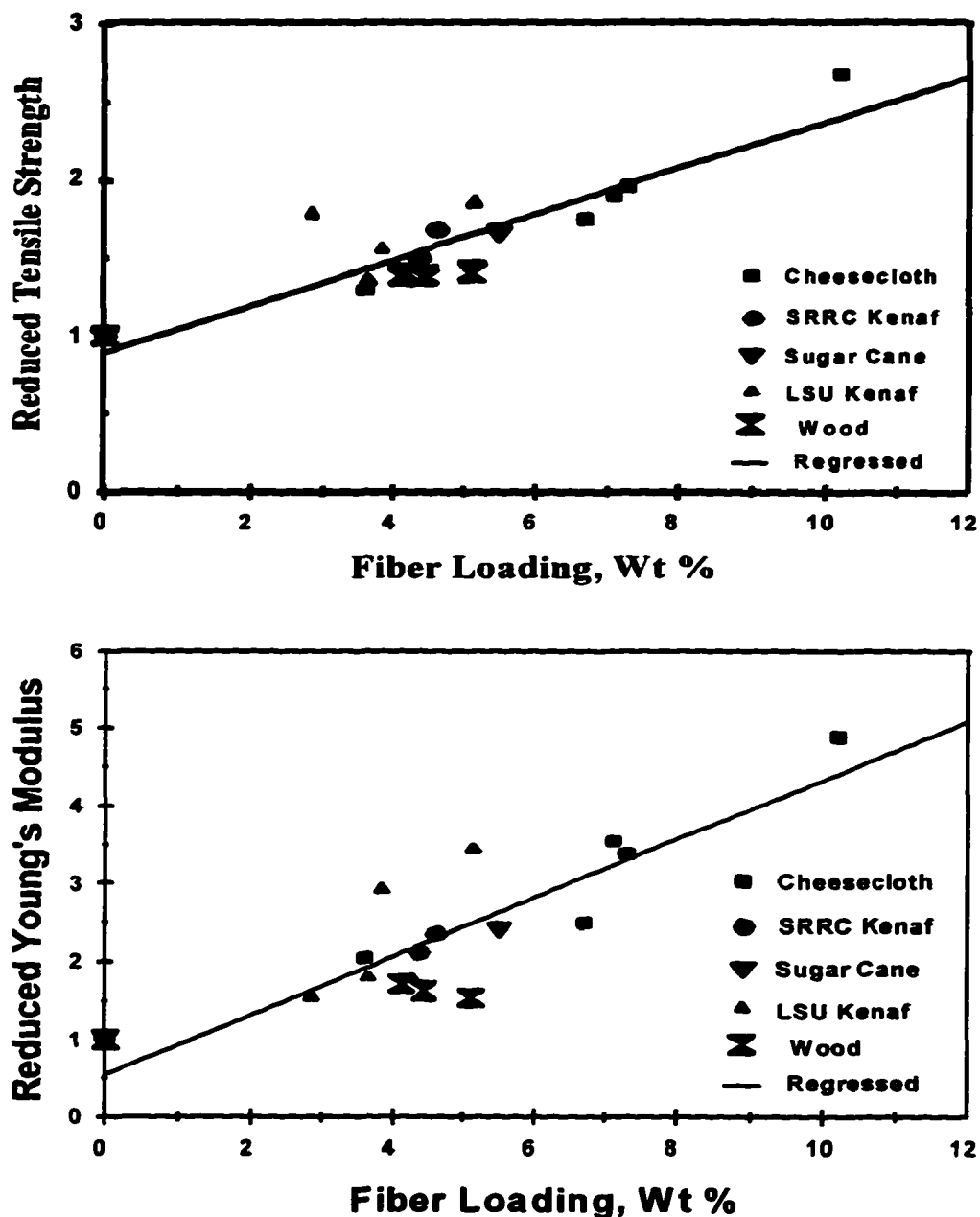


Figure 4.2 Effect of Fiber Properties on The Mechanical Properties
(From: Collier, et. al., 1996)

Figure 4.3 and 4.4 show the effects of fiber loading on tensile and bending properties of PU/cellulosic fiber composites. Spectrim MM 310 is a polycarbamate (polyurethane) formulation designed for load bearing applications. Figure 4.3 shows

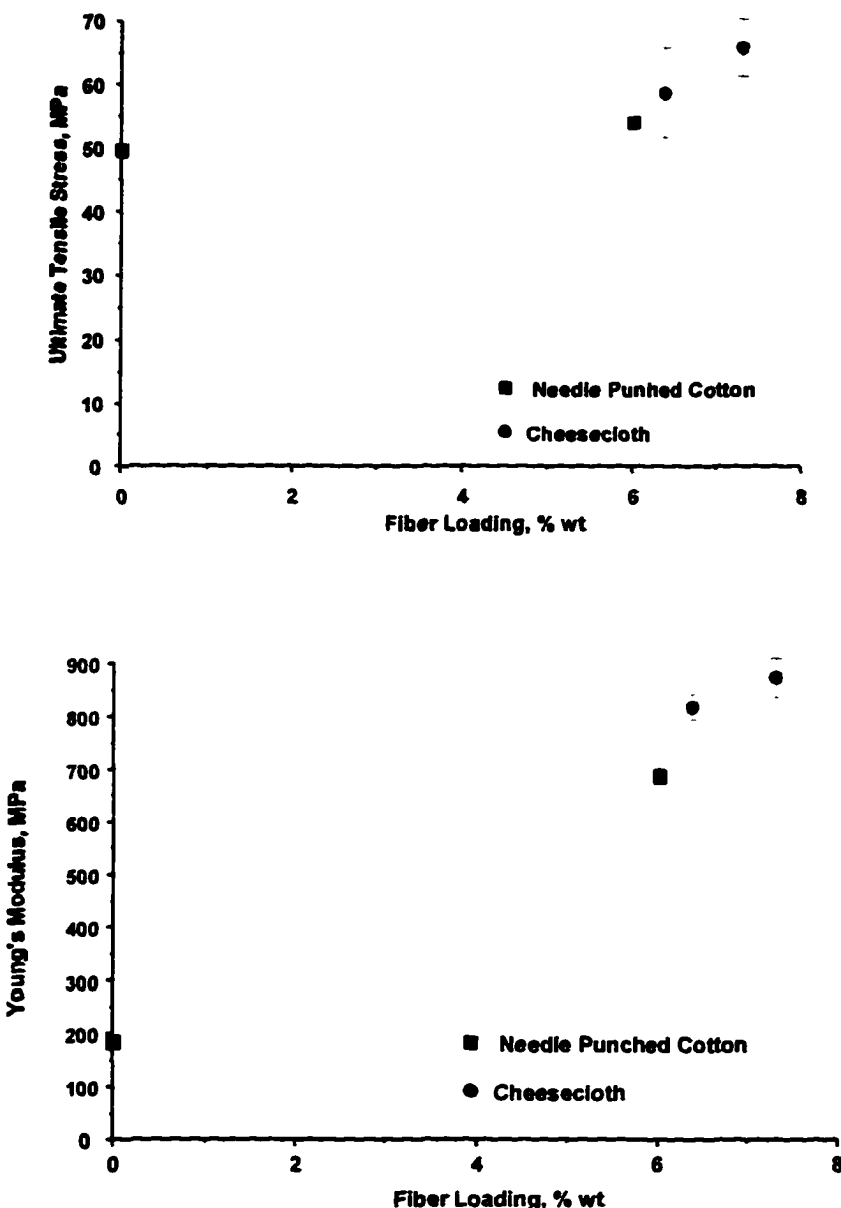


Figure 4.3 Effect of Fiber Loading on Tensile Properties of Spectrim MM 310/cotton Composites for Chemical Ratio = 1

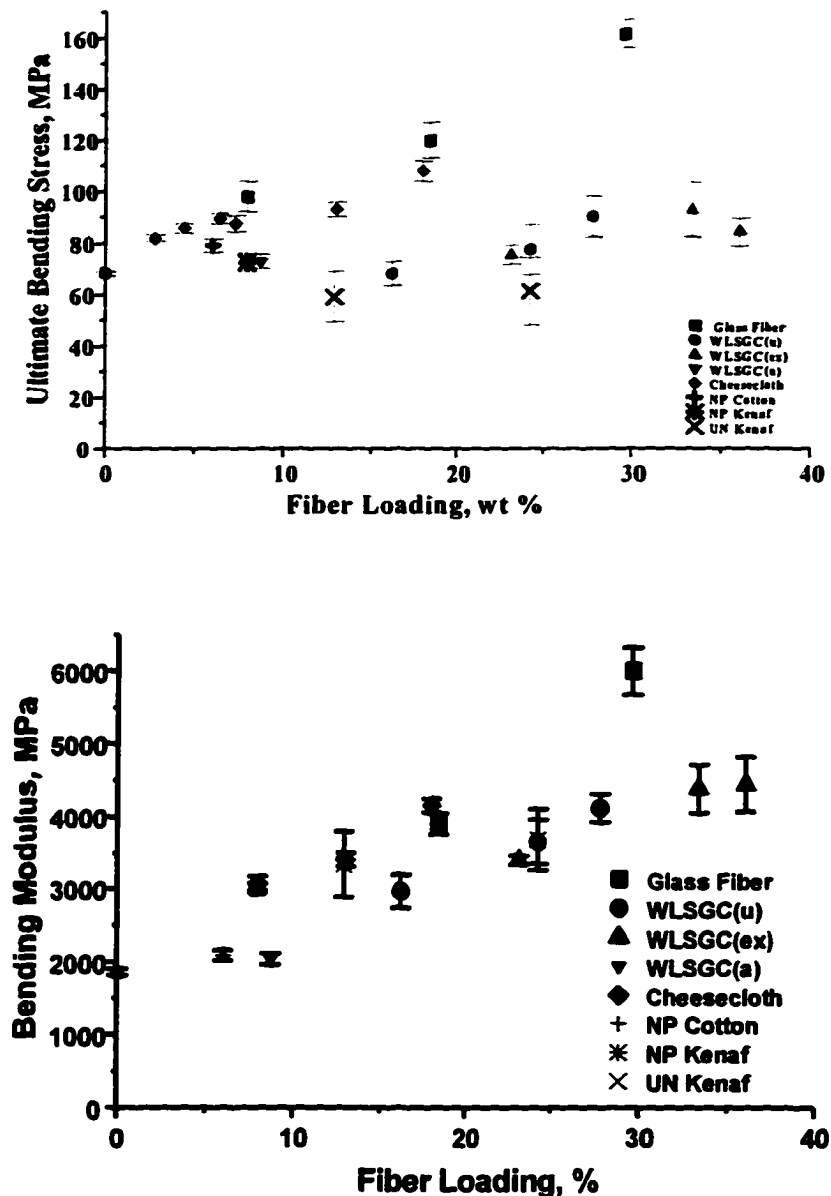


Figure 4.4 Effect of Fiber Loading on Bending Properties of Spectrim MM 310/Cellulosic Composites for Chemical Ratio = 1

that both woven (cheesecloth) and non woven (needle punched) cotton mats give 300 % improvement in Young's modulus and 30 % improvement in tensile strength

with 7 % fiber loading. Since the matrix strength of Spectrim MM 310 is already relatively high, its contribution to the composite mechanical properties is significant. In this case, fiber orientation starts playing a significant role. This is shown by the more efficient reinforcement performed by cheesecloth (bi-directional oriented) compared to the performance of the needle punched cotton mat (more randomly orientated). This assertion is supported by bending test results shown in Figure 4.4. Needle punched (NP) cotton samples have slightly lower bending strength and bending modulus compared to cheesecloth samples. The cheesecloth mats performed comparably to the fiber glass although the fiber glass has a much higher tensile strength. The fiber glass was in a random non-woven mat. Samples with other cellulosic fibers, however, have significantly lower bending strengths compared to the samples with cotton mats. This may be due to the weaker cohesive forces between the fibers in the bundles. It is important to note that by partial delignification, the lignin content inside the fiber bundles is reduced significantly. This may also weaken the cohesive bond between the fibers.

Figure 4.4 indicates that the mechanical strengths of the composites with water laid sugar cane (WLSGC) mats increase with the fiber loading. These fibers were prepared with three different treatment conditions: high temperature partial delignification and steam explosion (ex), high temperature partial delignification without steam explosion (u) and atmospheric pressure partial delignification without steam explosion (a). Samples prepared from untreated (UN) kenaf fibers have lower

bending strength compared to the neat PU while the sample with treated kenaf fibers in the form of NP mat have at least the same bending strength as neat PU. This may show that the bonds between the fibers inside the bundles are weaker than the matrix-fiber bonds, and therefore fiber treatment is important. The maximum fiber loading used in this work was approximately 50 % by weight. At this level of fiber loading, closing the aluminum mold by simply tightening the bolts was found to be insufficient. The clamping force needed to close the second mold was 15 ton force and this is the maximum capacity of hydraulic press available for this work. Higher fiber loading will give additional advantages in addition to mechanical properties improvement, such as lowering the material cost. This is because the prices of the cellulosic fibers used in this work are lower than the price of the resin. An improved clamping mechanism is clearly necessary in order to achieve higher fiber loadings.

4.2 Effect of Chemical Ratio

The effect of chemical ratio is very apparent for high fiber loading and high excess isocyanate as shown in Figure 4.5. For higher levels of excess isocyanate, the excess isocyanate will attack the urethane and urea bonds and form chemical cross links. This trend is shown by the increased tensile strength for neat PUU with excess isocyanate. This effect, however, levels off at excess isocyanate about 20 % (chemical ratio = 0.8). The leveling off trend is not observed for higher cellulosic fiber loading. The strengthening effect of excess isocyanate became more apparent for higher fiber loading since there are more hydroxyl groups available for

chemical bonds between the matrix and the fibers. This fact affirms the FTIR study that showed significant reaction of isocyanates and cellulosic fiber hydroxyls. For much higher cellulosic fiber loading, the amount of hydroxyl groups in the fiber should be taken into account in the chemical ratio calculation.

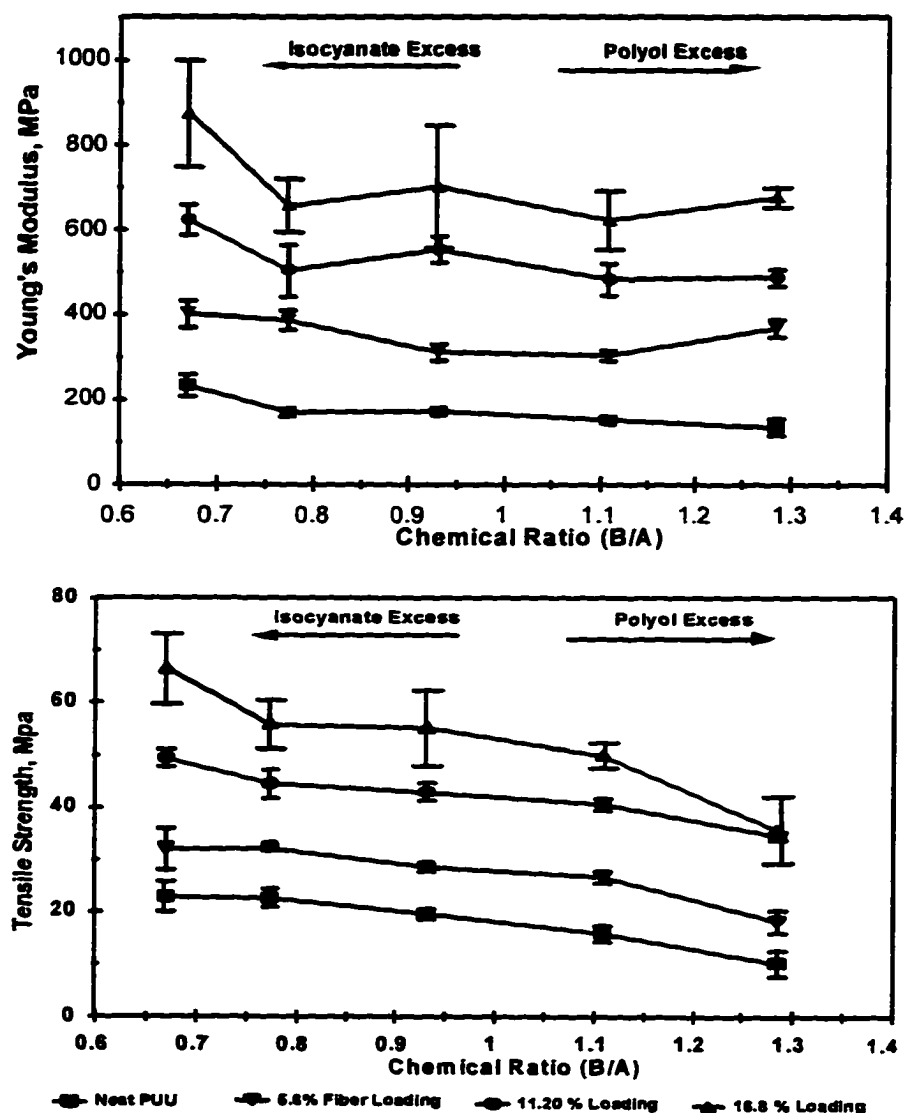


Figure 4.5 Effect of Chemical Ratio on Tensile Properties of Spectrim 50/Cheesecloth Composites

Another factor that may shift the chemical ratio effect is the moisture content of cellulosic fibers. Water is very reactive to isocyanate (Macosko, 1989). TGA analyses of some of the cellulosic fibers used in this work are shown in Table 4.1. Of all the fibers, cotton has the lowest moisture content at room temperature. Heating the fibers at 100 °C for two hours reduced the moisture content of the fibers very slightly. The effect of fiber moisture content on the composite mechanical properties was not studied in this work.

Table 4.1 TGA Analysis Result

Fiber	% Moisture (wt/wt)
Cotton (room condition)	7.9
Kenaf (room condition)	11.7
Kenaf (oven dried)	9.4
Sugar cane (room condition)	11.3
Sugar cane (oven dried)	7.9

4.3 Resin-Fiber Adhesion

Table 4.2 and 4.3 show surface tension (σ) and surface energy (γ) measurements for some of the materials used in the experiments. Superscripts d and p in Table 4.3 refer to dispersion and polar component of the surface energy, respectively. The surface energies of the mold release agents were estimated by measuring contact angles of a plate coated with the mold release agents with respect to water and methylene iodide. Since the solubility of mold release compounds (CT-101 and F-57) in both liquids was not studied in detail other than by visual

observation, the values in Table 4.3. serve only as estimates. The calculated dispersive component of sugar-cane fiber surface energy was slightly negative. This may be due to inaccuracy of the perimeter determination because the diameter of the fiber is not uniform. The measured surface energy value, however, shows that sugar cane fibers are polar. The plus sign next to the surface energy value of sugar cane fiber in Table 4.3 is to indicate that the total surface energy of the fiber is more than the listed value if the dispersion component is included.

Table 4.2 Surface Tension Properties of The Resins and Mold Release Agents

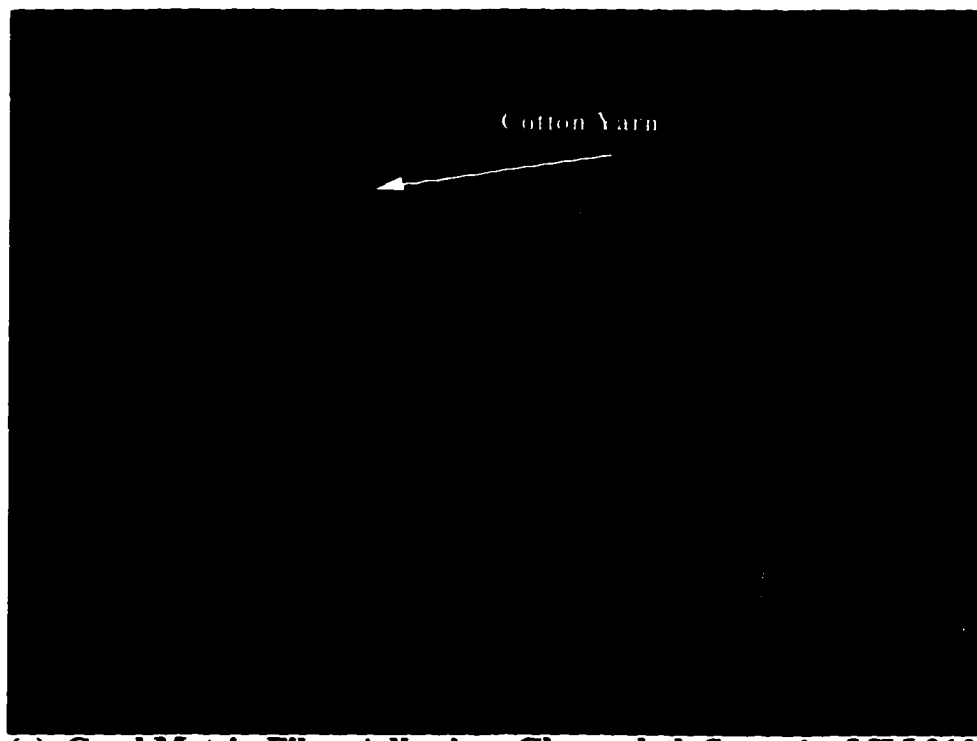
Liquid	σ , mN/m
Spectrim MM 310 A (Isocyanate)	40.55
Spectrim MM 310 B (Polyol)	34.5
Mold Release CT-101	26.4

Table 4.3 Estimated Surface Energy

Compound	γ^d (mN/m)	γ^P (mN/m)	γ (mN/m)
CT-101	25.6	9.9	35.5
F-57	25.1	14.3	39.4
Sugar Cane Fiber	close to zero	49.8	49.8+

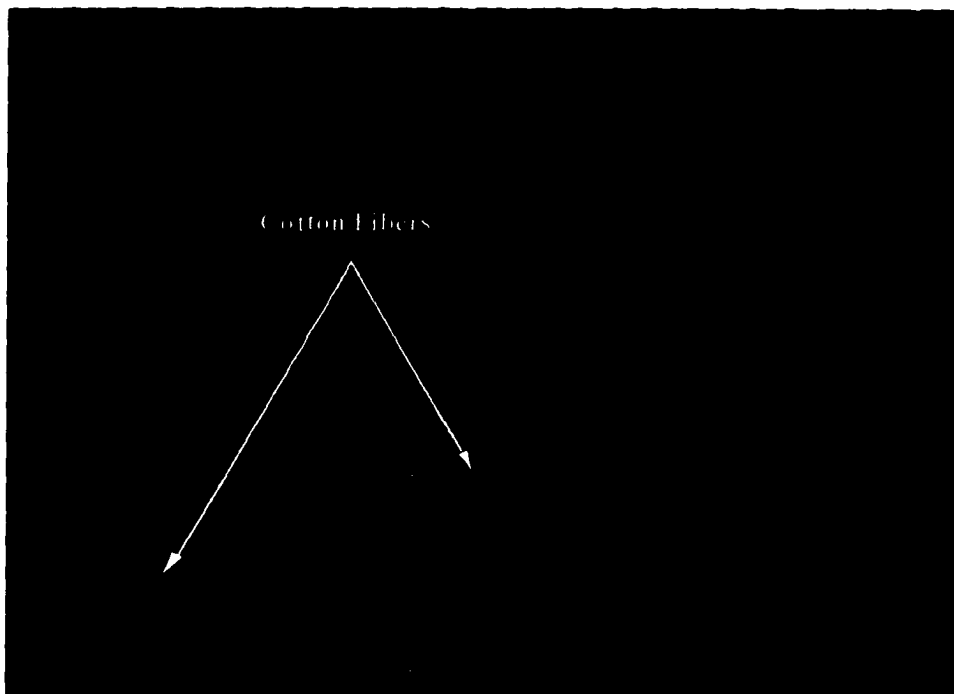
Due to the chemical properties of cellulosic fibers, good fiber-matrix adhesion can be expected to exist in the composite. This is shown by SEM

micrographs in Figure 4.6. Almost all samples with cotton fibers appeared to break because either the tensile strength of the fiber or the matrix-fiber adhesion strength was exceeded. As shown in Figure 4.6 (a) and (b), only very short cotton fibers (or bundles) extended beyond the broken surface contrary to the samples with the fiber glass where the fibers extended much farther beyond the broken surface (Figure 4.6(c)) because of much weaker matrix-glass fiber adhesion.

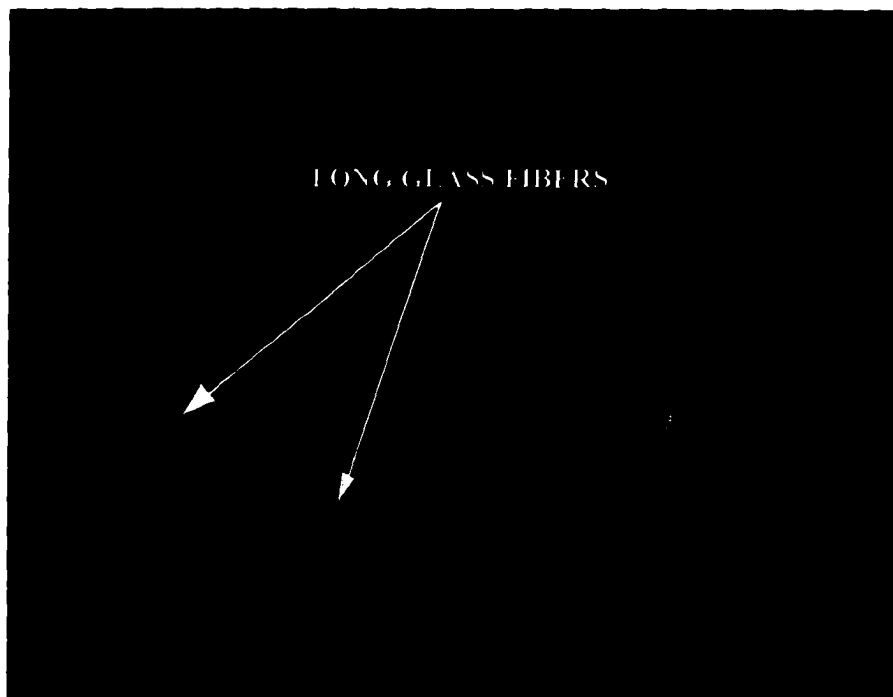


(a). Good Matrix-Fiber Adhesion: Cheesecloth-Spectrum MM 310

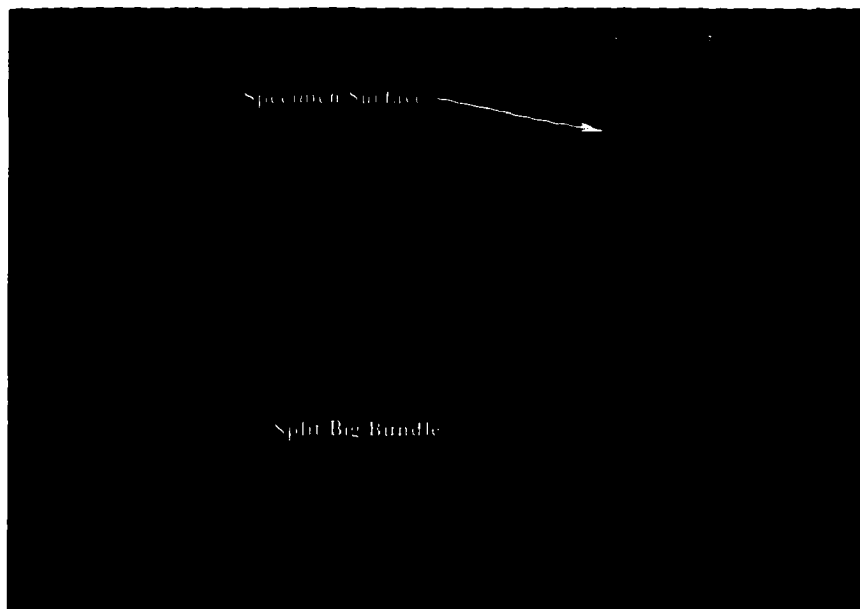
Figure 4.6 SEM Micrographs of Broken Parts of The Samples



(b). Good Matrix-Fiber Adhesion: Needle Punched Cotton-Spectrum MM



(c). Matrix-Fiber Adhesion Failure: Fiber-Glass/Spectrum MM 310



(d). Cohesion Failure inside a Big Fiber Bundle: Sugar Cane Rind/Spectrim MM 310

Figure 4.6 (a) also shows that micro voids are present especially in the vicinity of fiber-matrix interface. When compressed nitrogen is used in the RIM operation as a gas blanket for the chemical and as "blowing agent" to compensate for the volume shrinkage during the reaction, the present of microvoids is unavoidable. Under room conditions, moisture is always present inside the cellulosic fiber. This moisture can react with isocyanate and release carbon dioxide that can cause micro bubble formation. The macrovoids however may originate from air trapped during mold filling and this should be taken into consideration since this may cause a detrimental effect on the mechanical properties of the composites. The number of voids on the specimen surfaces seems also to be influenced by the mold release

agent used. It was found that CT-101 did a better job than F-57, although both have similar surface energy.

Figure 4.6(d) shows the micrograph for the broken surface of sugar-cane rind/PU samples. Most cracks in the samples with sugar cane and kenaf fibers were initiated at the surface near large fiber bundles. This problem may be overcome by properly adjusting the operating conditions for delignification and steam explosion. The best conditions should be able to reduce the diameter of large fiber bundles, thereby lowering the variability of the fiber diameter while preserving the average fiber aspect ratios. Higher normality of NaOH during delignification tends to give smaller diameter fibers with shorter lengths. Lower normality will give larger cross section, long fiber bundles. Much higher normality than used, however, will pulp the fiber and give low permeability mats that pose practical difficulties during molding. As shown by Figure 4.7, the injection pressure for sugarcane fibers treated with 1.0 N solution (Sgc7) is much higher than that of lower normality treated fiber (Sgc8 and Sgc9).

4.4 Kinetic Study

A typical recorded temperature profile from a shot is shown in Figure 4.8. The temperature versus time data could be corrected for heat loss before kinetic model fitting was performed. The temperature correction equation is a lumped heat balance on the whole system, i.e. the container, the reacted material and

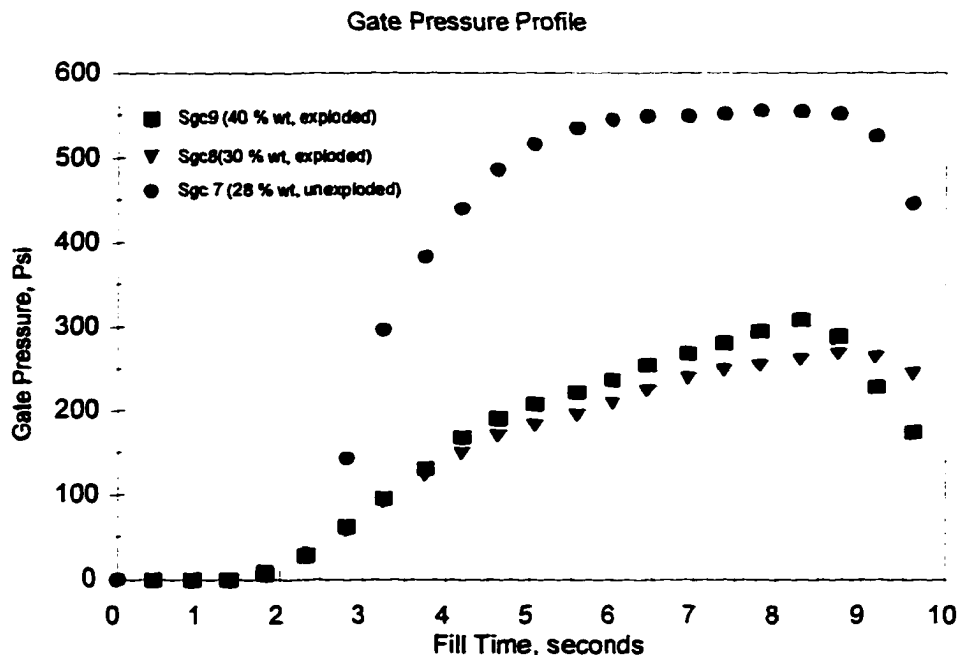


Figure 4.7. Gate Pressure Profiles for 27.94 cm x 28.575 cm x 0.65 cm Center Gated Rectangular Mold

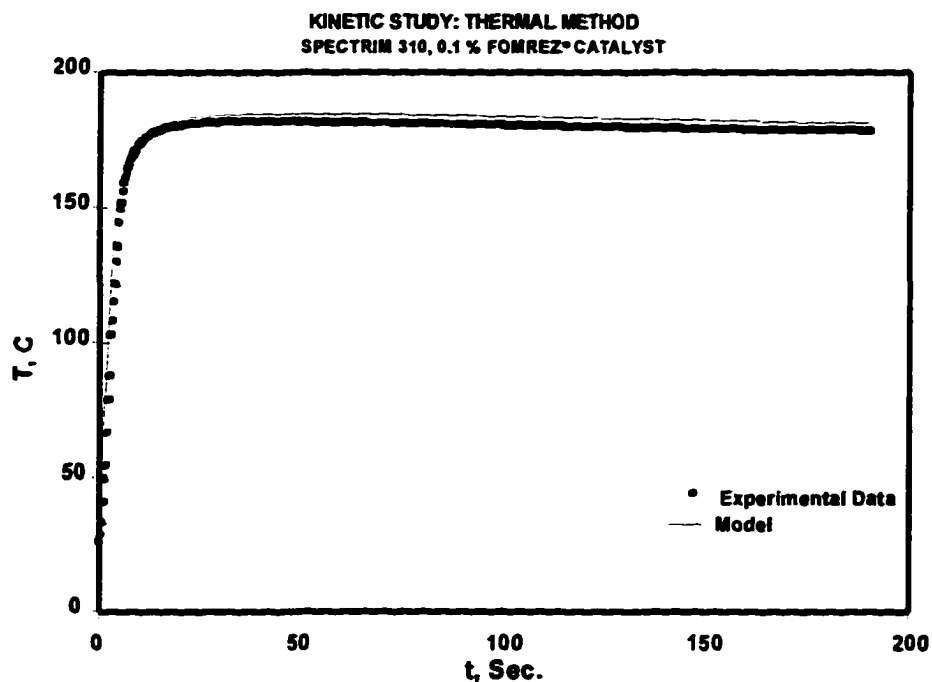


Figure 4.8 Experimental Temperature and The Kinetic Model Prediction

the thermocouple. When the reaction has been completed, the heat balance on the system can be rearranged as:

$$mC_p \frac{dT}{dt} = UA(T - T_a) \quad (4.1)$$

where A is the effective heat transfer area, m is the effective mass of the system, C_p is the average heat capacity of the system, and U is the heat transfer coefficient from the system to the surrounding air that has the temperature T_a . Equation 4.1 can be integrated from temperature T_0 at time t_0 to temperature T at time t to get temperature profile as function of time:

$$\ln\left(\frac{T - T_a}{T_0 - T_a}\right) = -m_h(t - t_0) \quad (4.2)$$

where m_h is the lumped parameters in equation 4.1, that is:

$$m_h = \frac{UA}{mC_p} \quad (4.3)$$

The parameter m_h can be obtained by fitting the temperature profile of the system where the reaction is already completed. The fitted value of m_h from the data in Figure 4.7 is small ($0.00022 \text{ }^{\circ}\text{C/sec}$). The heat loss effect therefore may be neglected in the kinetic study. In the case where the heat loss is significant, then the corrected temperature time gradient can be calculated:

$$\frac{dT_c}{dt} = \frac{dT_{ex}}{dt} + m_h(T_{ex} - T_0) \quad (4.4)$$

where T_c is the corrected temperature profile (adiabatic temperature profile) and T_{ex} is the experimental temperature profile. Equation 4.4 can be integrated

numerically. Since the experimental temperature data curve is relatively smooth, an Euler method of integration on a spread sheet is sufficient to obtain a corrected temperature profile from equation 4.4.

The kinetic model can be fitted for the whole range of the temperature profile by including the heat loss effect. Assuming that all the physical properties are constant and the reaction goes to completion, the partial conversion can be expressed as:

$$\alpha = \frac{T - T_0}{\Delta T_{\max}} \quad (4.5)$$

where T_0 is the initial temperature of the system, and ΔT_{\max} is the adiabatic temperature rise of the chemical system.

The data was fitted using a widely used empirical equation for polyurethane systems (Macosko, 1989; Lin et al., 1993) that can be written as:

$$\frac{d\alpha}{dt} = A e^{\frac{E}{kT}} (1 - \alpha)^b \quad (4.6)$$

Substituting equation (4.5) into equation (4.6) we obtain the final equation:

$$\frac{d(T - T_0)}{dt} = \Delta T_{\max} A e^{\frac{E}{kT}} \left(1 - \frac{T - T_0}{\Delta T_{\max}}\right)^b \quad (4.7)$$

Temperature T in equation 4.7 can be either the measured temperature or the corrected temperature, dependent on whether or not the heat loss is negligible. The parameters A , E , ΔT_{\max} , and b were obtained from the curve fitting procedure on a spreadsheet (Origin). The specific heat of reaction ΔH (cal/gram of mixture) can be

obtained from:

$$\Delta H = \Delta T_{\max} C_p \quad (4.8)$$

where C_p is the mixture specific heat [cal/(g °K)].

An example of a typical result is given in Figure 4.8 for the temperature plot for 0.1 % catalyst content (w/w % of polyol stream). The figure shows that the empirical equation fits the experimental data reasonably well. The experimental values of temperature in Figure 4.8 were slightly lower than the predicted values. The slight difference may be caused by the fact that the initial measured temperature was lower than the actual initial temperature (the temperature of the thermocouple tip was lower than the initial temperature of the chemical). The fitted empirical constants for the kinetic model for 0.1 % catalyst are:

$$\Delta T_{\max} = 149.24 \text{ } ^\circ\text{C}; A = 455.097 \text{ sec}^{-1}; E = 4900.001 \text{ cal/(gmole } ^\circ\text{K}); b = 2.03.$$

The data in Figure 4.8 can also be plotted as partial conversion versus time as shown in Figure 4.9. The rate of reaction is second order with respect to the partial conversion. Figure 4.9 shows that the adiabatic reaction reaches more than 95 % conversion in 10 seconds. According to the manufacturer recommendation, the in mold gel time for a heated mold (60°C) is about 10-12 seconds. For cross-linked PU systems, 70 % conversion is considered the gel points (Macosko, 1989). Therefore, the operating temperature should be designed properly for a specific mold dimension to avoid gelling before the completion of the mold filling.

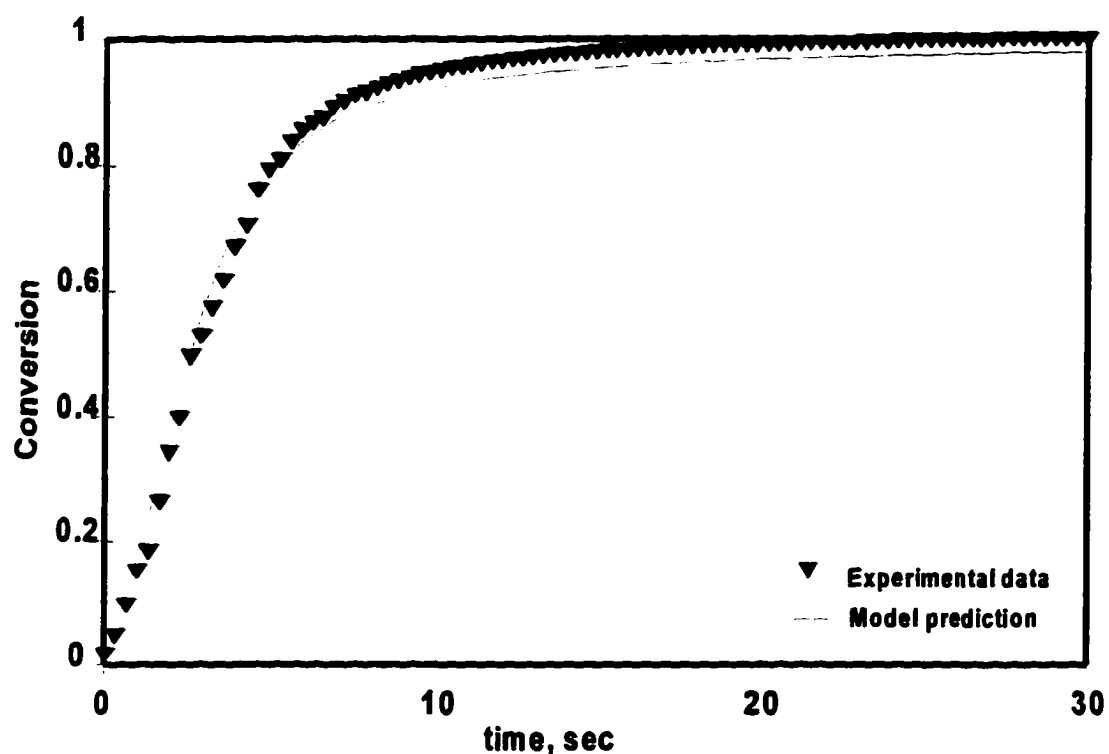


Figure 4.9 Conversion Versus Time

CHAPTER 5

CELLULOSIC COMPOSITES CONCLUSIONS

Good mechanical property improvement can be obtained in PUU/cellulosic and PU/cellulosic composites. The tensile strengths and Young's moduli of PUU-cellulosic composites are doubled compared to those of neat PUU with only 7 % and 5 % cellulosic fiber loading respectively. The bending modulus of the PU/cellulosic composites were doubled with 18 % loading while the bending strengths were increased up to 50 % at the same loading. This demonstrates the effectiveness of load transfer between the matrix and the fiber due to chemical bonds formed between the matrix and fiber. Higher fiber loading (above 50 %) could be achieved as long as the clamping force to close the mold is available.

Experiments with the PUU matrix (Spectrim® 50) shows that tensile mechanical properties of the composites are not sensitive to the cellulosic fiber properties and fiber macroscopic configurations in the mats. Fibers from different sources and different lignin content (ranging from zero lignin content up to at least 10 %) with different macroscopic arrangements of the textile reinforcement (water laid, needle punched and woven) perform comparably in PUU/cellulosic composites. Although the PU matrix (Spectrim® MM 310) is more than three times stronger than Spectrim® 50, its mechanical properties can be improved using cellulosic fibers as reinforcements. Cellulosic fiber properties and their macroscopic arrangement,

however, significantly influence the mechanical properties of PU/cellulosic composites. Bending strengths increase significantly for samples with cotton fiber reinforcements. Bending strength is also improved for samples with treated sugar cane and kenaf fibers especially with high fiber loading. Decreases in bending strengths in samples with untreated kenaf fibers were mostly caused by cohesive failure inside big bundles. This shows the importance of fiber treatments (partial delignification and steam explosion) since this affects bundle size..

Due to the polar nature of cellulosic fibers and the chemistry of isocyanate, good adhesion and chemical bonding between fiber and PU or PUU matrix could be obtained. The presence of the chemical bonds between the PU matrix and cellulosic fibers was confirmed by FTIR studies (Collier et al, 1996) and the effect of chemical ratio on mechanical properties of PUU/cellulosic composites. High excess isocyanate was found to decrease mechanical properties of neat PUU samples. Higher excess isocyanate, however, was found to increase the mechanical strength of samples with high fiber loading. This is because there are more hydroxyl groups to react with excess isocyanate to form carbamate bonds between the PU matrix and cellulosic fibers.

Using high normality caustic soda treatment for cellulosic fibers enables production of smaller diameter fibers without steam explosion. While the elimination of steam explosion is a clear process benefit, this method of treatment

produces more smaller fibers that in turn cause the mat produced from these fibers to have very low permeability. This low permeability mat requires high injection pressure. The operating conditions for fiber preparation need to be adjusted to obtain optimum fiber dimensions while allowing reasonable injection pressures.

The kinetic study of Spectrim® MM 310 shows the importance of mold filling design. According to the manufacturer recommendation the in-mold gelling time of the PU resin is 30 seconds. From the kinetic study, under close to adiabatic conditions, the reaction reached more than 90 % partial conversion within less than 10 seconds. Normally 0.7 conversion is considered to be the gel time for PU formulations (Macosko, 1989). Near adiabatic conditions may also be found within thick specimens because the thermal conductivity of the polymer is low. Clearly, mold design and SRIM modeling are necessary to avoid this.

CHAPTER 6

CELLULOSIC COMPOSITES RECOMMENDATIONS

- (1). As the achievement of high fiber loading is usually the goal in composites manufacturing, a better mold and clamping system needs to be designed. This is because a high clamping force is required to close the mold when a high fiber loading is sought .
- (2). The goal to achieve PU/cellulose composite mechanical strengths as high as can be achieved should be weighted against the practicality of the composite preparation. Therefore, more studies are needed to find optimal treatment conditions that give good fiber properties suitable for SRIM cellulose composite production.
- (3). Dimensional stability is an important issue in material selection especially for load bearing applications. High moisture absorption of cellulosic fibers is a big concern in any cellulosic/plastic composite application. A thorough study is important to quantify the effect of humidity on the performance of PU/cellulosic composites.

PART II

SRIM AND RTM MODELING

CHAPTER 7

LITERATURE SURVEY ON SRIM AND RTM MODELING

Liquid composite molding (LCM) that includes structural reaction injection molding (SRIM) and resin transfer molding (RTM) is increasingly becoming the process type of choice for manufacturing low cost, high quality surface finish, composite parts in one step (Macosko, 1989; -, 1983; Lindsay, 1993; Rogers, 1990, Valenti, 1992; Wilder, 1989). Growing interest in the SRIM thermosetting process has primarily been driven by higher productivity and design flexibility demands in the automotive industry (Lindsay, 1993; Rogers, 1990). This industry has been the major market for SRIM products, while RTM parts have been made primarily for the aerospace industry (Valenti, 1992). Strict regulation on emission limits and for occupational safety are two other factors that influence major composite processors to consider replacing traditional processing such as hand lay-up by closed-mold SRIM and RTM processing (Valenti, 1992). Operating using closed molds and also often under vacuum can minimize chemical release to the environment. Previously, preform preparation cost was the major factor in the material cost for SRIM parts. The advance of automated preform manufacturing is foreseen to attract wider SRIM and RTM applications (Lindsay, 1993; Rogers, 1990; Valenti, 1992; Wilder, 1989).

The demand for SRIM and RTM parts, especially in the automotive industry, is projected to increase significantly in the near future (Lindsay, 1993).

In both SRIM and RTM processes, fiber preformed mats are placed inside the mold cavity prior to filling the mold with resins. The resins subsequently react and form solid structures (Macosko, 1989; SPI, 1983). The differences between the two processes are in the way the reaction is started and in the cycle time. While impingement mixing between two streams initiates the reaction in SRIM, a catalyst is added and sometimes heating is also required to start the reaction in RTM. Typically RTM has a longer cycle time than SRIM (Lindsay, 1993). Polyurethane (PU) formulations are the most widely used for SRIM applications while there are more variations for RTM applications. The two most important for RTM are polyester based and epoxy based formulations. With the advance of resin synthesis, the distinction between SRIM and RTM is becoming more blurred. Some chemical manufacturers have developed two component formulations that can be used for both SRIM and RTM by allowing users to adjust the curing times from the order of a few minutes (suitable for SRIM) to as high as one hour (suitable for RTM) (Lindsay, 1993). One example of this type is Xycon (urethane polyester hybrid resin) developed by Amoco (Rogers, 1990).

Mold filling is a very crucial step in both SRIM and RTM. In the short duration of mold filling, which is from the order of a few seconds to as high as

only a few minutes, the resin should be able to penetrate into the mats and wet the fiber bundles. Incomplete filling, inadequate fiber wetting, and/or voids trapped in the mold can decrease the mechanical properties of the composites (Macosko, 1989). Determination of gate and air vent locations is also a crucial issue in mold design (Young, 1994). Proper inlet gate positioning can also reduce the filling time and the required injection pressure.

Recently, there has been some effort to utilize modeling in mold design and simulation of mold filling. Modeling can help minimize the time and cost involved in product development (Lindsay, 1993). Using modeling tools, a designer will be able to locate appropriate and adequate gates and vents so that void trapping and "line welding" resulting from collapsing two fronts into each other can be minimized. The modeling also helps to predict the effects of changing certain operating conditions on the overall performance of the process, so that mold filling optimization could be performed on a computer to minimize costly experimental trials.

7.1 SRIM and RTM Modeling

Fiber preform beds are customarily modeled as porous media (Macosko, 1989; Young, 1994; Friedrichs and Guceri, 1995; Lin et al., 1993; Gauvin et al., 1996; Liang et al., 1993; Calhoun et al., 1996; Trochu et al., 1993]. Therefore the macroscopic flow of resin inside the fiber bed can be represented by Darcy's law.

Although there were efforts to solve the Navier-Stokes equations on an idealized cell of fiber bed (Skartsis et al., 1992; Young, 1996) , for practical problems Darcy's law is considered sufficient and computationally more viable. Therefore all available simulation packages for RTM and SRIM are based on Darcy's law representations. The differences between these packages are mainly centered around the numerical methods adopted to solve the governing equations and the moving front location evolution during the filling.

There are two major approaches to SRIM modeling, namely: finite element (FE) and finite difference (FD) approaches. Although analytical solutions are also available; these are strictly limited, to simple geometries and non reacting systems (Gonzales-Romero and Macosko, 1985). However, the majority of SRIM and RTM applications involve complex geometries and very often include non-isothermal reacting systems during mold filling. Therefore this literature review will focus only on the two major classes of SRIM model, i.e. FD and FE based models.

7.2 Finite Difference Based Models

FD techniques are still widely used for solving flow problems although more recently FE methods are gaining popularity. Many commercial computational fluid dynamics (CFD) packages are based on FD or FE formulations (Freitas, 1995). Examples of FD based packages are : Flow-d® from

Flow Science Inc., Star-CD® from Computational Dynamics LTD, Fluent® from Fluent Inc. etc. FD approaches equipped with boundary fitted coordinate system (BFCS) have been used to solve moving boundaries problems during mold filling in SRIM and RTM (Friedrichs and Guceri, 1995; Trochu and Gauvin, 1992). While dynamically generated grids permit tracking of the front location accurately, there are still several obstacles when the geometry is complex.

In BFCS methods, the calculation domain boundaries are always coincident with physical boundaries. Therefore, the moving front is always located at the calculation boundary so that no approximation is needed to implement boundary conditions. This requires grid generation at the end of every time step. Obviously, this demands a very high computational time, in fact a main frame was needed just to solve a 2-D problem. Other complications will arise when the liquid front is split around a mold insert or a sharp edge, or when multiple gates are used, causing multiple liquid filled domains inside the mold. The requirement of the physical domain mapping into a rectangular domain (in 2-D) causes the computations to be very complicated thereby making the development of a general solution very difficult (Trochu and Gauvin, 1992).

Despite all these problems, BFCS offers the most accurate description of front location versus time because the front location is clearly defined (without any approximation) in this method (Trochu and Gauvin, 1992; Wang and Lee,

1989). The approach might be simplified by using a fixed grid instead of dynamic grid and tracking the front location using a different method. These are basically the underlying concept for other commercial solver packages.

7.3 Finite Element Based SRIM Model

Although FE methods originated as structural analysis tools, they are gaining wider application in engineering and science including in fluid flow simulation. Often the equations solved for a structural problem can be used for flow problems by redefining the meaning of variables, for instance plate bending formulations can be used for fluid flow by allowing the strain terms to be redefined as strain rate. The major advantage of FE methods is geometrical flexibility (Pittman, 1989). For example, irregular geometry in 2-D can be fitted by triangular elements. Most simulation packages developed for SRIM and RTM modeling are based on FE formulations using a fixed mesh with a few variations in methods for satisfying the conservation equation from element to element.

To track the front location accurately, it is essential that the numerical solution used be able to satisfy the continuity equation locally. The majority of the workers resort to control volume finite element (CV/FE) formulations (Young, 1994; Lin et al., 1993; Calhoun et al., 1996; Trochu et al., 1993). In these formulations, the solution is performed on a fixed mesh while the front location is determined by calculating a filling factor (F) using a fluid mass balance over all

front cells. Another variant of FE based packages is what is so called a non-conforming FE formulation used by Trochu et al. (1993). Using a non-conforming FE formulation, the continuity equation is satisfied locally from cell to cell, therefore, the cell filling factor calculation is straightforward.

In spite of the advantage of FE formulations, the difficulty is that the memory requirements to store the stiffness matrices and load vectors is very high (In FE analysis, the coefficients of the resulting algebraic equations are assembled into stiffness matrices and load vectors). Although some of the models developed can solve 3-D problems, the majority of FE analyses on SRIM mold filling are limited to 2-D space for the flow, especially when the mold filling is reacting non-isothermally. To calculate the temperature distribution in the mold thickness direction, different methods have been used. Young (1995) used CV/FE formulation on a 2-D mesh to solve the flow field and used a FD method to solve the temperature distribution in the gap-direction. Calhoun et. al. (1995) also used CV/FE formulation except that the temperature distribution in the thickness direction was calculated using a Chebyshev collocation spectral method. Liang et. al. (1993) solved a generalized Hele-Shaw (GHS)(often called 2½-D) model for mold filling in RTM and solved the gap-wise temperature distribution using FD. This approach is justified only for thin specimens. Despite these simplifications, all of these packages require at least a workstation platform. No FE based SRIM

model solver packages were specifically developed for personal computer (PC) applications, and to be broadly applicable, PC based models should be developed.

7.4 PC Based Modeling for Fully 3-D SRIM Mold Filling Problems

Most FD based CFD packages, solve the resultant algebraic equations iteratively. This approach reduces the memory requirement significantly compared to FE formulations. Using the CV FD formulation, the application of the front tracking algorithm is straightforward since the moving interface is always located at the control volume surfaces where the velocity information is stored. Front location can be tracked by approximate methods (Cividini and Gioda, 1984) as shown by Lo et al. (1994 (a) and 1994(b)). The application of a more robust front tracking method, volume of fluid (VOF), is also very straightforward as will be shown in this work.

The emphasis in this work is to develop a PC based model to simulate fully 3-D non-isothermal reacting mold filling in SRIM and RTM. The PC emphasis is because PC's are more accessible to users such as the small industries involved in SRIM and RTM and to personal users. The developed algorithm will be applicable to both simple geometries as well as complex geometries by using coordinate mapping or grid transformation (Guceri, 1989). By grid transformation, the physical domain is mapped into a simple rectangular domain in a 2-D space or into a tetrahedral calculation domain in a 3-D space. By this operation, the calculation

algorithm will be applicable for both simple geometries as well as complex geometries. Obviously this will require extra memory to store some coordinate transformation parameters. A complex geometry sometimes can be broken down into several simple geometries so that it can be modeled accurately without resorting to coordinate transformation. This multi-blocking approach will be implemented in some of the examples presented in this dissertation.

Finally, a computational fluid dynamic result should be presented in such a way that it can be interpreted easily. This is the role of a post processor. Some of the simulation results will be presented on a regular graphical application for PC's such as Surfer® (a trade mark of Golden Software Inc.) . But for more complex geometries, a post processor program will be developed on Matlab® (a trade mark of The Mathworks Inc.) platform that is also available on PC's. Over all, the entire program should be run on a PC from grid generation, through solution, and the post processing step.

CHAPTER 8

MATHEMATICAL REPRESENTATION FOR MOVING FRONT PROBLEMS IN RTM AND SRIM

Mold filling is a very crucial step in both SRIM and RTM. In the short duration of mold filling, which is on the order of a few seconds, the resin should be able to penetrate into the mats and wet the fiber bundles. Incomplete fiber wetting and voids trapped in the mold can decrease mechanical properties of the composites (Macosko, 1989). Mold filling in SRIM and RTM is inherently transient, reactive, non-isothermal, and involves moving boundaries (interface between liquid and gas phases). These conditions result in highly non-linear mathematical models with complex geometries which, in general, necessitate numerical method to solve them. The numerical methods should be equipped with means to described the location, the shape and the evolution of the free surfaces which are the major challenges in mold filling modeling.

This chapter discusses mold filling modeling in SRIM and RTM. All the governing equations to model mold filling problems in SRIM and RTM are discussed in the first two sections. This chapter will end with a discussion of front tracking methods.

8.1 Governing Equations

The macroscopic flow of polymeric resin through a fiber bed is usually modeled as flow through porous media (Macosko, 1989; Friedrichs and Guceri, 1995; Lin et al., 1993). The velocity-pressure relation is given by Darcy's equation (Macosko, 1989; Friedrichs and Guceri, 1995; Lin et al., 1993; Bird et al., 1960) as:

$$\underline{v} = -\frac{\underline{\underline{K}}}{\mu} \bullet (\nabla p - \rho \underline{g}) \quad (8.1)$$

where \underline{v} is the superficial velocity vector, μ is the viscosity, p is the pressure, \underline{g} is the gravity acceleration, and $\underline{\underline{K}}$ is the permeability tensor. In three-dimensional Cartesian coordinates, $\underline{\underline{K}}$ can be written as:

$$\underline{\underline{K}} = \begin{bmatrix} K_{xx} & K_{xy} & K_{xz} \\ K_{yx} & K_{yy} & K_{yz} \\ K_{zx} & K_{zy} & K_{zz} \end{bmatrix} \quad (8.2)$$

Therefore, Darcy's equation can be expressed in three-dimensional form as (Gebart and Lidstrom, 1996):

$$v_i = -\frac{K_{ij}}{\mu} \bullet \frac{\partial P}{\partial x_j} \quad (8.3)$$

where i and $j = x, y, z$. P is the modified pressure that combines both pressure gradients and gravity driving forces.

Assuming the fluid is incompressible and substituting equation (8.1) into the continuity equation:

$$\underline{\nabla} \bullet \underline{v} = 0 \quad (8.4)$$

we obtain the governing equation:

$$\underline{\nabla} \cdot \left(\frac{\mathbf{I}}{\mu} (\underline{\underline{K}} \bullet \underline{\nabla} p) \right) = 0 \quad (8.5)$$

In most practical situations, the permeability coefficient is measured in the principal directions of the fiber mats and then the off-diagonal elements are computed using mathematical equations (Gauvin et al., 1996). If the directions of the coordinate axes coincide with the principal directions of the fiber mats, the off-diagonal elements in the permeability tensor become zero (Young et al., 1991, Gauvin et al., 1996) and the continuity equation can be written as:

$$\frac{\partial}{\partial x} \left(\frac{\mathbf{K}_{xx}}{\mu} \frac{\partial p}{\partial x} \right) + \frac{\partial}{\partial y} \left(\frac{\mathbf{K}_{yy}}{\mu} \frac{\partial p}{\partial y} \right) + \frac{\partial}{\partial z} \left(\frac{\mathbf{K}_{zz}}{\mu} \frac{\partial p}{\partial z} \right) = 0 \quad (8.6)$$

where K_{ii} ($i=x, y, \text{ and } z$) are the diagonal elements of the permeability tensor. Discussion of permeability will be presented in the next section.

During filling, the filled region inside the mold cavity evolves with time. The quasi steady state assumption is the most common assumption used in modeling mold filling problems. By assuming this, the mold filling process is regarded as comprised of a sequence of steady state processes and the governing equations are solved only for filled regions, neglecting the density change with time in partially filled regions. To obtain the description of the moving front, other methods must be employed besides the governing equation. This approach uses what is commonly

called front tracking algorithms. The discussion on front tracking methods will be presented at the end of this chapter and in the next chapter.

Ideally, viscosity should remain low until mold filling is completed. This however does not happen for fast reacting chemical systems and mold filling longer than a few seconds. Viscosity changes with time due to polymerization and the related heat effect from the normally exothermic reactions. The injection pressure will increase dramatically for longer filling times due to increases of viscosity. For such situations the change in viscosity with time is no longer negligible and should be taken into account. This requires the solutions also of the energy and chemical species conservation equations.

8.2 Permeability

Permeability is the most important parameter in the mold filling model in RTM and SRIM. There have been some efforts to model permeability coefficients. The Blake-Kozeny-Carman equation (BKC equation) is the most widely used empirical equation to describe the change of permeability with the fiber configuration in the mats (Williams et al., 1974, Skartsis et al., 1992). It models porous media as a system of parallel capillaries with diameters estimated as the hydraulic diameters of the system. The equation is obtained from applying the Hagen-Poiseuille equation for capillary flow with correction for the true velocity in

the porous medium, the resultant permeability expression is then coupled with Darcy's Law (Williams et al., 1974). The BKC equation is written as:

$$K = \frac{\varepsilon^3}{(1-\varepsilon)^2} \frac{I}{s^2 k} \quad (8.7)$$

where ε is porosity, s is the specific surface of the medium particle, and k is the Kozeny constant (1992).

Within certain porosity limits, k was thought to be constant, and determined by geometry and orientation of the packing materials (Williams et al., 1974). Equation 8.7 adequately predicts permeability for random porous beds, and k has been observed experimentally to have values around 5 for a wide variety of isotropic porous media with a range of porosity is between 0.4 and 0.7 (Skartsis et al., 1992). For higher and lower porosities, k changes drastically from the constant value (i.e. 5).

There were efforts to calculate permeability in an aligned fiber bed by solving the Navier-Stokes equations for a single unit cell of the fiber bed (Skartsis et al., 1992(b); Cai and Berdichevsky, 1994). Skartsis et al (1992(b)) solved the Navier-Stokes equations for unit cells of square and staggered square arrays of fiber beds numerically, and computed the theoretical value of the transverse permeability. The prediction agreed well with experimental observation. Cai and Berdichevsky (1994) gave analytical expressions for permeability in aligned fiber bundle and tows by solving the momentum equation for viscous flow (i.e. the inertia terms are

negligible), and Darcy's equation applied on a multiple region unit cell in the form of composites cylinders. The equation gave reasonable agreement with the numerical result.

Despite the impressive success of the theoretical prediction of permeability, the theoretical prediction can at best predict it in ideal configurations. In practical situations, permeability is still measured experimentally, and then the data expressed in the form of empirical equations for future use. Young et al (1991) gave empirical expressions based on their experimental measurement for random glass fiber mats and stitched bi-directional fiber mats (the fiber strands in the mat are oriented in two directions. One part is oriented into 90° to the other). Their results show that permeabilities in flow direction K_x and K_y are not only function of porosity but also functions of superficial velocity as well. The empirical equations were written as:

Random fiber mat:

$$K_x = K_y = 241v' + 40e^{5.45\varepsilon} \quad (8.8)$$

$$K_z = \frac{62\varepsilon^3}{(1-\varepsilon)^2} \quad (8.9)$$

Bi-directional fiber mat:

$$K_x = 47e^{5.92\varepsilon} + (2018\varepsilon - 592)v' \quad (8.10)$$

$$K_y = \frac{4}{5}k_x \quad (8.11)$$

$$K_z = \frac{272 \varepsilon^3}{(1 - \varepsilon)^2} \quad (8.12)$$

where v' (cm/sec) is the superficial velocity, and the units of permeability are in Darcy (1 Darcy=9.8697 x 10 -9 cm 2). They claimed that equations 8.8-8.9 are applicable in the porosity range between 0.54-0.95, and equations 8.10-8.12 are applicable in the porosity range between 0.45-0.67, while the applicable superficial velocity for all equations is between 1 cm/s to 11 cm/s.

If the axes of the calculation coordinate do not coincide with the principle axes of the mat, the permeability matrix should be transformed into the calculation domain. This can be accomplished using tensor analysis. Young et al. (1991) gave the transformation of the permeability tensor from the coordinate based on the mat principle axes x_1 , x_2 , and x_3 to the calculation coordinate system x , y , z as:

$$\begin{bmatrix} K_{xx} & K_{xy} & K_{xz} \\ K_{yx} & K_{yy} & K_{yz} \\ K_{zx} & K_{zy} & K_{zz} \end{bmatrix} = \begin{bmatrix} l_{11} & l_{12} & l_{13} \\ l_{21} & l_{22} & l_{23} \\ l_{31} & l_{32} & l_{33} \end{bmatrix} \begin{bmatrix} K_{11} & 0 & 0 \\ 0 & K_{22} & 0 \\ 0 & 0 & K_{33} \end{bmatrix} \begin{bmatrix} l_{11} & l_{12} & l_{13} \\ l_{21} & l_{22} & l_{23} \\ l_{31} & l_{32} & l_{33} \end{bmatrix} \quad (8.13)$$

where l_{ij} are the directional cosines of x , y , and z with respect to the principle axes x_i . K_{11} , K_{22} , and K_{33} are the permeability values measured in the principle axes of the mat.

8.3 Energy and Reaction Equations

Assuming local thermal equilibrium, the energy equation can be written as (Macosko, 1989; Lin et al., 1993):

$$\rho C_p \frac{\partial T}{\partial t} + \rho_r C_{pr} \left(u \frac{\partial T}{\partial x} + v \frac{\partial T}{\partial y} + w \frac{\partial T}{\partial z} \right) = k \left(\frac{\partial^2 T}{\partial x^2} + \frac{\partial^2 T}{\partial y^2} + \frac{\partial^2 T}{\partial z^2} \right) + \varepsilon \Delta H R_{rxn} \quad (8.14)$$

where T is temperature, ρ is density, C_p is specific heat, k is thermal conductivity, ε is the porosity, ΔH is the heat of reaction, R_{rxn} is the reaction rate. r and f subscripts refer to resin and fiber respectively. u, v, and w are the x, y, and z components of the superficial velocity, respectively. C_p and k are the averaged values of the related quantities of the fiber and the resins. Heat capacity and conductivity are usually given as weighted averages of those of the resin and the fiber as (Lin et al., 1993):

$$C_p = \omega_r C_{pr} + \omega_f C_{pf} \quad (8.15)$$

$$\rho = \varepsilon \rho_r + (1 - \varepsilon) \rho_f \quad (8.16)$$

$$k = \frac{k_r k_f}{k_f \omega_r + k_r \omega_f} \quad (8.17)$$

$$\omega_r = \frac{\varepsilon \rho_r}{\varepsilon \rho_r + (1 - \varepsilon) \rho_f} \quad (8.18)$$

$$\omega_f = 1 - \omega_r \quad (8.19)$$

where ω is the weight fraction. This formulation is often called the one temperature equation and was found to give a good approximation for the two separate equations for resin phase and the fiber phase (Lin et al., 1993). The assumption of local equilibrium will break down and two temperature equations have to be used when the temperature changes very rapidly (Tucker, 1996). This can happen when the reaction is very fast or when the filling time is very short (the convective heat transfer is much higher than the conductive heat transfer, i.e. at high Peclet numbers) (Tucker, 1996; Whitaker, 1986; Whitaker, 1991). Since the filling is usually much shorter than the curing step in SRIM and RTM, the one temperature equation still gives a good over all temperature profile. While the pressure equation is solved only for the filled region, the temperature equation (equation 8.14) should be solved for the whole domain including the mold if necessary.

The reaction rate, R_{rxn} , is a function of the species concentration (or partial conversion α) and temperature. α can be obtained from the solution of the balance of the reacting species that is given by:

$$\frac{\partial \alpha}{\partial t} + \frac{I}{\varepsilon} \left(u \frac{\partial \alpha}{\partial x} + v \frac{\partial \alpha}{\partial y} + w \frac{\partial \alpha}{\partial z} \right) = R_{rxn} \quad (8.20)$$

This equation should be solved only for the filled region.

8.4 Rheokinetic Model

The reaction term R_{rxn} is usually obtained from fitting experimental data for a specific chemical formulation. The most widely used empirical equation to represent reaction kinetics of polyurethane systems is (Lin et al., 1993; Macosko, 1989):

$$R_{rxn} = A e^{\frac{-E_1}{RT}} (\alpha_f - \alpha)^n \quad (8.21)$$

Equation (8.21) is applicable for mole ratios close to 1. For other thermosetting materials including epoxy, unsaturated polyester and phenolic systems, the kinetic data are usually fitted with the following equation (Kamal and Ryan, 1989; Calhoun et al., 1996):

$$R_{rxn} = \left(A_1 e^{\frac{E_1}{RT}} + A_2 e^{\frac{E_2}{RT}} \alpha^{ml} \right) (1 - \alpha)^{m2} \quad (8.22)$$

Resin viscosity is usually related to the conversion, α , and temperature as (Macosko, 1989; Lin et al., 1993):

$$\mu = \mu_0 \left[\frac{\alpha_g}{\alpha_g - \alpha} \right]^{f(\alpha, T)} \quad (8.23)$$

where μ_0 is given by:

$$\mu_0 = A_\mu e^{\frac{E_\mu}{RT}} \quad (8.24)$$

A_μ and E_μ are constants, and $f(\alpha, T)$ is a function of conversion and temperature. α_g is the gel conversion which theoretically is 0.71 for polyurethane systems (Macosko,

1989; Lin et al., 1993). Equations 8.23 and 8.24 were also used to represent the viscosity kinetic relationship for epoxy systems and unsaturated polyester systems (Chick, et al., 1996) and other thermosetting polymers (Young et al., 1991).

8.5 Boundary Conditions

Boundary conditions for the pressure equation can be given either in terms of pressure or velocity since both are related through Darcy's equation. At the front, the liquid pressure is equal to the cavity pressure, P_o .

$$P_{front} = P_o \quad (8.25)$$

At the wall the velocities are zero, i.e.:

$$u_{wall} = 0,$$

$$v_{wall} = 0, \quad (8.26)$$

$$w_{wall} = 0.$$

and at the gate either pressure or velocity is known, i.e.:

$$u_{gate} = u_o,$$

$$v_{gate} = v_o, \quad (8.27)$$

$$w_{gate} = w_o.$$

or

$$P_{gate} = P_g \quad (8.28)$$

where P_g , P_o , u_o , v_o , and w_o are the gate pressure, cavity pressure and velocity components at the cell where the gate is located, respectively.

The most commonly used boundary conditions for the temperature and reaction equations are known values at specified locations, such as:

$$\begin{aligned}\alpha_{\text{gate}} &= 0 \\ T_{\text{gate}} &= T_o.\end{aligned}\tag{8.29}$$

Interphase convective type boundary conditions at the wall can also be specified for the temperature equation. For a metal mold, however, it has been found that a constant wall temperature boundary condition gives good results since the mold heat conductivity is much higher than that of the resin (Young, 1995).

8.6 Front Tracking Methods

Difficulties arise from the changing geometry due to the moving front. One remedy for this problem is the use of dynamic grid generation using a boundary fitted coordinate system (BFCS) (Friedrichs and Guceri, 1995; Guceri, 1989). Using BFCS the calculation domain will always coincide with the physical geometry. This method however requires significant extra calculations and complications especially when geometries are complicated or multiple gate inlets are used since the grid generation should be performed for every time step (Trochu and Gauvin, 1992).

For fast calculations especially during the preliminary design, the use of a simpler front tracking method may be more justifiable. An example of this category is the approximate method that was proposed by Cividini and Gioda (1984) and later implemented by Lo et. al. (1994(a), 1994(b)) for a FD scheme. This method however, will work best only for regular grids. To handle more complex geometries and irregular grids without necessitating a complicated algorithm, a more general front tracking method should be used, e.g. the volume of fluid method (VOF) (Hirt and Nichols, 1981). The VOF method uses a marker variable (F) to specify the fractional filling of the cells by liquid. F is 1 for a completely filled cell, and zero for an empty cell. In a partially filled cell, the F value is between 0 and 1. F values are obtained by solving a convective type differential equation:

$$\varepsilon \frac{\partial F}{\partial t} + u \frac{\partial F}{\partial x} + v \frac{\partial F}{\partial y} + w \frac{\partial F}{\partial z} = 0 \quad (8.30)$$

where u, v , and w are the superficial velocity in the x , y , and z directions. The implementation of these two front tracking methods can not be separated from the chosen numerical method. Therefore the discussion of the front tracking method will be included in the next chapter.

CHAPTER 9

DEVELOPMENT OF THE NUMERICAL METHODS

FD and FE methods are usually employed to solve the governing equations presented in the previous chapter. Although FE methods are gaining more popularity due to their flexibility in handling more complex geometries, FD methods are simpler to use (Guceri, 1989; Patankar, 1980) and less computationally intensive. This is because of the FD adaptability to different iterative schemes used in solving the resultant simultaneously algebraic equations (Patankar, 1980). FD methods can handle complex geometries more efficiently, comparable to FE methods, by using BFCS and numerical grid generation (Guceri, 1989). Although problem cases solved in this work are generally only for regular geometries, the numerical method formulated will be applicable as well when the grid generation and coordinate transformation are employed.

Mass and heat transfers in SRIM mold filling can be categorized as diffusion-convection problems. The control volume approach is the most widely used formulation to solve diffusion-convection type equations using FE and FD. The most important feature of this technique is that the resultant discretized equation enables direct physical interpretation of the results (Patankar, 1980).

In this work, the control volume FD method with a fixed grid (as opposed to the dynamic grid used in the BFCS method discussed in the previous chapter) is used to solve the moving front model in mold filling. The front location is computed either using the approximate method (Cividini and Gioda, 1984; Lo et al, 1994 (a) and 1994 (b)) or by using a modified VOF method (Hirt and Nichols, 1981).

9.1 Control Volume Finite Difference Formulation

For programming purposes, the diffusion-convection phenomena in a non-compressible fluid is often represented by a general equation (Patankar, 1980) as:

$$\rho \frac{\partial}{\partial t}(\phi) + \rho U \frac{\partial \phi}{\partial x} - \frac{\partial}{\partial x}\left(\Gamma \frac{\partial \phi}{\partial x}\right) + \rho V \frac{\partial \phi}{\partial y} - \frac{\partial}{\partial y}\left(\Gamma \frac{\partial \phi}{\partial y}\right) + \rho W \frac{\partial \phi}{\partial z} - \frac{\partial}{\partial z}\left(\Gamma \frac{\partial \phi}{\partial z}\right) = S \quad (9.1)$$

where ϕ is the transported quantity under consideration and Γ is "diffusivity/conductivity" for ϕ . U, V, and W are x, y and z components of the "convective mass flux". Γ , U, V, and W can be interpreted differently than the conventional conductivity and velocity. Table 9.1 shows the expression of α , U, V, and W for variables involved in the SRIM mold filling problem. In Table 9.1, α is chemical conversion, and K, μ , k, C_p and D represent permeability, viscosity, heat conductivity coefficient, specific heat capacity, and diffusivity respectively. The diffusivity coefficient for a polymer molecule or a macromolecule is usually very

low and thus diffusion mass transfer in mold filling is negligible compared to the convection mass transfer. Therefore D is usually set equal to zero.

Table 9.1 Expressions for U, V, W and Γ

ϕ	U	V	W	Γ
P	0	0	0	K/μ
T	u	v	w	k/C_p
α	u	v	w	D
F	u	v	w	0

The Γ may have different values in x, y, and z directions such as when a non isotropic material is used. The source term (S) in equation (9.1) represents the actual source term plus any additional terms that are not included in the diffusion and convection terms. Generally, S is a non-linear function of variable ϕ and other variables. For example, in the equation for α , the source term is the reaction rate term that is a non linear function of α (the ϕ) and temperature (T). In the computation, S is often linearized in term of ϕ as:

$$S = S_p \phi + S_c \quad (9.2)$$

where S_p and S_c are constants.

Being expressed in the same general equation, all variables can be treated in the same way in the computation, and therefore can be computed in the same program. To implement the control volume method, the calculation domain is divided into several control volumes in which grid points are placed (as shown by shaded area in Figure 9.1 in a 2-D space). Grid points are locations for storing all variables except the velocity components which are stored at the control volume interface (or often called staggered grid). The capital letter P refers to the grid point under consideration whereas E, W, N, S, T, and B (T and B are not shown in 2-D space) refer to the neighboring grid points. The lower case letters e, w, n, s, t, and b refer to the interface between the control volume surrounding grid point P and the corresponding neighboring grid points.

In general the working equation is obtained by integrating the governing equation over the control volume. Performing this operation over the whole domain of calculations will give a system of algebraic equations for the variable of interest each of which can be expressed as:

$$a_P \phi_P = a_E \phi_E + a_W \phi_W + a_N \phi_N + a_S \phi_S + a_T \phi_T + a_B \phi_B + b \quad (9.3)$$

The coefficients in equation (9.3) (a_E , a_W , a_N , a_S , a_T , and a_B) are functions of the Peclet number (thus the flow and physical properties) at the interfaces that are given as¹:

¹ Operator $\|x_1, x_2\|$ takes the largest value of its arguments.

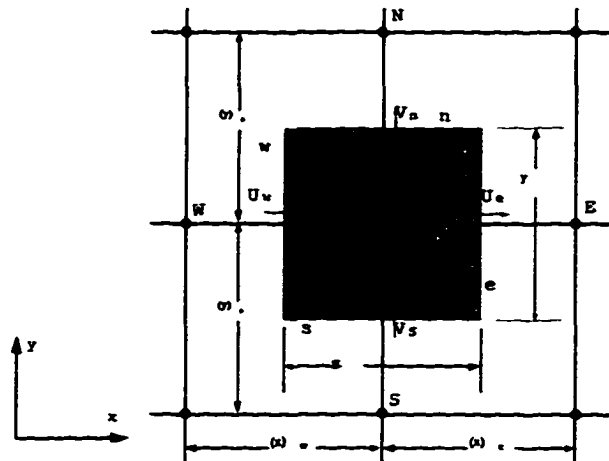


Figure 9.1 Control Volume for Two-dimensional Space

$$a_E = D_E A(|P_E|) + \left\| -F_E, 0 \right\| \quad (9.4-a)$$

$$a_W = D_W A(|P_W|) + \left\| F_W, 0 \right\| \quad (9.4-b)$$

$$a_N = D_N A(|P_N|) + \left\| -F_N, 0 \right\| \quad (9.4-c)$$

$$a_S = D_S A(|P_S|) + \left\| F_S, 0 \right\| \quad (9.4-d)$$

$$a_T = D_T A(|P_T|) + \left\| -F_T, 0 \right\| \quad (9.4-e)$$

$$a_b = D_b A(|P_b|) + \left\| F_b, 0 \right\| \quad (9.4-f)$$

$$a_p = a_E + a_W + a_N + a_S + a_T + a_b + a'_p - S_p \Delta x \Delta y \Delta Z \quad (9.4-g)$$

$$a'_p = \frac{\rho'_p \Delta x \Delta y \Delta z}{\Delta t} \quad (9.4-h)$$

$$b = S_c \Delta x \Delta y \Delta Z + a'_p \phi'_p \quad (9.4-i)$$

The superscript o refers to the previous time step (known values at the current time step). The "flowrates" $F_e, F_w, F_n, F_s, F_t, F_b$ and the "conductance's" $D_e, D_w, D_n, D_s, D_t, D_b$ are defined by:

$$\begin{aligned}
 F_e &= (\rho U)_e \Delta y \Delta z, \\
 F_w &= (\rho U)_w \Delta y \Delta z, \\
 F_n &= (\rho V)_n \Delta x \Delta z, \\
 F_s &= (\rho V)_s \Delta x \Delta z, \\
 F_t &= (\rho W)_t \Delta x \Delta y, \\
 F_b &= (\rho W)_b \Delta x \Delta y.
 \end{aligned} \tag{9.5}$$

and

$$\begin{aligned}
 D_e &= \frac{\Gamma_e \Delta y \Delta z}{(\delta x)_e}, \\
 D_w &= \frac{\Gamma_w \Delta y \Delta z}{(\delta x)_w}, \\
 D_n &= \frac{\Gamma_n \Delta x \Delta z}{(\delta y)_n}, \\
 D_s &= \frac{\Gamma_s \Delta x \Delta z}{(\delta y)_s}, \\
 D_t &= \frac{\Gamma_t \Delta x \Delta y}{(\delta)_t}, \\
 D_b &= \frac{\Gamma_b \Delta x \Delta y}{(\delta)_b}.
 \end{aligned} \tag{9.6}$$

and the Peclet number at any interface i is given by:

$$P_i = \frac{F_i}{D_i} \quad (9.7)$$

where $i = e, w, n, s, t$, and b .

The exact expression of the function $A(|P|)$ depends on the interpolation scheme chosen to describe the ϕ profile between grid points. Patankar (1980) discussed various approaches to compute the coefficients. For example, using a power law scheme gives the expression (Patankar, 1980):

$$A(|P|) = \left\{ 0, (1 - 0.1|P|)^5 \right\} \quad (9.8)$$

A power law will be used in this work to express the variation of all dependent variables between grid points.

9.2 Implementing Boundary Conditions

Due to the transient nature of the location of the front, the exact implementation of the front pressure boundary condition may cause the program to be more complicated and more geometrically dependent. An approximate method is used in this work to express front boundary conditions by assigning extremely large conductance's in the unfilled part of mold cavities. This results in negligible drop in the calculated dependent variable values in the unfilled region so that the moving front boundary conditions can be replaced by specifying the dependent variable values at some fictitious points fixed at the wall. This approach works as well if the

boundary condition is expressed in terms of the flux (constant velocity in this case).

This approach can be justified by the following reason:

1. The velocity calculation is performed only for the filled region, therefore an accurate pressure profile is needed only for the filled region.
2. The viscosity of the gas phase is much lower than the resin viscosity. Since the "conductance" for the pressure equation is permeability divided by viscosity, the actual "conductance" in empty region is always much higher compared to filled region's.

This simple method can be illustrated by solving a one-dimensional pure diffusion problem given in the following equation:

$$\frac{d}{dx} \left(\Gamma \frac{d\phi}{dx} \right) = 0 \quad (9.9)$$

Assume that the concern is only the profile of ϕ at point 1-5 shown in Figure 9.2.

Using the simple approach gives the same ϕ profile at point 1-5 compared to the results obtained by specifying the boundary conditions at the exact location (point 5).

This is shown in Figure 9.3. In this example Γ_1/Γ_2 is taken equal to 1×10^{10} . The circles in Figure 9.3 refer to flux boundary condition, while the triangles correspond to the constant ϕ boundary condition.

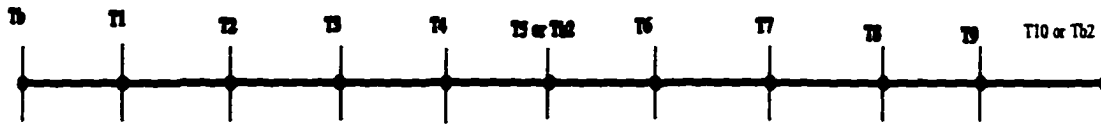


Figure 9.2 One-dimensional Diffusion Problem

Special treatment should also be made for partially filled cells when the conversion and temperature equations are also solved. While the velocity (pressure) calculation is only performed at the filled region by assuming quasi steady state conditions, the transient and source term contributions in the energy and kinetic equations can not be neglected in the partially filled region. Variables in the partially filled cells can be obtained by using a conservation equation as follows:

$$V_{cell}^{cell}(C_p, \rho T)^{new} = V_{cell}^{cell}(C_p, \rho T)^{old} + V_{cell}^{cell} F^{new} \varepsilon r_{rxn} \Delta H \Delta t^{new} + \sum_{nb} v_{nb} A_{nb} C_{pr} \rho_r T_{nb} \Delta t^{new} \quad (9.10)$$

and

$$V_{cell}^{cell} \varepsilon (F \alpha)^{new} = V_{cell}^{cell} \varepsilon (F \alpha)^{old} + V_{cell}^{cell} \varepsilon F^{new} r_{rxn} \Delta t^{new} + \sum_{nb} v_{nb} A_{nb} \alpha_{nb} \Delta t^{new} \quad (9.11)$$

where V_{cell} is the cell volume. The summation is over the filled neighboring cells with the corresponding velocity component flow from them to the partially filled cell. In the above equation F^{new} (new value of fluid volume fraction) and Δt^{new} will be computed at the end of every iteration since the front location is moved at the end of the current time step. Therefore both values have to be approximated for the purpose of the calculation. The estimated values will automatically be equal to the calculated

values when the iterations converge. In these calculations the diffusion contributions are neglected.

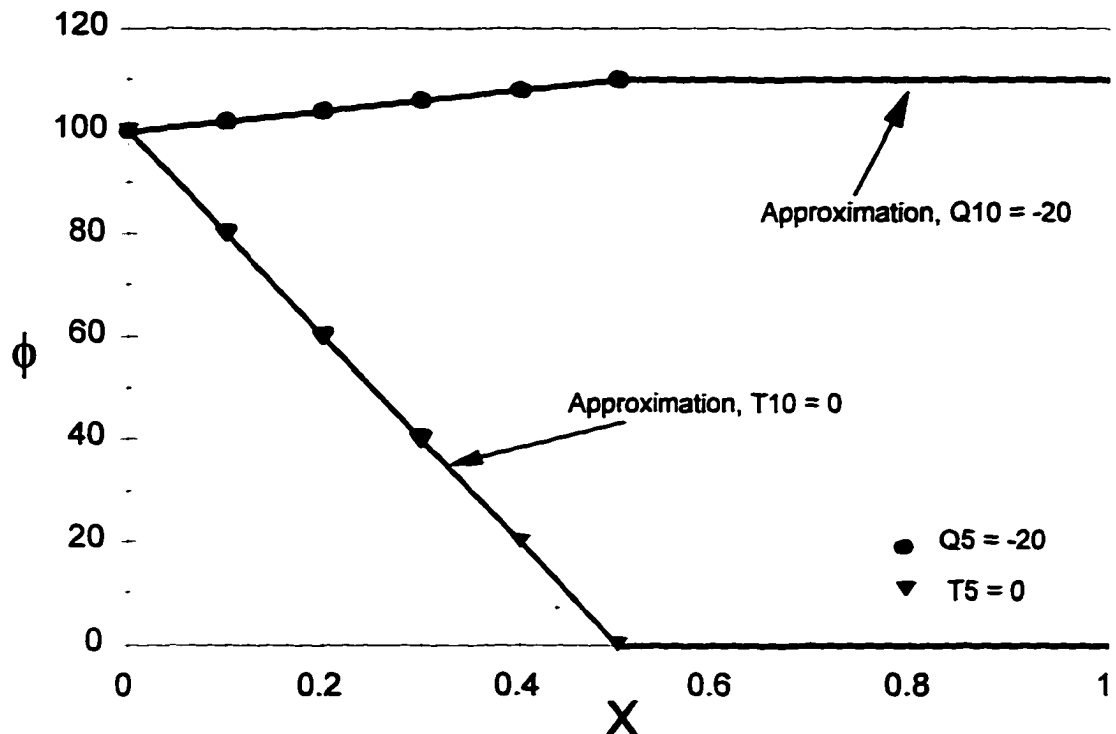


Figure 9.3 An Illustration for The Approximate Boundary Conditions

9.3 Convergence Consideration

Applying the working equation (equation 9.3) over all grid points in the entire calculation domain generally results in a system of non linear equations which requires an iterative solution procedure. In order to assure the achievement of convergence, the system of equations should meet the Scarborough criterion that is expressed as (Patankar, 1980):

$$\frac{\sum |a_{nb}|}{|a_P|} \leq 1, \quad (9.12-a)$$

for all equations

$$\frac{\sum |a_{nb}|}{|a_P|} < 1, \quad (9.12-b)$$

for at least one equation

The summation in equation 12 is over all the unknown neighboring grid points. Any known neighboring values will be dropped from the summation. This condition implies that the chance to achieve convergence can be improved by specifying the values of ϕ at as many grid points as possible.

9.4 Front Tracking

Difficulties arise from the changing geometry due to the moving front. One remedy for this problem is the use of dynamic grid generation using BFCS (Wang and Lee, 1989; Friedrichs and Guceri, 1995). Using BFCS the calculation domain will always coincide with the physical geometry. This method however requires significant extra calculation since the grid generation should be performed for every time step and gives rise to untractable complications for multiple injection port problems. For fast calculation, especially during the preliminary design, employing simpler front tracking methods on a fixed grid may be more justifiable. An example of this category is the approximate method that was proposed by Cividini and Gioda (1984) and later implemented by Lo et. al. for a FD scheme (1994(a), 1994(b)). For problems with more complex geometries or when multiple injection ports are

required, the VOF method (a more robust front tracking method) will be used. These methods will be described in the following section.

9.4.1 Approximate Method for Front Tracking

After the velocity field and the related variables are obtained, the new front location should be determined before moving to the next time step. The approximate method is illustrated in Figure 9.4. This procedure is started by computing the average flux through each free surface (f_j) using the known velocity field. The decisions to move the fronts are made based on the ratio of the average flux in through each free surface divided by a base flux. The choice of base flux was made arbitrarily, and was selected as the maximum flux (Cividini and Gioda, 1984; Lo et al., 1994(a) and 1994 (b)). Thus the criterion to move the front is given by:

$$\delta_j = \left| \frac{f_j}{f_{\max}} \right| \quad (9.13)$$

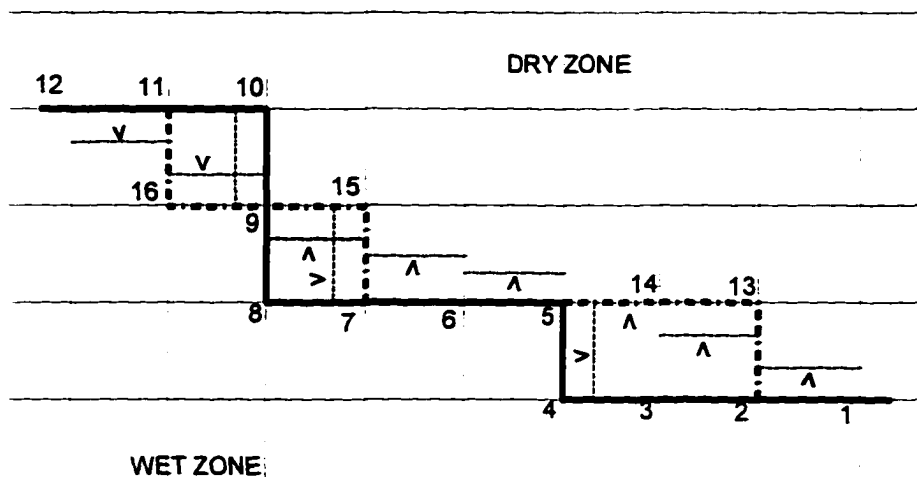
If δ_j is greater than a pre-assigned value, δ_b , the j front is moved to the adjacent elements, otherwise the front position is not changed.

In Figure 9.4, the heavy solid lines represent the original fronts, and the heavy dashed lines are the new fronts. The arrows and light dashed lines represent the value of δ_j for each segment. The maximum value of δ_j is reached for example at segments 2-3 and 3-4, with the outward direction, therefore segments 2-3 and 3-4 are replaced by segments 13-14 and 5-14. However other segments, for example 1-2, 5-

6, and 6-7 are not moved because the corresponding values of δ_j are less than δ_b . This procedure is repeated for each time step until the mold is full (the front coincides with the walls). The time step is calculated as:

$$\Delta t = \frac{l}{n} \sum_{j=1}^n \frac{\Delta L_j \phi_j}{f_j} \quad (9.14)$$

where ΔL_j is the distance between the old and the new positions of j^{th} segment.



- > Flux Direction and the level OF * for each segment
- ... Moved Free Surface

Figure 9.4 Approximate Method for Front Movement
(Cividini and Gioda, 1984)

9.4.2 Volume of Fluid Method

More accurate methods for front tracking suitable for FD implementation are available (Wang and Lee, 1989; Friedrichs and Guceri, 1995). In general they

require one additional differential equation to be solved. Of those, the most widely used is VOF proposed by Hirt and Nichols (1981). An excellent review of front tracking methods is given by Wang and Lee (1989). Here, a brief description of a modified implementation of the VOF method will be presented.

To describe front movement using this method, equation 8.30 should be solved. Any solution method employed for this purpose should be able to maintain the distinct nature of the moving front; i.e. the property jumps from the empty cells to neighboring filled cells. To describe this feature, F should have value equal to 1 at the filled regions and zero at all empty regions. F is allowed to have value between 0 and 1 only at one layer of front cells. Solving F by direct discretization of equation (8.30) tends to smooth out the profile of Hirt and Nichols (1981) proposed a special approach to get around this problem. Fortunately by implementing the CV approach to solve the governing equations, equation (8.30) can be solved with little effort.

As has been described in the previous chapter, velocity is calculated from the pressure profiles using Darcy's law and it is stored at the interfaces. Since the pressure profile already satisfies the continuity equation, equation (8.30) is automatically satisfied in the filled region. Calculations for F have to be performed only at the front cells and this is very straightforward. At the front cells F can be calculated from:

$$F^{new} = \frac{F^{old} * V^{cell} \varepsilon + \sum_i v_i A_i \Delta t}{V^{cell} \varepsilon} \quad (9.15)$$

where V_{cell} is the volume of cell, ε is porosity, v_i is velocity component at interfaces surrounding the cell, A_i is the interface area, and Δt is the time increment. i includes all interfaces surrounding cell P, as shown in Figure 9.1, i.e. e, w, n, s, t, and b. Applying equation 9.15 to filled cells automatically gives F equal to 1, and applying it to empty cells automatically gives F equal to 0. Therefore calculation with equation 9.15 needs to be performed only on front cells.

The crucial parameter in equation (9.15) is Δt . In general the time step should be determined in such a way that only one layer of cells will be filled in that step. Many cells may be filled at the same time, however no cell should be overfilled. This can be translated into the following operation:

$$\Delta t = \min \left[\frac{V^{cell} \varepsilon^{cell} (1 - F^{cell})}{\sum_{nb} Fm_{nb}} \right] \quad (9.16)$$

where Fm_{nb} is the mass flux from neighboring cells. nb includes all the neighbors. By applying equation 9.16 to all cells (in practice this needs to be applied only to the front cells) the time step obtained is the minimum time to completely fill any one cell in the whole domain. After selecting a proper time step, new values of F at the front cells can be back calculated from equation (9.16) as:

$$F^{new} = \frac{V^{cell} \varepsilon F^{old} + (\sum_{nb} Fm_{nb}) \Delta t}{V^{cell} \varepsilon} \quad (9.17)$$

The new filled status of any front cells will be decided by comparing the values of the new calculated fluid volume fraction (F) with a base value (F^{base}) which is equal to 1. In practical calculations, rounding of errors always occurs. Therefore the value of F^{base} is normally set to a value close enough to one.

9.5 Iterative Scheme

Since all the governing equations are coupled, the discretized equations will be in the form of non linear algebraic equations. Therefore an iterative calculation will be used. A line by line tri-diagonal matrix algorithm (TDMA) has been adopted widely for solving the type of equations obtained in the discretized equations (Patankar, 1980). The main advantage of this algorithm is the low memory space required to store the values of variables and the coefficients. Therefore, even in the non reacting and isothermal problem where non-linear discretized equations will result, this iterative scheme also will be adopted. Adopting this scheme allows the solution of fairly complex geometries on a personal computer (PC).

The complete iterative scheme is described schematically in Figure 2. Different convergence criteria (Tol) can be defined. The simplest criterion is to stop the iteration when the values of the variables changing from two consecutive iterations is less then a pre-specified value. This criterion is generally used in the calculation.

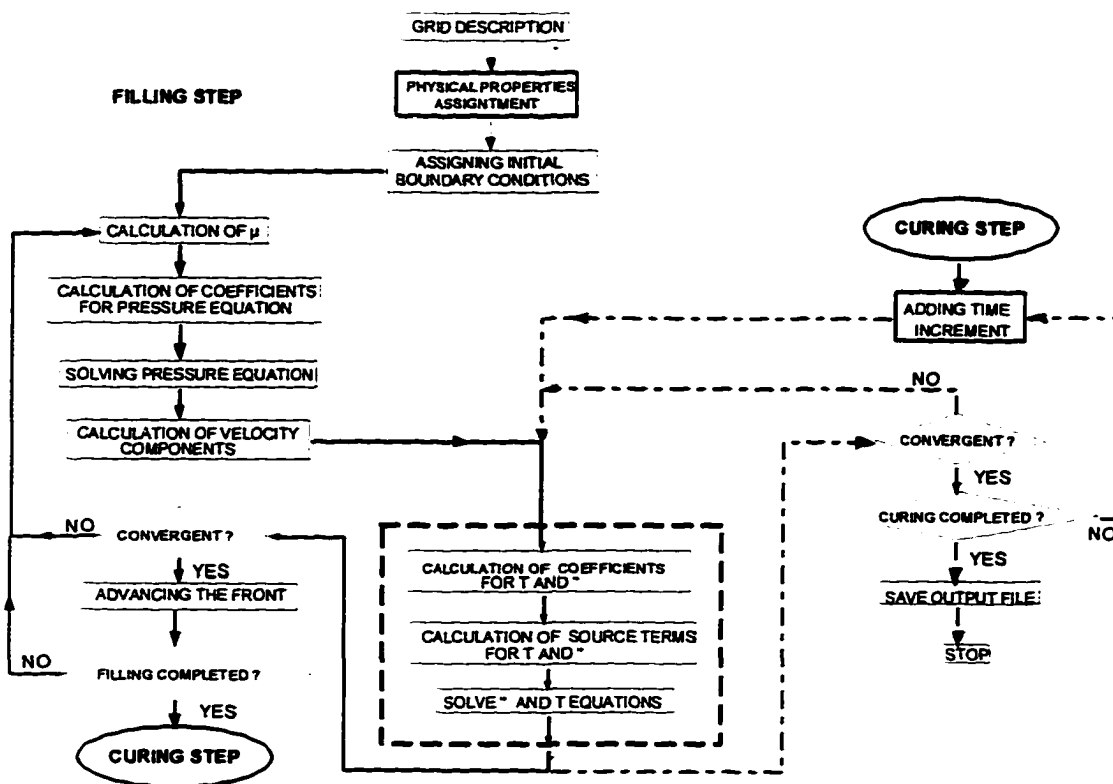


Figure 9.5 Iterative Algorithm

9.6 Programming Implementation

The numerical solution was coded on a Microsoft FORTRAN 4.0 project developer package (a trade mark of Microsoft Corporation) running on Windows 95. The most important feature of this FORTRAN compiler is that it permits the access of the memory for calculation that are only limited by the hardware (the size of hard disk (HD) memory plus the RAM). Since most new PC's come with HD around 2.5 giga byte, any practical problem can be solved on a PC relatively accurately, provided sufficient time is permitted. Another interesting feature of this compiler is the dynamic array. Using dynamic array, the required size memory is allocated only when it is needed, therefore no storage space is wasted if this feature

is implemented. Old versions of FORTRAN compilers only allowed the use of fixed arrays. If a fixed array is implemented, a pre-specified space should be allocated to store matrices and arrays and this remains fixed until the dimension statement is changed. The dynamic array was implemented, however, only for the post-processor program. The application of dynamic array for the whole program should be considered in the near future.

The skeleton of the program was originally obtained from Dr. Sumanta Acharya of the Mechanical Engineering Department and from the work by Lo et. al (1994 (a) and 1994 (b)). The program was modified for a specific application in SRIM modeling. The implementation of the multi-blocking approach is also included. The program allows the full solution of 3-D mold filling and curing. Important physical properties and the kinetic model have to be specified by the user. Non-isometric materials can be handled by the program by supplying different mechanical properties for different blocks. Finally the program can handle simple cylindrical coordinates as well as simple Cartesian coordinates. A complex geometry can be tackled by dividing it into several simple geometries. To handle this multiblock, users need only specify the interconnectivity information among the blocks. Iterative schemes among the blocks will be tackled by the program automatically. Boundary conditions can be supplied either in the form of constant values or constant wall fluxes.

The FORTRAN code of the program was stored in several separate files for easy management. The names of the files and their roles are listed in Appendix A.

In the next chapter, the program will be tested against some experimental data from literature. Comparison of the program with FE solutions for non isothermal reacting systems will also be performed. A sample of a relatively complex geometry (stub-flange) will follow. In this stub-flange example, the multiblocking approach will be illustrated. The implementation of coordinate mapping will not be done in this work. The illustration of this however is presented in the Appendix C. Here, the governing equation will be mapped and then rearranged in the form that is solvable by this program (Equation 9.1).

CHAPTER 10

MODEL VERIFICATION AND DEMONSTRATION

In this chapter analysis result of the FD program will be compared with FE analysis results published in the literature and where possible, with experimental data. A simulation on manufacturing a stub-flange with RTM will also be presented at the end of this chapter.

Some workers have conducted experimental verification for mold filling using non-reactive, isothermal fluids. Among those are Young et al. (1991), Gauvin et al. (1996), and Trochu et. al. (1993). The analysis results obtained using the model developed in this work will be compared to the experimental results obtained by Young et al. (1991). Early this year, a FE code for RTM mold filling was obtained from Dr. Frederick R. Phelan Jr. of National Institute of Standards and Technology (NIST). The code was designed to solve isothermal non-reacting mold filling for complex geometries and was originally run on workstations. The program was then compiled using Microsoft Fortran Powerstation® so that a comparison with the program developed in this work is possible. The FE program used flow analysis network (FAN) to track the front (Phelan, 1997).

Experimental data for non-isothermal reactive system mold filling such as those obtained by Lin et al. (1993) and Calhoun et al. (1996) are very rare. Lin's

data (Lin et al., 1993) were obtained from mold filling experiments using polyurethane. During the injections neither the pressure nor the flow-rate was constant, and the authors did not provide the quantitative profiles of either variable. It is impossible to simulate their experimental results without quantitative information on either the injection pressure or injection flowrate used in the experiment. Calhoun's experiments (Calhoun et al., 1996) used a RTM unit that is commonly used in the industry. As noted by Calhoun et al. (1996), it is necessary to scale up their FE and analytical results to match their experimental data. This uncertainty makes it difficult to simulate their data. As an alternative, the analysis results for reactive systems obtained from the developed model will be compared to FE analysis results from the literature.

10.1 Comparison with Experimental Data from Literature: Non Reactive System

Young et al. (1991) performed several mold filling experiments on a center-gated rectangular mold filled with random and bi-directional mats. The dimensions of the mold were 40 cm x 13.5 cm x 0.58 cm. The non reactive fluid used was diphenyl-octyl-phthalate (DOP) with a viscosity of 80 cp. The simulation was performed for Young's experiment with an inlet flow-rate of 22 ml/sec and a porosity 0.82 for a random mat. The permeability of the random mat (OCF-M8610) was calculated as a function of porosity and velocity. These equations are cited in Chapter 7 (equations 8.8 and 8.9). The gate pressure prediction given by

the 2-D and 3-D models developed in this dissertation and the experimental data are shown in Figure 10.1.

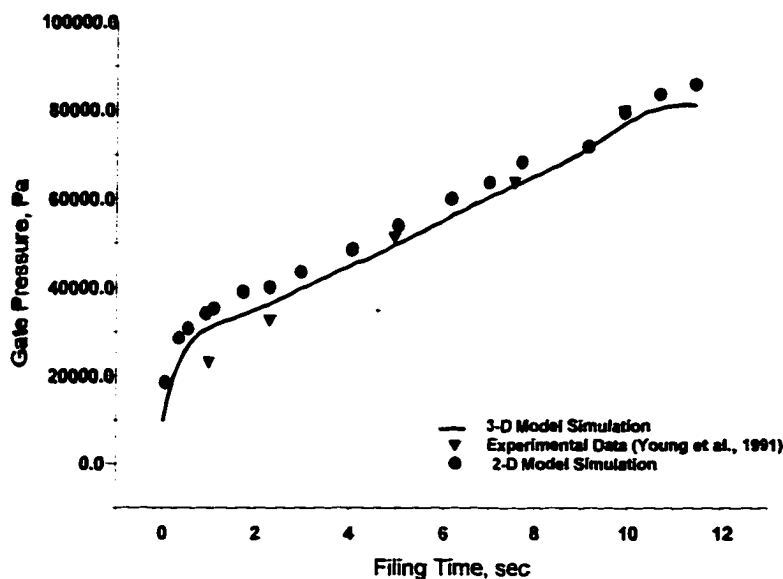


Figure 10.1 Simulation Results: Non Reactive System

Figure 10.1 shows that both the 2-D and 3-D models give reasonably good predictions of the experimental data. The calculation with the 2-D program was performed on 49×17 grids, while the 3-D solution was obtained using $33 \times 11 \times 3$ grids. Figure 10.2 shows a comparison of filling patterns obtained from the 2-D model using different grid sizes. It shows that both grid sizes give very similar patterns of filling, i.e. radial flow in the beginning and axial flow in the end. Figure 10.3 shows a comparison of filling pattern predictions by 2-D and 3-D model using a similar number of grid points. It shows that the models agree with each other very well.

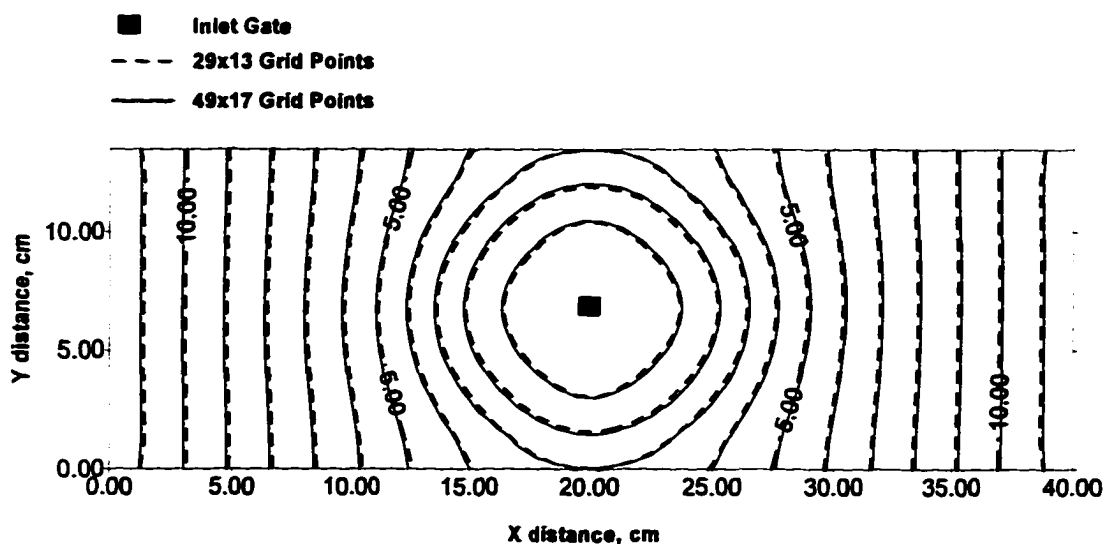


Figure 10.2 Filling Patterns: Effect of Grid Refinement

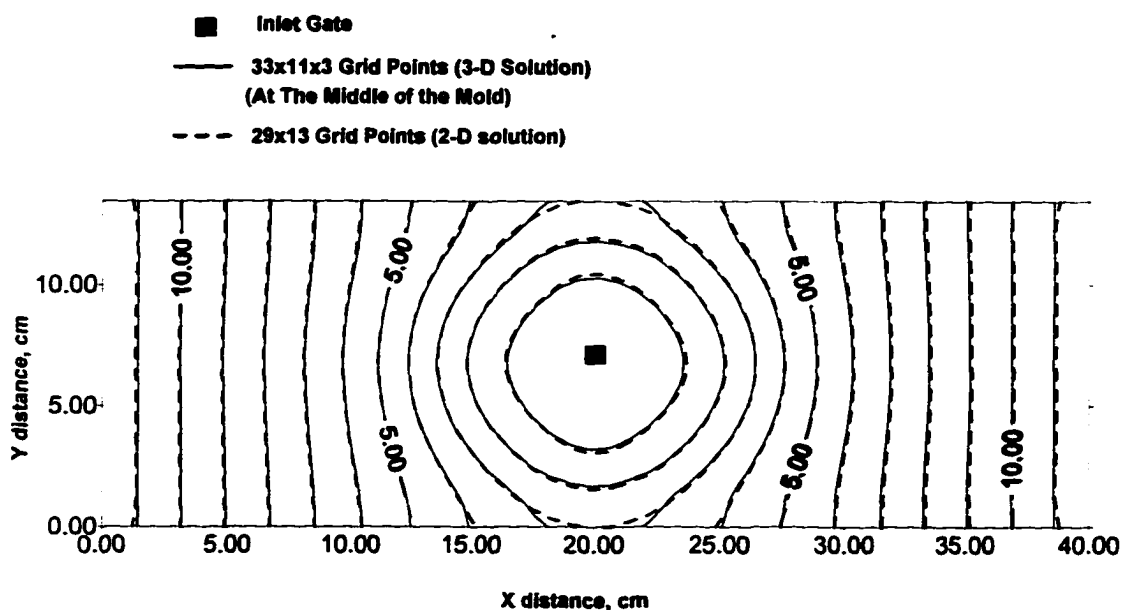


Figure 10.3 Filling Patterns: Comparison of 2-D and 3-D Model Predictions

10.2 Comparison with Results Obtained using NIST's FE Program

A 2-D FE mesh was created for a simple rectangular mold with the dimension of 29.76 cm x 251.5 cm on Geostar® [a platform (both a pre and post-

processor) to run FE analysis package Cosmos®; both are the trade marks of Structural Research and Analysis Corporation (SRAC)] . The total number of nodes and elements was 44 and 64, respectively. The mesh information was then translated into a Nastran (one of the most widely used FE code version) format that is readable by Dr. Phelan's code. Calculations were preformed using both NIST's FE program and the 2-D version of the FD code. The FD calculation was done on 14x12 grid points. The viscosity of the non-reactive fluid was 100 cp. The preform porosity was 0.8 and its isotropic permeability was 1.85×10^{-5} cm². The gate was located at one of the corners. The fluid injection was assumed to be a constant flow-rate of 10 ml/sec. By using a constant flowrate, the theoretical fill time can be computed since the cavity volume is known.

Both codes could predict the theoretical filling time accurately (i. e. 58.7 seconds). The slight difference in front location prediction, as shown in Figure 10.4, may be caused by the fact that in the FE code the constant flowrate boundary condition is treated as a point source in the corner node, while in the FD code the constant flowrate boundary condition is handled by equally distributing the flow over the area of the inlet gate (the corner control volume). The difference may also originate from the difference in locations to store the filling time information (the FE uses triangular elements with three nodes in each element; FD uses rectangular control volumes with one grid point in the middle of each control

.

volume). Gate pressure predictions from both codes are very close to each other as shown in Figure 10.5.

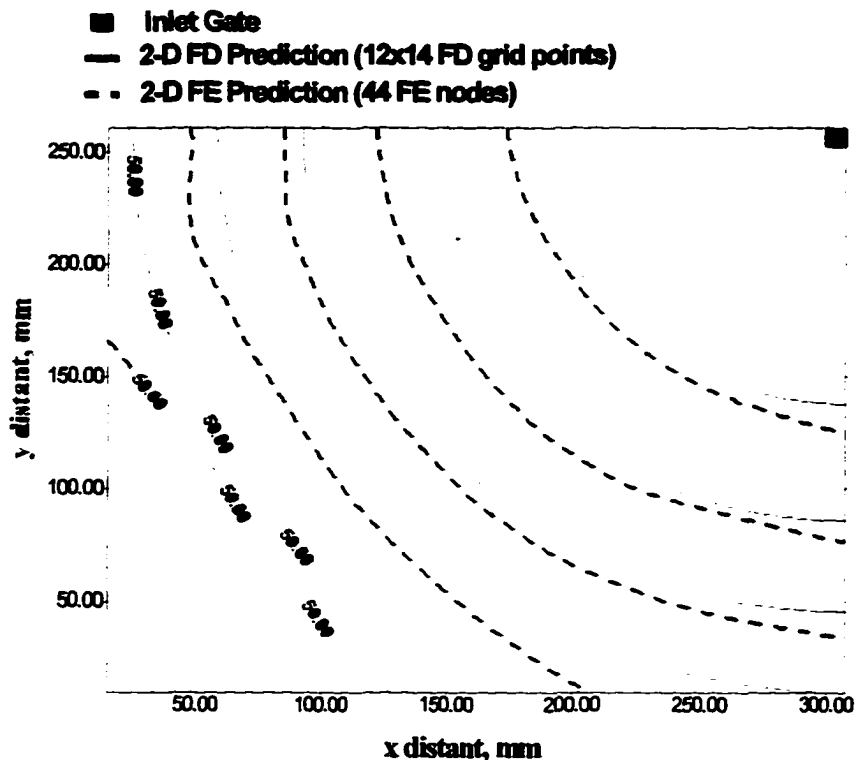


Figure 10.4 Comparison with NIST FE Solution: Filling Patterns

Overall, the FD and FE agreement is fairly good. It can be expected solutions obtained from both codes will match each other better with finer grids (mesh).

The run times of both programs are very similar for same number of nodes (grid points); for example for 44 grid points (nodes), run time for both programs is on the order of two seconds. Figure 10.6 shows run time versus number of grid

points for LSU's 2-D model. It shows that the run time increases significantly with number of grid points.

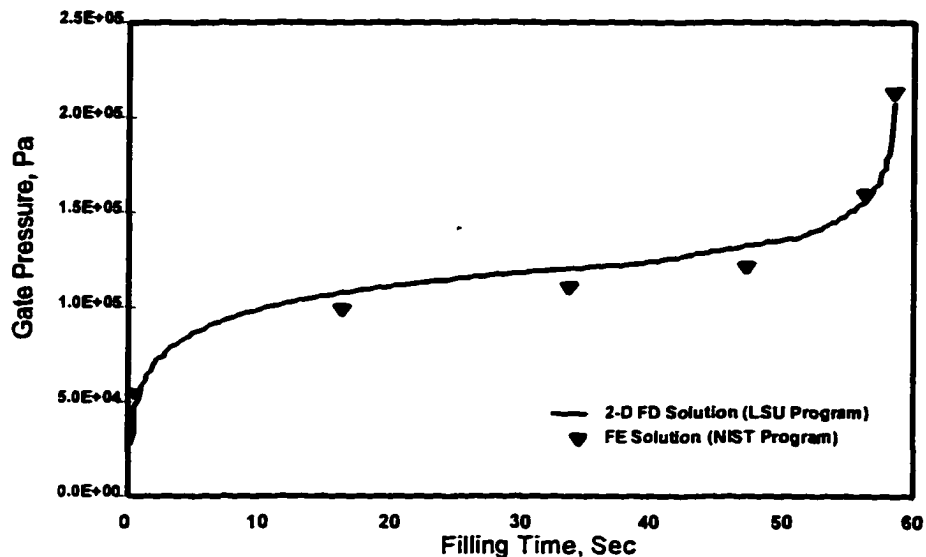


Figure 10.5 Comparison with NIST FE Solution: Gate Pressure Profiles

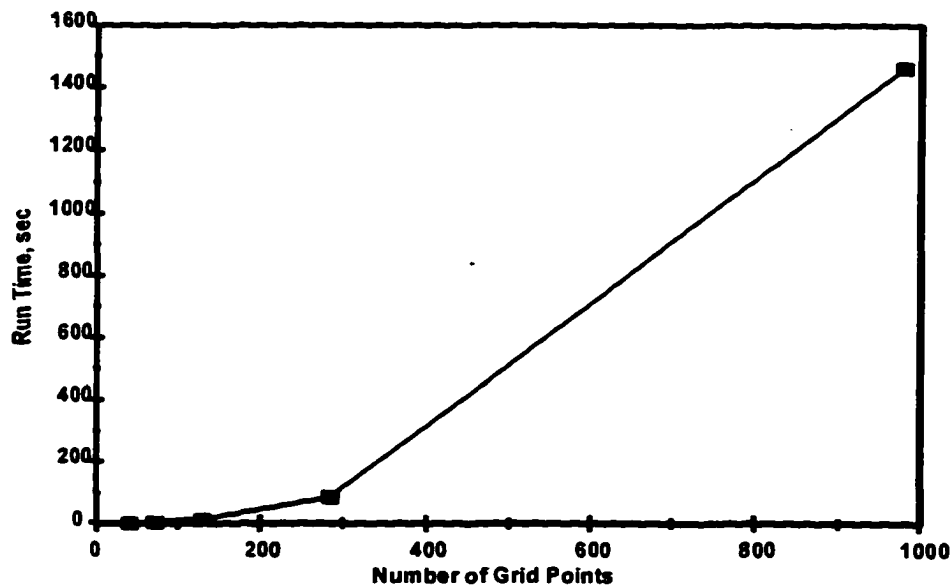


Figure 10.6 Run Time versus The Number of Grid Points for the 2-D Model

10.3 Mold Filling and Curing Simulation

Mold filling and curing simulation were performed on a 20 cm x 8 cm rectangular mold with 1 cm cavity thickness. The gate is located along one of the corners and has a constant pressure of 0.69 MPa. The mold and the preform temperatures were 60 °C prior to the injection of the liquid. In this simulation the effect of heat transfer and chemical reaction were taken into account. Kinetic and heat transfer data were obtained from an article by W.B. Young (1995). First, the problem was solved for a mold with an insulated (adiabatic) wall and the result compared to a non-flow adiabatic solution without heat transfer using a Runge-Kutta numerical method on a common mathematical software such as MathCad® (a trademark of MathSoft Inc.). Although the mold filling simulation takes into account the effects of fluid flow and heat transfer, the overall heat balance should be equal to the adiabatic non-flow solution because both assume no heat loss to the surroundings. The average temperature and conversion from the 3-D simulation should match the adiabatic solutions. Next, the simulation was performed for constant outside mold wall temperatures and the results were compared to the FE solution obtained by Young (1995).

The kinetic model for the resin is given by Equation 8.22 in Chapter 8. Temperature and kinetic influences on viscosity are given by:

$$\mu = A_\mu e^{\frac{E_u}{kT}} \left(\frac{\alpha_g}{\alpha_g - \alpha} \right)^{a+b\alpha} \quad (10.1)$$

where α_g is the gel conversion, E_u , A_μ , a , and b are constants determined experimentally. Thermal, kinetic and viscosity parameters are listed in Table 10.1 (Young, 1995).

In all of these simulations, the mold cavity was divided into $21 \times 9 \times 3$ control volumes along the width, length, and thickness. In cases where the mold is included, the top and bottom parts (both of 2 cm thickness) were divided into 4 control volumes in the thickness direction. The effect of the side walls was neglected in accordance with the solution in the reference article (Young, 1995). The mat was, according to the reference (Young , 1995), a bi-directional woven glass mat (TGFW-800) with a porosity of 0.8, and permeabilities in the transverse directions given by:

$$k_x = 8.85 \times 10^{-13} \times 10^{4.64\varepsilon} \text{ m}^2 \quad (10.2)$$

and

$$k_y = 3.59 \times 10^{-13} \times 10^{4.64\varepsilon} \text{ m}^2 \quad (10.3)$$

where ε is porosity. The mat principle directions are assumed to coincide with the coordinate axis directions.

Table 10.1 Thermal, Kinetic, and Rheological Parameters (Young, 1995)

Thermal Parameters	Kinetic Parameters	Viscosity
$C_{pr} = 1.680 \text{ (J/g}^{\circ}\text{C)}$	$A_1 = 3.783 \times 10^{-5} \text{ (l/sec)}$	$A_\mu = 2.78 \times 10^{-4} \text{ (Pa sec)}$
$C_{pr} = 0.670 \text{ (J/g}^{\circ}\text{C)}$	$A_2 = 6.783 \times 10^{-5} \text{ (l/sec)}$	$E_\mu = 18000 \text{ (J/mole)}$
$k_r = 0.168 \text{ (W/m}^{\circ}\text{C)}$	$E_1 = 54418 \text{ (J/mole)}$	$\alpha_g = 0.1$
$k_f = 0.0335 \text{ (W/m}_0\text{C)}$	$E_2 = 50232 \text{ (J/mole)}$	$a = 1.5$
$\rho_r = 1.1 \text{ (g/cm}^3)$	$m_1 = 0.3$	$b = 1.0$
$\rho_f = 2.560 \text{ (g/cm}^3)$	$m_2 = 1.7$	
	$\Delta H = 247.5 \text{ (J/cm}^3)$	

10.3.1 Adiabatic Solution

Since the density and heat capacity are constant, the temperature profile can be given in term of partial conversion as:

$$T = T_o + \frac{\epsilon \Delta H \alpha}{C_p \rho} \quad (10.4)$$

This equation can be substituted into equation (8.22) to obtain the conversion profile as function of time. This equation was solved as discussed using a Runge-Kutta method on MathCad® and the results at selected points are represented by the symbols in Figure 10.7. The initial temperatures of the resin and the mats were assumed to be 60°C.

The 3-D simulation was performed by assigning zero thermal conductivity on the wall. The calculation was performed from the beginning of the filling and then continued through the curing step until the partial conversion was close enough to 1. The simulation results are given by lines in Figure 10.7.

Figure 10.7 shows that the 3-D simulation results match the adiabatic solution well. Since the mold walls are assumed to be adiabatic, the total amount of heat inside the system is equal to the heat content inside an adiabatic system. The results in Figure 10.7 assure that the program gives the proper values for temperature as well as the partial conversion.

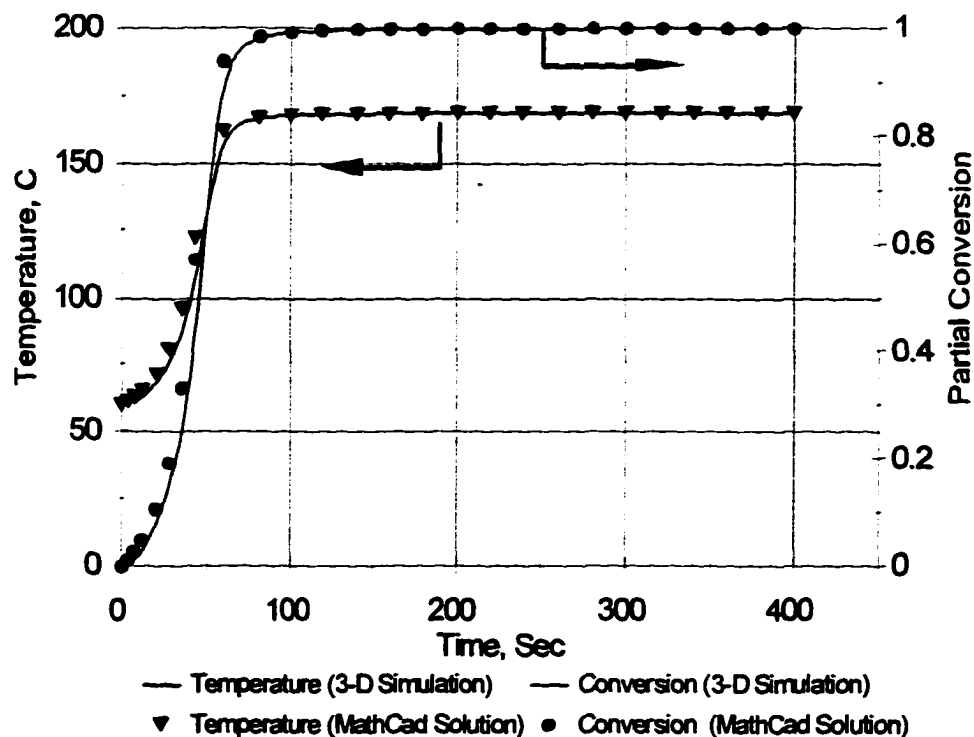


Figure 10.7 Adiabatic Mold Filling and Curing

10.3.2 The Mold Thermal Effect

The heat transfer contribution was determined by including the effect of the mold. Since the thickness dimension is much smaller than the other dimensions, the heat transfer is more pronounced in this direction. Therefore the effect of the side walls was neglected by simply setting the side wall temperatures to a constant 60 °C. The top and bottom outside surface temperatures of the mold were set to a constant 60 °C also. The initial resin temperature was 20 °C. The mold diagram is shown in Figure 10.8.

The simulation results (represented by lines in Figure 10.9) were compared to some selected results from FE analysis by Young (1995). Young solved the filling problem using a control volume FE on 2-D mesh. However, the heat conduction in the thickness direction was discretized using a FD expression (Young, 1995).

In the FD analysis, the mold cavity and the upper and bottom parts of the mold are included into one domain. The filling status of the mold grid points were set equal to a solid status. The program will not perform the filling calculation in grid points with solid filling status. The heat transfer calculation, however, was performed for the whole calculation domain.

The temperature profiles for points T1 and T2 (as shown in Figure 10.8) are plotted in Figure 10.9 along with several selected points from FE analysis obtained by Young (1995). Point T1 and T2 are located at the center of the mold cavity. T1 is

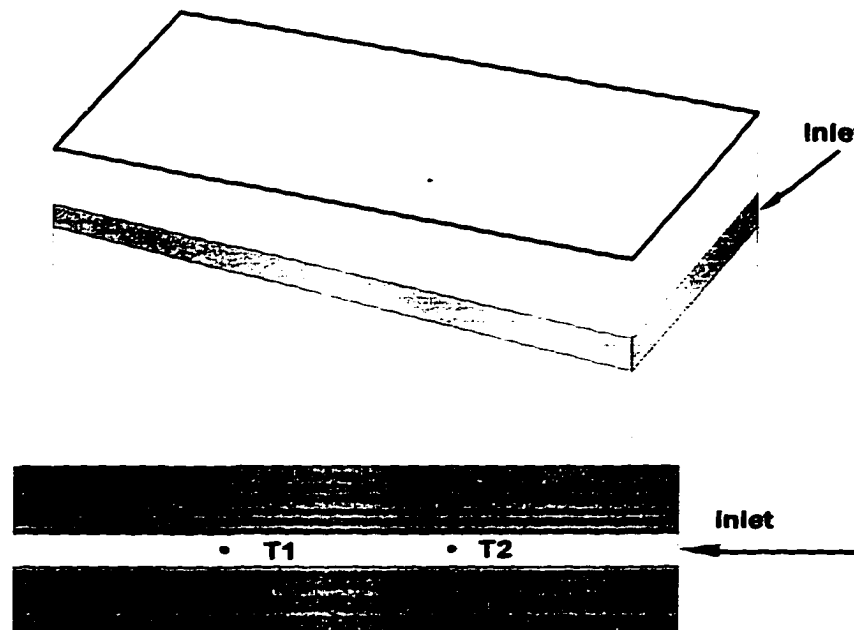


Figure 10.8 Young's Mold

located 14.28 cm from the inlet side, while T2 is located 7.14 cm from the inlet side.

Figure 10.9 illustrates that the FD and FE solutions show similar trends and similar shapes of curves. The FE solution curves reached the maximum faster than the FD solutions. This may either be because the FE solution got “extra heat” resulting from improper calculation of boundary conditions or the FD solution “lost some heat” from the same reason. To support this assertion, the problem was solved for two different inlet temperatures. As shown in Figure 10.10, increasing the inlet temperature from 20°C to 30°C , thus adding extra heat, speeds up the reaction significantly. Therefore the curve for the inlet temperature 30°C reaches the peak quicker than the curve for the 20°C inlet temperature. This trend is similar to what is observed in Figure 10.9.

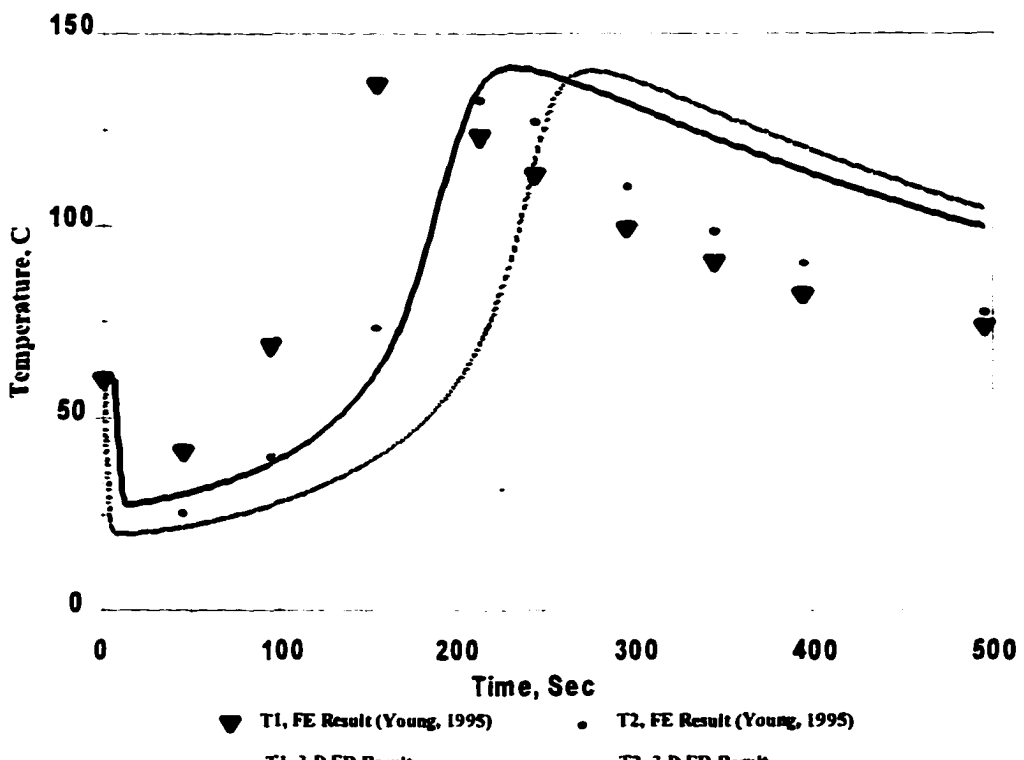


Figure 10.9 Non-isothermal Reactive Systems: A Comparison with FE Solution

10.4 Comparison with Molding Experimental Data with Cellulosic Preform

Several in-mold pressure measurements were done during the course of this work. These were mainly intended for preform permeability characterization. Typical pressure profiles are given in Figure 4.7. As indicated in the section discussing the kinetic study, the Spectrim® MM 310 reaction is very fast. Therefore, the viscosity should be influenced by the reaction during the mold filling. Since the viscosity-conversion relation for this chemical is not available, the simulation for the experimental data was done by lumping the permeability and viscosity into one factor, and it was assumed that an averaged value can be used for the calculation.

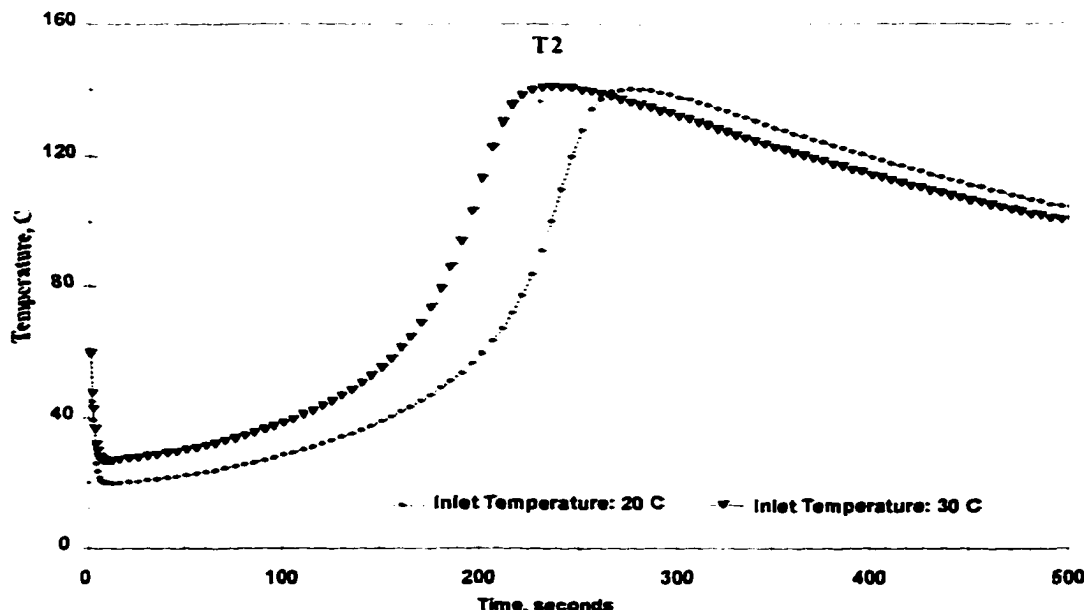


Figure 10.10 Non-isothermal Reactive Systems: Effect of Inlet Temperature

The detailed mold geometry is given in Figure 3.1. In these experiments, the center gate was used, and the triangular part surrounding the other gate was plugged. Therefore, the injection was done into a rectangular mold with a gate slightly off center. Figure 10.11 shows the simulation results for experimental data Sgc7 and Sgc 9. The figure shows that calculation results can at best match the order of magnitude of the experimental results. However it should be noted the viscosity is increasing during mold filling rather than having the assumed averaged value. Lower initial viscosities would cause the gate pressure to be lower initially. Furthermore, if the time scale of the experimental data is corrected by a certain factor, the calculation results will match the experimental data better. This time scale correction

may also indicate a slow response of the pressure transducer to the fast filling time.

The lumped permeability-viscosity parameters used in these calculation are:

$$\left(\frac{\kappa}{\mu}\right)_{Sgc7} = 1.76 \times 10^{-6} \text{ cm}^2 \text{ poise}^{-1}$$

and

$$\left(\frac{\kappa}{\mu}\right)_{Sgc9} = 3.367 \times 10^{-6} \text{ cm}^2 \text{ poise}^{-1}$$

These values show that the unexploded mat (Sgc7) has much less permeability compared to the steam exploded mat (Sgc 9).

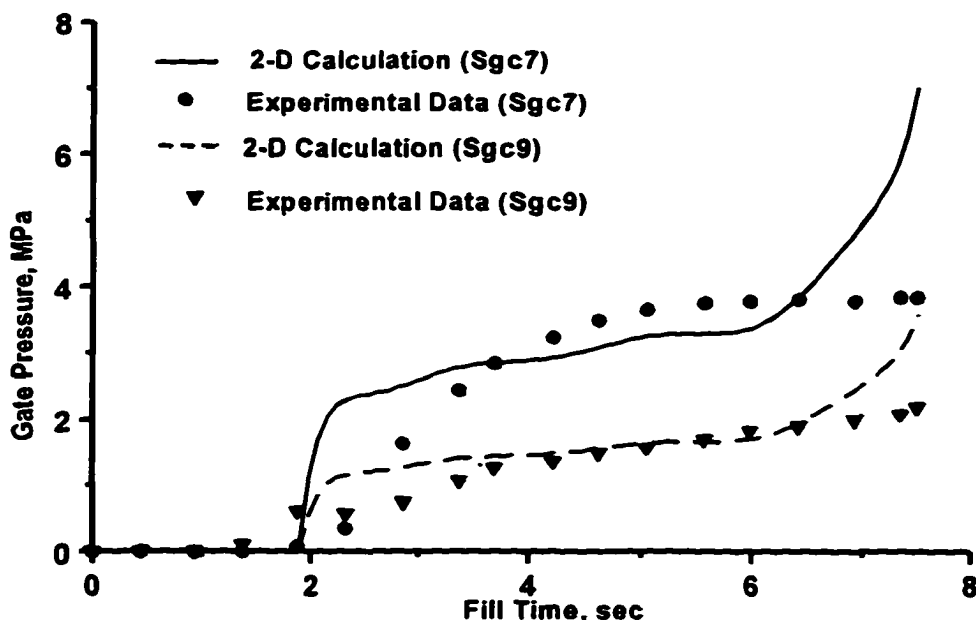


Figure 10.11 Molding Experimental Data with Sugar Cane Fiber

10.5 Simulation of Stub Flange Filling

All the simulations presented in the previous sections have dealt with simple rectangular geometries. In this section, a simulation on stub-flange

manufacture with RTM will be performed. The objective of this simulation is twofold. The first objective is to demonstrate the capability of the 3-D code developed in this work to handle a relatively complex geometry, and the second objective is to demonstrate a newly developed post-processor program to visualize the 3-D model results in 3-D space.

The post processor program is still in the early development stage. This section, presents some preliminary results of this work. The program will read the filling pattern information or other variables calculated using the 3-D model along with the geometry information, and then write a “M” file that can be executed on Matlab® (a trade mark of The MathWork, Inc.) platform by calling the name. An optional interpolation subroutine is also provided in the post processor. The interpolation could be performed prior to the Matlab® file creation. The interpolation is intended to refine the data grid points so that the visualization quality could be enhanced. This goal can be achieved only if the quality of data output from the numerical calculation is good as well. Matlab® will create a contour plot of the variable on the top of the 3-D geometry. More work needs to be done to improve the quality of the Matlab® display.

The calculation is performed in a cylindrical geometry. The geometry is then broken into three simple geometries (multiblocking) so that coordinate mapping is not required to handle the geometry accurately. For more complex

geometries both coordinate mapping and multiblocking may be necessary to achieve an accurate description of the physical geometry efficiently. Efficient in this context means that the required data space and computation effort are kept as low as possible. The discretized geometry and the multi-blocking method for the stub-flange are illustrated in Figure 10.11.

The inner diameters of both the flange and the pipe are 4 inches, and the outside diameters of the flange and the pipe are 9.5 inches and 5.5 inches, respectively. The pipe length is 6 inches and the total length of the stub-flange is 6.75 inches. The preform mat is a random mat with an isotropic permeability of $6 \times 10^{-6} \text{ cm}^2$. Since RTM reactions are normally much slower compared to SRIM reactions, the resin viscosity of 1.0 poise is assumed to be constant during the mold filling; therefore, the calculations of temperature and species concentration are not necessary. The injection was at a constant flowrate of $6 \text{ cm}^3/\text{sec}$. This flowrate may be distributed into several gates.

The filling pattern for two-pipe inlet gates is given in Figure 10.13. The reason to chose the inlet gates in the pipe is that the last part to be filled will be the flange side thereby the void trapping inside the pipe-flange connection will be minimized. This objective seems to be achieved. As shown in Figure 10.13, the front moves out of the pipe side almost in a plug flow manner and the flange side is filled almost at the same time. The gate location chosen however is not

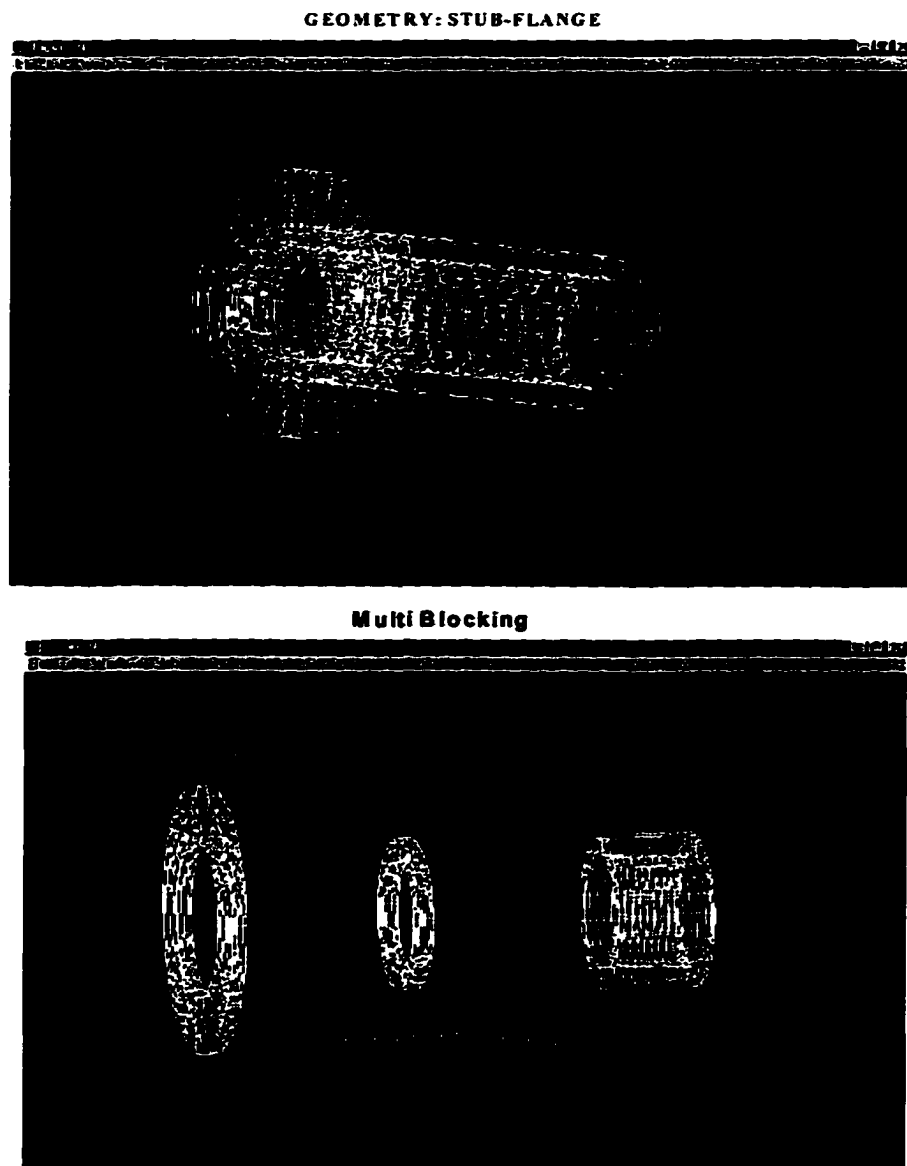


Figure 10.12 Matlab Screen Capture: Discretized Geometry and Multi-Blocking of Stub Flange

necessarily the best option if the injection pressure is the criterion. Lower injection pressures to fill the mold cavity in a given filling time are better. Similar

simulations can be performed using the 3-D program until the appropriate design criteria can be met.

It is important to note that the contour line in Figure 10.13 is not smooth. This is the result of the discrete approach in the FD analysis. This contour could be smoothed out by selecting more appropriate interpolation methods, or by a subsequent smoothing sub-routine. Although an optional interpolation sub-routine has been added into the program, full advantage from it can not be achieved without the ability to control line density. Simply displaying all the contour line on the screen will make the 3-D graph very messy in the area where the variable changes very quickly. Therefore extra work needs to be done to achieve this.

Screen Capture of The Matlab Display**Figure 10.13 Simulation Result: Filling Patterns**

CHAPTER 11

MODELING CONCLUSIONS

All of the simulations performed in Chapter 10 show that the FD control volume program gives good predictions for experimental results, as well as some of the FE solutions. Differences in prediction values between the FD solution and the FE solution may be caused by the different ways to store the variables. This may be the case for the trend observed in Figure 10.4. Figure 10.4 shows that there is slight difference in the detailed front locations versus time predicted by FE and FD analysis although both models predict the same overall filling time. This type of difference should diminish as the number of nodes used in the calculation increases.

The difference in the temperature prediction by the FD code and FE solutions from literature may be caused by more serious problems. In section 10.3.1, the prediction from the FD program was compared with the numerical solution for an adiabatic system by neglecting the heat transfer and flow effects. Both solutions are in excellent agreement. The same FD program was used to simulate Young's problem (Young, 1995) except that heat conductivities at the walls were set to non-zero values. The FD program gave a different prediction from the FE solution obtained by Young, although both solutions gave the same curve shapes. To assure

that the FD program predict the curing step properly, more comparison with experimental data or with other FE predictions should be done.

An attempt was made to simulate some experimental data obtained in this work. The model can at best give only an order of magnitude of the pressure profile experimental data. The predicted pressure profiles will be closer to experimental if the dependencies of viscosity and permeability on conversion are known and if a correction factor were subtracted from the time scales. This may show that the pressure reading system used in the experiment responds too slowly to the fast pressure change inside the mold.

The role of 3-D simulation and visualization in mold RTM design was also demonstrated in this chapter. Multiblocking is able to handle complex geometries that can be divided into several simple regular geometries. For more complex irregular geometries, BFCS and coordinate transformation may be needed. Accurate visualization of calculation results is as important as the calculation method itself, because only by an accurate display of the results in the most appropriate way can a correct interpretation of the result be made. The post processor program developed in this work is expected to play this role although some improvement is needed, notably a more precise control of the color associated with a certain variable value.

CHAPTER 12

MODELING RECOMMENDATIONS

Memory requirement is one of the major concerns in any PC application. Although current operating systems for PC's allow practically unlimited access of the available memory [hardisk (HD) and random access memory (RAM)], efficient memory usage is of practical importance. The access of HD is usually several orders of magnitude slower than RAM access. Therefore, a program with more efficient memory management runs faster than a program with a poor one. Except for the post processor part, the computer code written as part of this work still uses static arrays and matrices. Clearly the first important improvement to the program is to limit the usage of static arrays to the minimum (because this type of array can not be removed completely), and to use more dynamic arrays.

The second improvement to the program is to equip the program with a grid generation package that will allow more accurate modeling of a physical geometry. Grid generation is usually not separate from coordinate transformation. By adding a coordinate transformation option to the program, complex geometries can be solved with a simple general algorithm because the calculation domain is always Cartesian geometry.

The third improvement needed is in the post processing area. This work demonstrated that a good PC based 3-D RTM/SRIM model (including numerical

solution and visualization) could be developed by utilizing widely available commercial applications for PC's. Further work should also include the visualization aspect. Mastering "color algebra" in Matlab® is necessary to accomplish this goal. With the improvement of this aspect and the other two mentioned previously, the developed program will be a more efficient PC based SRIM/RTM model.

Experimental verification is an important aspect in any model development. From experiments conducted in this work and from the literature, it is noted that obtaining quantitatively accurate experimental data for reactive mold filling is very difficult. This is caused partly by the fast mold filling process and also caused by the slow response of data reading systems used in the experiment. In order to be able to interpret experimental data properly, quantitative information on the data reading system response delays is necessary. A study in this field with a specific RTM/SRIM application will be useful for both research and industrial applications.

REFERENCES

- Agarwal, P., Textile Fibers from Sugar Cane, Unpublished MS. Thesis, Louisiana State University (1992).
- Baser, S.A., D.G. Shetty, and D.V. Khakhar, "Jet Impingement Mixing in an L. Type Mixhead: Comparison of Mixing Criteria", Polymer Engineering & Science, 33(24), 1611-1618 (1993).
- Berin, M.L., SPI Plastic Engineering Hand Book, Fifth Edition, Van Nostrand Reinhold, New York.
- Birch, A.J., J.L. Stanford, and A.J. Ryan, " The Effect of Hard Segment Content on Microphase Separation and Physical Properties of Non-Linear-Segmented Copolyureas Formed by RIM", Polymer Bulletin, 22, 629 635 (1989).
- Bird, R.B., W.E. Stewart and E.N. Lightfoot, Transport Phenomena, John Wiley & Sons, New York (1960).
- Boukolbal, S., S. Fellahi, and M. Litim, " Study of Geometrical and Processing Parameters Effect on Impingement Mixing in Reaction Injection Molding", SPE Antez Tech. Papers, 35, 826-829 (1989).
- Brandrup, J., and E.H. Immergut, Polymer Handbook, John Wiley & Son , New York (1989).
- Brunelte, C.M., S.L. Hsu, and W.J. Mac Knight, "Hydrogen-Bonding Properties of Hard Segment Model Compounds in Polyurethane Block Copolymers", Macromolecules, 15, 71-77 (1982).
- Cai, Z., and A.L. Berdichevsky, " Numerical Simulation on the Permeability Variations of a Fiber Assembly", Polymer Composites, 14(6), 529-539 (1993).
- Cai, Z., and A.L. Berdichevsky, " Estimation of the Resin Flow Permeability of Fiber Tow Preforms Using the Self-Consistent Method", Polymer Composites, 15(3), 240-246 (1993).

- Calhoun, D.R., S. Yalvac, D.G. Wetters, C.H. Wu, T.J. Wang, J.S. Tsai, and L.J. Lee, "Mold Filling Analysis in Resin Transfer Molding", Polym. Comp., 17(2), 251-264 (1996).
- Camberlin, Y., and J.P. Pascault, "Quantitative DSC Evaluation of Phase Segregation Rate in Linear Segmented Polyurethane and Polyureas", J. Polym. Sci. : Polym. Chem. Ed., 21, 415-423 (1983).
- Chen, T.Y., and V.W. Wang, " A Unified Simulation For Reactive Polymer Processing: RIM, SRIM and RTM", SPE Antez Tech. Papers, 39, 2421-2425 (1993).
- Chen, Y., Textile Application of Sugar cane Fibers, MS. Thesis, Louisiana State University (1993)
- Chick, J.H., C.D. Rudd, P.A. Van Leeuwen, and T.I. Frenay, Polym. Comp., 17(1): 124-135 (1996)
- Cividini, A., and G. Gioda, " An Approximate F.E. Analysis of Seepage with a Free Surface", Int. J. for Num. Analyt. Meth. in Geomechanics, 8, 549-566 (1984).
- Coleman, M.M., K.H. Lee, D.J. Skrovanek, and P.C. Painter, " Hydrogen Bonding in Polymers. 4. Infrared Temperature Studies of a Simple Polyurethane", Macromolecules, 19, 2149-2157 (1986).
- Collier, J.R., M. Lu, M. Fahrurrozi, and B.J. Collier, "Cellulosic Reinforcement in Reactive Systems", J. Appl. Polym. Sci., 61, 1423-1430 (1996).
- Collier, J.R., and B.J. Collier, Cellulose/Polymeric Composites, LEQSF Proposal (1993).
- Collier, B.J., J.R. Collier, P. Agarwal, and Y.W. Lo, "Extraction and Evaluation of Fibers from Sugar Cane", Textile Res. J., 62 (12), 741-748 (1992).
- Dean, J.A., Handbook of organic Chemistry, McGraw-Hill (1987).
- Eagles, D.B., B.F. Blumentritt, and S.L. Cooper, " Interfacial properties of Kevlar-49 Fiber-Reinforced Thermoplastics", Journal of Applied Polymer Science, 20, 435-448 (1976).

- Elsunni, M.M., J.R. Collier, "Processing of Sugarcane Rind into Non-Woven Fibers", J. American Soc. of Sugar Cane Tech., 16, 94-110 (1996).
- Elsunni, M.M., Processing of Sugar cane Rind into Textile, Unpublished MS Thesis, Louisiana State University (1993).
- Feldman, D., and M.A. Locasse, " Polymer-Filler Interaction in Polyurethane Kraft Lignin Polyblends", Journal of Applied Polymer Science, 51, 701-709 (1994).
- Finlayson, B.A., Numerical Methods For Problems With Moving Fronts, Ravenna Park Publishing, Inc., Seattle (1992).
- Freitas, C.J., "Perspective: Selected Benchmarks From Commercial CFDS Codes", J. of Fluids Eng., 117 (1995).
- Friedrichs, B., and S.I. Guceri, "A Hybrid Numerical Technique to Model 3_D Flow Fields in Resin Transfer Molding Processes", Polymer Engineering and Science, 35, 1834-1851 (1995).
- Furukawa, M., and T. Yokoyama, Journal of Applied Polymer Science, 53, 1723 (1994)
- Gao, Y., Y.Y. Xiu, Z.Q. Pan, D. Wang, C.P. Hu, and S.K. Ying, " Effect of Aromatic Diamine Extenders on The Morphology and Property of RIM Polyurethane-Urea", Journal of Applied Polymer Science, 53, 23-29 (1994).
- Gauvin, R., F. Trochu, Y. Lemenn, and L. Diallo, "Permeability Measurement and Flow Simulation Through Fiber Reinforcement", Polym. Comp., 17(1), 34-42 (1996)
- Gonzalez-Romero, V.M., and C.W. Macosko, "Adiabatic Filling Packed Beds in Composite Reaction Injection Molding", Polym. Process Eng., 3(1&2), 173-184 (1985).
- Grulke, E.A., Polymer Processing, PTR Prentice Hall, New Jersey (1994).

Guceri, S.I , Finite Difference Solution, Chapter 5 of Computer Modeling for Polymer Processing Fundamentals, Hanser Publisher, Munich (1989).

Gum, W.F., W. Riese, and H. Ulrich (Editors), Reaction Polymers, Hanser Publisher, Munich (1992).

Hedenberg, P. and P. Gatenholm, "Conversion of Plastic/Cellulose Waste into Composites. I. Model of the Interphase", J. of App. Polym. Sci., 56, 641-651 (1995).

Hirt, C.W., and B.D. Nichols, " Volume of Fluid (VOF) Method for Dyanamics of Free Boundaries", Journal of Computational Physics, 39, 201-225 (1981)

Hon, D.N.S., and N. Shiraishi (Editors), Wood and Cellulosic Chemistry, Marcel Dekker Inc., New York (1991).

Kamal, M.R., M.E. Ryan, Models of Material Behavior, Chapter 2 of Computer Modelling for Polymer Processing Fundamentals, by C. L. Tucker III (Editor), Hanser Publisher, Munich (1989).

Kontou, E., G. Spathis, and M. Ni, "Physical and Chemical Cross-Linking Effects in Polyurethane Elastomers", Colloid Polym. Sci., 268, 636-644 (1990).

Lam and J.L. Kardos, R.C., " The Permeability and Compressibility of Aligned and Cross-Plied Carbon Fiber Beds During Processing of Composites", SPE Antez Tech. Papers, 35, 1408-1412 (1989).

Lee, H.S., Y.K. Wang, W.J. Macknight, and S.L. Hsu, "Spectroscopic Analysis of Phase-Separation Kinetics in Model Polyurethane", Macromolecules, 21, 270-273 (1988).

Lee, H.S., Y.K. Wang, and S.L. Hsu, "Spectroscopic Analysis of Phase Separation Behavior of Model Polyurethanes", Macromolecules, 20, 2089-2095 (1987).

Liang, E.W., H.P. Wang, and E.M. Perry, "An Integrated Approach for Modeling the Injection Compression, and Resin Transfer Molding Processes for Polymer" , Advances in Polymer Technology, 12(3), 234-282 (1993).

- Lin, R.J., L.J. Lee, and Ming J. Liou, "Mold Filling and Curing Analysis in Liquid Composite Molding", Polymer Composites, 14(1), 71-81 (1993).
- Lindsay, K.F., "Automation of Preform Fabrication Makes SRIM Viable for Volume Parts", Modern Plastics, 70(13), 48 (1993)
- Lo, Y.W., D.D. Reible, J.R. Collier, and C.H. Chen, "3-Dimensional Modelling of Reaction Injection Molding 1.", Polymer Engineering and Science, 34(18), 1393-1400 (1994a).
- Lo, Y.W., D.D. Reible, J.R. Collier, and C.H. Chen, "3-Dimensional Modelling of Reaction Injection Molding 2: Application", Polymer Engineering and Science, 34(18), 1401-1405 (1994b).
- Lo, Y.W., Three-Dimensional Modelling of Reaction Injection Molding, Unpublished PhD. Dissertation, Chemical Engineering, LSU (1991).
- Luo, N., Z. Pang, D. Wang, and S. Ying, "The Effect of Catalyst Concentration on The Structure and Properties of Polyurethane-urea Elastomers Produced by Reaction Injection Molding", Polymer Science, Ser. B, 36(5), 683-686 (1994).
- Macosko, C.W., RIM: Fundamental of Reaction Injection Molding, Hanser Publisher, New York (1989).
- McGeehan, J.A., and J.W. Gillespie, J.R., "Processing Performance Relationships Considering Voids in Structural Reaction Injection Molding", Polymer Engineering and Science, 33(24), 1627-1633 (1993).
- Meister, J.J., and F.F. Chang, "Polyol Prepolymers from Natural Products and Their Use in Urethane", SPE Antez Tech. Papers, 38, 1481-1483 (1992).
- Methews, F.L., and R.D. Rawlings, Composite Materials: Engineering and Science, Chapman & Halls (1994).
- Michaeli, W., and Th. Gernot, "New Software Tools For The Filling Simulation of Thermosets", SPE Antez Tech. Papers, 39, 2406-2414 (1993).
- Pannone, M.C., C.W. Macosko, "Kinetic of Isocyanate Reaction", Journal of Applied Polymer Science, 34, 2409-2432 (1987).

Patankar, S.V., Numerical Heat Transfer and Fluid Flow, Hemisphere Publishing Co. (1980).

Peebles, S.M., and A.B. Corripi, "Transient Temperature Model for Reaction Injection Molding", AIChE J., 41(5): 1273-1280 (1995)

Peebles, S.M., Control of One Percent Yield Offset In reaction Injection Molding, Unpublished PhD. Dissertation, Louisiana State University (1994).

_____, Personal Communication with Mr. Roy Morgan of Dow Chemical, Freeport, Texas.

_____, Personal Communication with Dr. Ioan Negulescu of School of Human Ecology , Louisiana State University (1993).

Pittman, J.F.T. , Finite Element for Field Problems, Chapter 6 of Computer Modeling for Polymer Processing Fundamentals, Hanser Publisher, Munich (1989).

Progelhof, R.C., J.L. Throne., Polymer Engineering Principles, Hanser Publisher, Munich (1993).

Richardson, M.O.W., Polymer Engineering Composites, Applied Science Publisher LTD., London (1977).

Rogers, J.K., "RTM and SRIM - ready for main stream Market ?", Modern Plastics, 67(12), 44-48 (1990).

Romanoschi, O., S. Romanoschi, J.R. Collier, and B.J. Collier, "Kenaf Alkali Processing", Accepted for Publication in Cellulose Chemistry and Technology (1997a).

Romanoschi, O., S. Romanoschi, J.R. Collier, and B.J. Collier, "Optimization of Process Variables for the Atmospheric Pressure Delignification of Sugar Cane Rind", Accepted for Publication in Cellulose Chemistry and Technology (1997b).

- Ryan, A.J., J.L. Stanford, and R.H. Still, "Thermal and Mechanical Properties of Reaction Injection-Molded Poly(urethane-urea)s", Polymer, 32 (8), 1426-1439 (1991).
- Ryan, A.J., J.L. Stanford, and A.J. Birch, "Copolyureas Formed by Reaction Injection Molding: Correlation Between Chemical Structure, Thermal Properties and Microphase Separation", Polymer, 34, 4874-4881 (1993).
- Ryan, A.J., "Spinodal Decomposition During Bulk Copolymerization Reaction Injection Molding", Polymer, 31, 707-712 (1990).
- Silverstein, R.M., G.C. Bassler, T.C. Morril, Spectrometric Identification of Organic Compound, John Wiley & Sons Inc., New York (1991).
- Skartis, L., J.L. Kardos, and B. Khomami, "Resin Flow Through Fiber Beds During Composites Manufacturing Processes, Part I: Review of Newtonian Flow Through Fiber Beds", Polymer Engineering and Science, 32(4), 221-230 (1992).
- Skartis, L., B. Khomami, and J.L. Kardos, "Resin Flow Through Fiber Beds During Composites Manufacturing Processes, Part II: Numerical and Experimental Studies of Newtonian Flow Through Ideal and Actual Fiber Beds", Polymer Engineering and Science, 32(4), 231-239 (1992).
- Spathis, G., M. Niaounakis, E. Kontou, L. Apekis, P. Pissis, and Christodoulides, "Morphological Changes in Segmented Polyurethane Elastomers by Varying the NCO/OH Ratio", Journal of Applied Polymer Science, 54, 831-842 (1994).
- Spiegelhoff, T.J., and T.A. Osswald, "Modelling and Simulation of High Reynold Number Flows During Reaction Injection Mold Filling", SPE Antez Tech. Papers, 39, 2415-2420 (1993).
- Stanford, J.L., "Rheological and Mechanical Property Studies on Polyurethane Composite Materials Formed by Reaction Injection Molding (RIM)", New Polymer Technology For Auto Body Extensions, AIChE Symposium Series no 260, Vol 84, AIChE, New York (1988).

Tadmor, Z., and C.G. Gogos, Principles of Polymer Processing, John Wiley & Sons, NY (1979)

Tao, W., Interfacial Adhesion in Rayon/Nylon Sheath/Core Composites Fibers, Unpublished PhD. Dissertation, Louisiana State University (1991).

Tortora, P.G., and B.J. Collier, Understanding Textiles, Prentice-Hall, Inc., NJ (1997).

Trevino, L., K. Rupel, W.B. Young, M.J. Liou, and L.J. Lee, "Analysis of Resin Injection Molding in Mold, with Preplaced Fiber Mats, I: Permeability and Compressibility Measurement", Polymer Composites, 12(1), 20-29 (1991).

Trochu, F., R. Gauvin, and D.M. Gao, "Numerical Analysis of the Resin Transfer Molding Process by the Finite Element Method", Advances in Polym. Technology, 12(4), 329-342 (1993).

Trochu, F., and R. Gauvin, "Limitations of a Boundary-Fitted Finite Difference Method for Simulation of the Resin Transfer Molding Process", J. of Reinf. Plastics and Comp., 11(7), 772-786 (1992).

Trezvova, A.V., O.G. Fortunatov, E.V. Zolotova, V.V. Orlov, and D.Y. Korol'kov, "The molecular structure of Block copolyurethanes as related to the synthetic Procedure Used for Their Preparation", Polymer Science, Ser. A, 36(8), 1047-1049 (1994).

Valenti, M., "Resin Transfer Molding Speed Composite Making", Mechanical Engineering, November (1992).

Viola, G.G., and W.R. Schmeal, "Isocyanate Trimerization Kinetics and Heat Transfer in Structural Reaction Injection Molding", Polymer Engineering & Science, 34(15), 1173-1186 (1994).

Wang, H.P. and H.S. Lee, Numerical Techniques for Free and Moving Boundary Problems, Chapter 8 of Computer Modeling for Polymer Processing Fundamentals, Hanser Publisher, Munich (1989).

Whitaker, S., "Local Thermal Equilibrium: An Application to Packed Bed catalytic Reactor Design", Chem. Eng. Sci., 41(8): 2029-2039 (1986)

Whitaker, S., "Improved Constraints for The Principle of Local Thermal Equilibrium", Ind. Eng. Chem Res., 30: 983 (1991)

Wilder, R.V, "Resin Transfer Molding Finally Gets Some Real Attention from Industry", Modern Plastics, July (1989).

Williams, J.G., C.E.M. Morris, and B.C. Ennis, " Liquid Flow Through Aligned Fiber Beds", Polymer Engineering and science, 14(6), (1974).

Williams, M.A., B.D. Bauman, and D.A. Thomas, " Incorporation of surface modified UHMWPE Powders and Fibers in Tough Polyurethane Composites", Polymer Engineering and Science, 31(13), 992-998 (1991).

Wu, S., Polymer Interface and Adhesion, Marcel Dekker Inc., NY (1982)

Yokoyama, T., and M. Furukawa, " Model polyurethane network: Dependence of Elastomeric properties on Chain Length distribution and Polar Group Concentration", Journal of Applied Polymer Science: Applied Polymer Symposium, 50, 199-211 (1992).

Young, R.A, and R.M. Rowell (editors), Cellulose Structure, Modification and Hydrolysis, John Wiley & Sons, New York (1986).

Young, W.B., " The Effect of Surface Tension on Tow Impregnation of Unidirectional Fibrous Preform in Resin Transfer molding", J. of Comp. Materials, 30(11):1191-1209 (1996)

Young, W.B., " Thermal Behavior of The Resin and Mold in the Process of Resin Transfer Molding", J. of Reinf. Plastics and Comp., 14 (4), 310-332 (1995).

Young, W.B., "Gate Location Optimization in Liquid Composite Molding Using Genetic Algorithms", J. of Comp. Material, 28(12) -1098-1113 (1994).

Young, W.B., K. Rupel, K.Han, J.M. Lee, and M.J. Liou, " Analysis of Resin Injection Molding in Mold, with Preplaced Fiber Mats, II: Numerical Simulation and Experiments of Mold Filling", Polymer Composites, 12(1), 20-29 (1991).

APPENDIX A

COMPUTER PROGRAM STRUCTURE

Both the 3-D and 2-D versions of the program were written in FORTRAN and were compiled using Microsoft FORTRAN Powerstation version 4.0. The program is grouped into several files according the tasks that need to be done. Each file usually contains at least one subroutine, and each subroutine can have one or more callable entry (s). One group of files is shared by users because they do a general task, and another group are user defined to accommodate types of problems to be solved. Although the user defined subroutines require the user to write few lines of computer code to solve the problems, effort has been done to put default options and parameters as much as possible so that the user effort could be minimized.

The files of the 3-D version of this program are:

1. SHARED FILES:

BLMAIN.FOR¹: Main program that manage all the Subroutine.

BLSETUP.FOR: Controlling the iteration calculation.

BLCOEFF.FOR: Calculation of coefficients for the discretized equation.

¹ Files names start with BL refer to multiblocking capability as explained in Chapter 10

BLDEFAULT.FOR: Assigning default values for the variable. Impose default boundary conditions and cell filling status.

BLFRONT.FOR: Tracking the front location.

BLSUPPLY.FOR: Writing the output files for post processing

2. USER DEFINED FILES:

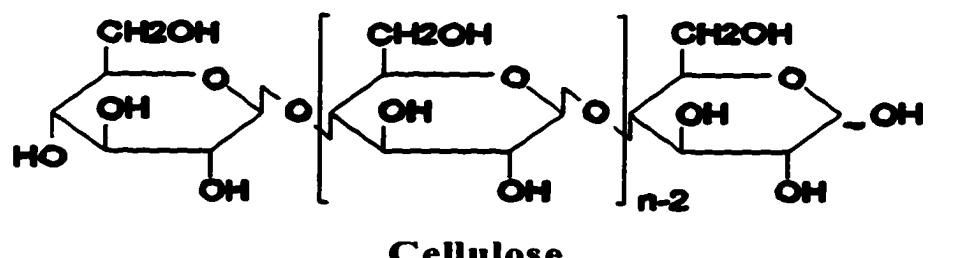
BLGRID.FOR: Inputting the grid and geometry information. The user first step in solving any problem is to input grid information.

BLUSER.FOR: Assigning physical properties. Non-default boundary conditions. This is the second step in solving a problem.

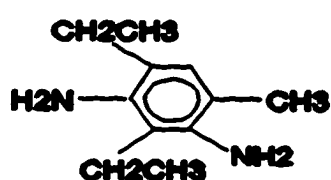
BLGAMSOR.FOR: Assigning source terms and the “diffusivity” coefficient.

The output written by Subroutine Supply will be read by the post processor program (Visualize). Visualize will write two “M” file, i. e. contour.m and geo.m both can be run on Matlab platform just by calling the names. Contour will draw contour plot of the variable on the top of the geometry. The resulted Matlab picture can be view from different angles.

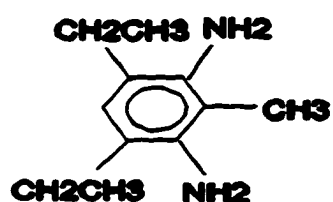
APPENDIX B
CHEMICAL STRUCTURES



Cellulose



2,4 DETDA



2,6 DETDA



4,4 diphenylmethane diisocyanate [u-MDI]

APPENDIX C

A REVIEW ON MAPPING OF GOVERNING EQUATIONS

All the governing equations for the fluid flow in SRIM fall into the category of diffusion-convection equations and can be represented by general equation as:

$$\begin{aligned}
 & \rho \frac{\partial \phi}{\partial t} + \rho U \frac{\partial \phi}{\partial x} + \rho V \frac{\partial \phi}{\partial y} + \rho W \frac{\partial \phi}{\partial z} + \\
 & \phi \left[\frac{\partial \rho}{\partial t} + \frac{\partial}{\partial x}(\rho U) + \frac{\partial}{\partial y}(\rho V) + \frac{\partial}{\partial z}(\rho W) \right] = \\
 & \Gamma_x \frac{\partial^2 \phi}{\partial x^2} + \Gamma_y \frac{\partial^2 \phi}{\partial y^2} + \Gamma_z \frac{\partial^2 \phi}{\partial z^2} + S_\phi + \\
 & \left(\frac{\partial \Gamma_x}{\partial x} \frac{\partial \phi}{\partial x} + \frac{\partial \Gamma_y}{\partial y} \frac{\partial \phi}{\partial y} + \frac{\partial \Gamma_z}{\partial z} \frac{\partial \phi}{\partial z} \right)
 \end{aligned} \tag{C.1}$$

For incompressible systems, the terms inside the square bracket on the left hand side are zero. Likewise for constant diffusivity coefficients, the terms inside the parenthesis on the right hand side are zero.

MAPPING THE GOVERNING EQUATION INTO THE CALCULATION DOMAIN

Let ξ , η and ν be the coordinate system in the calculation domain. Mapping the governing equation from the physical domain x, y , and z can be accomplished using the equation:

$$\begin{pmatrix} \frac{\partial f}{\partial \xi} \\ \frac{\partial f}{\partial \eta} \\ \frac{\partial f}{\partial v} \end{pmatrix} = \begin{bmatrix} x_\xi & y_\xi & z_\xi \\ x_\eta & y_\eta & z_\eta \\ x_v & y_v & z_v \end{bmatrix} \begin{pmatrix} \frac{\partial f}{\partial x} \\ \frac{\partial f}{\partial y} \\ \frac{\partial f}{\partial z} \end{pmatrix} \quad (\text{C.2})$$

The first derivatives with the respect of the physical domain coordinates can be expressed in terms of the derivatives with respect of the calculation domain coordinates as:

$$\begin{pmatrix} \frac{\partial f}{\partial x} \\ \frac{\partial f}{\partial y} \\ \frac{\partial f}{\partial z} \end{pmatrix} = \begin{bmatrix} x_\xi & y_\xi & z_\xi \\ x_\eta & y_\eta & z_\eta \\ x_v & y_v & z_v \end{bmatrix}^{-1} \begin{pmatrix} \frac{\partial f}{\partial \xi} \\ \frac{\partial f}{\partial \eta} \\ \frac{\partial f}{\partial v} \end{pmatrix} \quad (\text{C.3})$$

For simplicity of the presentations, first derivatives of any function g with respect to any variable β (i. e. x , y , z , ξ , η , or v) is written as g_β . After some mathematical manipulations, equation (C.3) can be written as:

$$\begin{pmatrix} f_x \\ f_y \\ f_z \end{pmatrix} = \begin{pmatrix} f_\xi \xi_x + f_\eta \eta_x + f_v v_x \\ f_\xi \xi_y + f_\eta \eta_y + f_v v_y \\ f_\xi \xi_z + f_\eta \eta_z + f_v v_z \end{pmatrix} \quad (\text{C.4})$$

where the derivatives of the calculation coordinates can be expressed as:

$$\begin{aligned}\xi_x &= \frac{I}{J}(y_\eta z_v - y_v z_\eta) & \xi_y &= \frac{I}{J}(x_v z_\eta - x_\eta z_v) & \xi_z &= \frac{I}{J}(x_\eta y_v - x_v y_\eta) \\ \eta_x &= \frac{I}{J}(y_v z_\xi - y_\xi z_v) & \eta_y &= \frac{I}{J}(x_\xi z_v - x_v z_\xi) & \eta_z &= \frac{I}{J}(x_v y_\xi - x_\xi y_v) \\ v_x &= \frac{I}{J}(y_\xi z_\eta - y_\eta z_\xi) & v_y &= \frac{I}{J}(x_\eta z_\xi - x_\xi z_\eta) & v_z &= \frac{I}{J}(x_\xi y_\eta - x_\eta y_\xi)\end{aligned}\quad (\text{C.5})$$

where J is the Jacobean of the transformation or determinant of the transformation matrix. Similarly, the second derivatives can be obtained using the same principles. The second derivatives can be expressed as:

$$\begin{aligned}\frac{\partial^2 f}{\partial x^2} &= \xi_x^2 f_{\xi\xi} + \eta_x^2 f_{\eta\eta} + v_x^2 f_{vv} + 2\xi_x \eta_x f_{\xi\eta} \\ &\quad 2\xi_x v_x f_{\xi v} + 2\eta_x v_x f_{\eta v} + \xi_{xx} f_\xi + \eta_{xx} f_\eta + v_{xx} f_v\end{aligned}\quad (\text{C.6})$$

$$\begin{aligned}\frac{\partial^2 f}{\partial y^2} &= \xi_y^2 f_{\xi\xi} + \eta_y^2 f_{\eta\eta} + v_y^2 f_{vv} + 2\xi_y \eta_y f_{\xi\eta} \\ &\quad 2\xi_y v_y f_{\xi v} + 2\eta_y v_y f_{\eta v} + \xi_{yy} f_\xi + \eta_{yy} f_\eta + v_{yy} f_v\end{aligned}\quad (\text{C.7})$$

$$\begin{aligned}\frac{\partial^2 f}{\partial z^2} &= \xi_z^2 f_{\xi\xi} + \eta_z^2 f_{\eta\eta} + v_z^2 f_{vv} + 2\xi_z \eta_z f_{\xi\eta} \\ &\quad 2\xi_z v_z f_{\xi v} + 2\eta_z v_z f_{\eta v} + \xi_{zz} f_\xi + \eta_{zz} f_\eta + v_{zz} f_v\end{aligned}\quad (\text{C.8})$$

The transformation of cross derivatives follow in the same ways and will not be discussed here.

If the source term (S_ϕ) contains some derivative terms, it should also be mapped following the above procedure. The final mapped governing equation should be cast into a general diffusion convection equation (Equation 9.1) as will be shown in the following section.

INCOMPRESSIBLE CONSTANT DIFFUSIVITY SYSTEMS

Applying the above transformation to equation (C.1) for constant density and diffusivity, we will get:

$$\begin{aligned}
 \rho \frac{\partial \phi}{\partial t} + \rho (U \xi_x + V \xi_y + W \xi_z) \frac{\partial \phi}{\partial \xi} + \rho (U \eta_x + V \eta_y + W \eta_z) \frac{\partial \phi}{\partial \eta} + \rho (U v_x + V v_y + W v_z) \frac{\partial \phi}{\partial v} = \\
 (\Gamma_x \xi_x^2 + \Gamma_y \xi_y^2 + \Gamma_z \xi_z^2) \frac{\partial^2 \phi}{\partial \xi^2} + (\Gamma_x \eta_x^2 + \Gamma_y \eta_y^2 + \Gamma_z \eta_z^2) \frac{\partial^2 \phi}{\partial \eta^2} + \\
 (\Gamma_x v_x^2 + \Gamma_y v_y^2 + \Gamma_z v_z^2) \frac{\partial^2 \phi}{\partial v^2} + 2(\Gamma_x \xi_x \eta_x + \Gamma_y \xi_y \eta_y + \Gamma_z \xi_z \eta_z) \frac{\partial \phi}{\partial \xi \partial \eta} + \\
 2(\Gamma_x \xi_x v_x + \Gamma_y \xi_y v_y + \Gamma_z \xi_z v_z) \frac{\partial \phi}{\partial \xi \partial v} + 2(\Gamma_x \eta_x v_x + \Gamma_y \eta_y v_y + \Gamma_z \eta_z v_z) \frac{\partial \phi}{\partial \eta \partial v} + \\
 (\Gamma_x \xi_{xx} + \Gamma_y \xi_{yy} + \Gamma_z \xi_{zz}) \frac{\partial \phi}{\partial \xi} + (\Gamma_x \eta_{xx} + \Gamma_y \eta_{yy} + \Gamma_z \eta_{zz}) \frac{\partial \phi}{\partial \eta} + (\Gamma_x v_{xx} + \Gamma_y v_{yy} + \Gamma_z v_{zz}) \frac{\partial \phi}{\partial v} \\
 + S_\phi
 \end{aligned}
 \tag{C.9}$$

..... (C.9)

Equation (C.9) can be rearranged in a more compact form as:

$$\begin{aligned}
 \rho \frac{\partial \phi}{\partial t} + \rho \omega_\xi \frac{\partial \phi}{\partial \xi} + \rho \omega_\eta \frac{\partial \phi}{\partial \eta} + \rho \omega_v \frac{\partial \phi}{\partial v} = D_\xi \frac{\partial^2 \phi}{\partial \xi^2} + D_\eta \frac{\partial^2 \phi}{\partial \eta^2} + D_v \frac{\partial^2 \phi}{\partial v^2} \\
 + S_\phi + S_{tr}
 \end{aligned}
 \tag{C.10}$$

where ω_β ($\beta = \xi, \eta, v$) is "the apparent velocity" in the direction of β coordinate of the calculation domain. Similarly, D_β is the corresponding "apparent diffusion" coefficient. S_{tr} is an extra "source term" resulting from the coordinate transformation. It is important to note that equation C.10 has the appearance of diffusion-convection type of equation (Equation 9.1)

IMPOSING THE BOUNDARY CONDITIONS

If the boundary conditions are given in the form of known values of the dependent variables such as (P , T , or α), the implementation is straightforward since the locations (in x , y , z as well as in ξ , η , v coordinate systems) are known.

If a boundary condition is given in terms of the gradient of the dependent variable, the boundary condition should be mapped following the above procedure [equations (C.4) and (C.4)].

VELOCITY CALCULATIONS

In the SRIM model, velocity is not the primary dependent variables calculated from the governing equations, but it is calculated using Darcy's equation. Since, Darcy's equation involves the pressure gradient, it should be mapped as well into the calculation domain. The mapped equations for velocity calculation can be derived using equations (C.4) and (C.5) as follow:

$$u = \frac{K_x}{\mu} \frac{\partial P}{\partial x} \quad (C.11)$$

$$u = \frac{K_x}{\mu} \left(\xi_x \frac{\partial P}{\partial \xi} + \eta_x \frac{\partial P}{\partial \eta} + v_x \frac{\partial P}{\partial v} \right) \quad (C.12)$$

where u is x component of the velocity. Using the same procedure, velocity components in the y and z direction can be written as:

$$v = \frac{K_y}{\mu} \left(\xi_y \frac{\partial P}{\partial \xi} + \eta_y \frac{\partial P}{\partial \eta} + v_y \frac{\partial P}{\partial v} \right) \quad (\text{C.12 & 13})$$

$$w = \frac{K_z}{\mu} \left(\xi_z \frac{\partial P}{\partial \xi} + \eta_z \frac{\partial P}{\partial \eta} + v_z \frac{\partial P}{\partial v} \right)$$

It is important to note that all the velocities are in physical domain (x, y, and z) base vectors. To utilize this velocity value in the control volume formulation, the above velocity has to be translated into the calculation domain base vectors. This will not be discussed here.

Note: The quantity $x_\beta, y_\beta, z_\beta$ ($\beta = \xi, \eta, \text{ and } v$) are given by the grid generation program used to discretize the geometry.

VITA

Mohammad Fahrurrozi was born on September 18, 1965, in Malang, a district in east province of Java Island, Indonesia. He received his bachelor of science degree in Chemical Engineering from Gadjah Mada University in Indonesia in August 1989. After working with the same university for two years, he then came to Louisiana State University in the Fall of 1991 to enroll in the graduate program in Chemical Engineering. He received his master of science degree in May 1993. He is currently a doctor of philosophy degree candidate in Chemical Engineering to be conferred in August 1997.

DOCTORAL EXAMINATION AND DISSERTATION REPORT

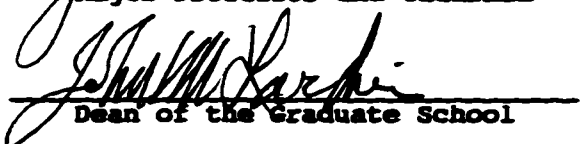
Candidate: Mohammad Fahrurrozi

Major Field: Chemical Engineering

Title of Dissertation: Cellulose Reinforced Composites and SRIM and RTM Modeling

Approved:

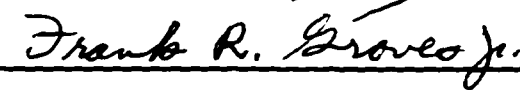

John R. Collier
Major Professor and Chairman

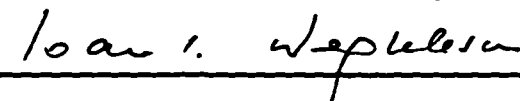

John W. Karcher
Dean of the Graduate School

EXAMINING COMMITTEE:


Bruce Collier


Amanda B. Fojtik


Frank R. Grove Jr.


Ioan I. Vepkuloson


Radell C. Gandy

Date of Examination:

July 3, 1997